PROGRAMA DE DOCTORADO EN INGENIERÍA ENERGÉTICA Y SOSTENIBLE

CONTROL INTELIGENTE DE PLANTAS HÍBRIDAS CON AEROGENERADORES, SISTEMAS SOLARES FOTOVOLTAICOS Y SISTEMAS DE ALMACENAMIENTO DE ENERGÍA

INTELLIGENT CONTROL OF HYBRID POWER PLANTS WITH WIND TURBINES, PV SOLAR SYSTEMS, AND ENERGY STORAGE SYSTEMS

UNIVERSIDAD DE CÁDIZ

ESCUELA TÉCNICA SUPERIOR DE INGENIERÍA DE ALGECIRAS

JULIO 2023

AUTOR: EHSAN HOSSEINI

DIRECTORES: LUIS M. FERNÁNDEZ RAMÍREZ

RAÚL SARRIAS MENA

CONTROL INTELIGENTE DE PLANTAS HÍBRIDAS CON AEROGENERADORES, SISTEMAS SOLARES FOTOVOLTAICOS Y SISTEMAS DE ALMACENAMIENTO DE ENERGÍA

INTELLIGENT CONTROL OF HYBRID POWER PLANTS WITH WIND TURBINES, PV SOLAR SYSTEMS, AND ENERGY STORAGE SYSTEMS

Por

EHSAN **H**OSSEINI

Vº. Bº de los Directores de la Tesis:

Fdo: Luis M. Fernández Ramírez Fdo: Raúl Sarrias Mena

Trabajo presentado para optar al grado de Doctor por la Universidad de Cádiz.

A thesis submitted for the degree of Doctor at the University of Cádiz

Algeciras, Julio 2023

تو کز محنت دیگران بی غمی
نشاید که نامد نهند آدمی

"If you've no sympathy for human pain,
the name of human you cannot retain".
Sadi, Persian poet

Agradecimientos

A lo largo de este viaje, he tenido la enorme suerte de estar rodeado de grandes personas que me han ayudado a llegar hasta la meta, que han hecho de mi proyecto el suyo, y que han puesto su tiempo y esfuerzo a mi disposición. Con estas líneas, me gustaría expresar mi enorme agradecimiento a todas ellas.

A mis queridos directores, Luis M. Fernández Ramírez y Raúl Sarrias Mena, que me han guiado hasta aquí con la sabiduría de su experiencia. Gracias Raúl, por tus consejos directos y certeros. Gracias Luis, por tus palabras de ánimo, por tantas respuestas a tantos correos, por tu implicación, pero sobre todo, gracias por confiar en mi trabajo. Muchas gracias por tu apoyo en los momentos difíciles, por tu paciencia, por dejarte robar el tiempo; en definitiva, gracias por estar siempre a mi lado.

A mis compañeros del grupo de investigación, con los que he compartido muy buenos ratos y también otros menos buenos. He compartido las dudas y la incertidumbre, los éxitos. Muchas gracias por vuestro apoyo y vuestra disposición para ayudarme en todo. Dr. Carlos, Dr. Pablo, Dr. Paco y mis queridos amigos y futuros doctores Pablo y David. No olvido los tintos de verano que nos hemos tomado ni tampoco los manchados.

A mis padres, Ali y Shahindokht, de cuyo ejemplo he aprendido a manejar las herramientas que más me han ayudado a completar este camino: el valor del esfuerzo y del trabajo. Gracias por vuestro apoyo y cariño incondicional.

A Cristina y Antonio, mis compañeros de piso en España que me han acompañado y ayudado durante todo este tiempo.

A todos, mil gracias.

Resumen

El concepto de sistemas de energía de múltiples fuentes, como por ejemplo en microrredes basadas en fuentes de energía renovable (RES), almacenamiento y conexión a la red, tiene como objetivo participar activamente en el equilibrio de la producción y el consumo de electricidad. Esta tesis estudia los desafíos de la integración de RES respaldados por sistemas de almacenamiento de energía (ESS) a la red principal en un sistema de energía de gran escala, además de considerar la eficiencia de ESS y los posibles problemas a largo plazo.

Aerogeneradores (WT) y sistemas solares fotovoltaicos (PV) son fuentes de energía accesibles y dos de los sistemas de energía renovable de más rápido crecimiento que juegan un papel vital en las microrredes eléctricas. Esta creciente penetración de las energías renovables en la generación de energía implica una conexión precisa entre la red principal, las cargas potenciales y los recursos de energía. En este contexto, los convertidores electrónicos de potencia y las técnicas avanzadas de control son aspectos relevantes que han motivado a los investigadores a desarrollarlos.

El convertidor es un componente crucial para la conexión de una fuente de energía a la red o a la carga local. En cuanto a la conexión a la red, la mayoría de los estudios se han centrado en los inversores para proponer nuevas topologías y estructuras de control. Los inversores basados en fuente de impedancia, también llamados inversor de fuente Z (ZSI), han captado el interés de los investigadores en los últimos años. Estos inversores pueden reducir o elevar la tensión, realizar la conversión en una sola etapa e integrar un ESS sin un convertidor adicional como característica principal. Muchas modificaciones estructurales se han desarrollado para mejorar su estructura. Uno de ellos es el cuasi-ZSI (qZSI), que tiene varias ventajas sobre la topología ZSI básica. Debido a las interesantes características que los hacen adecuados para aplicaciones con RES, el qZSI ha sido seleccionado en esta tesis para integrar plantas híbridas con energía eólica y PV a la red principal.

En aplicaciones de sistemas de energía a gran escala, un solo inversor no puede satisfacer la potencia requerida; por lo tanto, se pueden necesitar varios inversores para construir un inversor multinivel de puente H en cascada (CHBMLI). El concepto ZS/qZS, integrado con inversores multinivel, hereda los méritos del CHBMLI con una mayor fiabilidad del inversor gracias a la inmunidad a los cortocircuitos. Cuando se aplica a sistemas de energía a escala de MW, qZS-CHBMLI se puede escalar fácilmente agregando más módulos en cascada.

El sistema de gestión de energía (EMS) es otro tema importante que debe abordarse mediante el uso de un esquema de control adecuado. Un esquema de control apropiado debe generar las señales de control relevantes para extraer la potencia demandada de las fuentes de entrada de forma individual o simultánea mientras se mantiene la tensión o corriente de salida regulada. Desde una perspectiva amplia, el estudio del EMS para RES es importante para lograr una operación eficiente de los sistemas de generación de energía respaldados por ESS y la conversión de energía con cargas locales o red, y satisfacer los requisitos de calidad de la energía.

Esta tesis propone EMS inteligentes innovadores para lograr el correcto funcionamiento de un EMS estructural basado en la eficiencia de ESS y problemas a largo plazo para plantas híbridas con WT, PV, ESS y qZS-CHBMLI. Se propone una función multivariable no lineal restringida para aumentar la eficiencia de los almacenamientos de energía de la batería (BES) utilizados en una planta híbrida y conectada a una red a través de qZS-CHBMLI. Se utilizan algoritmos inteligentes para resolver la función objetivo propuesta. La función Fmincon de

MATLAB y el algoritmo de aprendizaje por refuerzo (RL), que aprovecha una función de recompensa no lineal, son los algoritmos de resolución usados para el problema de optimización propuesta. Además, un nuevo EMS basado en lógica difusa ha sido implementado.

Este tema merece un mayor esfuerzo de investigación, ya que no hay estudios publicados que hayan abordado el estudio de BES-qZS-CHBMLI con plantas híbridas que integran WT y PV, combinando RL y nuevas estrategias de control basadas en la eficiencia de las BES. En cuanto a la topología del sistema, pocos estudios han abordado la dinámica de la microrred AC con plantas híbridas, BESS y un optimizador-EMS conectado a la red. En la mayoría de los estudios, se ha utilizado un convertidor CC/CC para implementar la estrategia MPPT para fuentes de energía PV y WT, y habitualmente se utilizó un inversor de fuente de tensión (VSI) para la conversión CC/CA. La topología propuesta aquí se basa en ES-qZS-CHBMLI, sin convertidor CC/CC adicional. Además, todos los estudios previos publicados han utilizado una configuración de planta basada en un BES-qZS-CHBMLI integrando los mismos sistemas PV y BES en cada módulo en serie e integrando sistemas PV o WT con diferente potencia nominal en cada módulo. Finalmente, la evaluación del funcionamiento de la red en términos de potencias activas y reactivas desde el punto de vista del operador de red no han sido considerado en estos estudios previos. Con respecto al EMS, los trabajos previos han implementado un EMS basado en distribuir la potencia entre los BES según su estado de carga (SOC), donde se ha pasado por alto la eficiencia de los BES porque el EMS se centró solo en los valores del SOC y la potencia demandada.

Esta investigación ha desarrollado nuevas soluciones para mejorar el control y operación de las plantas eléctricas híbridas con sistemas WT, PV y EES mediante el uso de inversores más eficientes y estrategias de control basadas en algoritmos de control inteligente.

Abstract

The concept of multi-source energy systems, i.e., microgrids based on renewable energy sources (RES), storage, and grid connection, aims to actively participate in the balance of electricity production and consumption. This thesis studies the integration challenges of RES supported by energy storage systems (ESS) to the main grid in a large-scale power system, considering ESS efficiency and long-term issues.

Wind turbines (WT) and solar photovoltaic (PV) systems are accessible variable sources and two of the fastest growing renewable energy systems that play a vital role in microgrids as energy sources. This growing penetration of RES in power generation entails precise connection between the main grid, potential loads, and power resources. In this context, power electronic converters and advanced control techniques are relevant aspects, having motivated researchers to develop them.

The converter is a crucial component for the connection of a power source to either the grid or local load. Regarding the grid connection, most studies have focused on inverters to propose new topologies and control structures. Inverters based on impedance sources, also known as Z-source inverters (ZSI), have attracted the interest of scientists in recent years. These inverters can implement voltage buck/boost, perform conversion on a single stage, and integrate an ESS without an additional converter as the main feature. Many structural modifications have been made to improve their structure. One of them is the quasi-ZSI (qZSI), which has several advantages over the basic ZSI topology. Owing to the interesting characteristics that make them suitable for RES applications, the qZSI has been selected in this thesis to integrate WT-PV power plants into the main grid.

In large-scale power system applications, a single inverter cannot satisfy the required power; therefore, several inverters can be arranged to build a cascaded H-bridge multilevel inverter (CHBMLI). The ZS/qZS concept, integrated with multilevel inverters, inherits the merits of CHBMLI with improved inverter reliability owing to short-circuit immunity. When applied to MW-scale power systems, qZS-CHBMLI can be easily scaled by adding more cascaded modules.

The energy management system (EMS) is another important issue that must be addressed using a suitable control scheme. An appropriate control scheme must generate relevant control signals to draw the demanded power from the input sources individually or simultaneously while maintaining the regulated output voltage or current. From a broad perspective, studying the EMS for RES is important to achieve efficient operation of power generation systems supported by ESS and power conversion with local loads or grid, and to satisfy the power quality requirements.

This thesis proposes innovative intelligent EMSs to achieve proper operation of a structural EMS based on ESS efficiency and long-term issues for hybrid power plants with WT, PV, ESS and qZS-CHBMLI. A constrained nonlinear multivariable function was proposed to increase the efficiency of the battery energy storage (BES) used in a hybrid power plant and connected to a grid through qZS-CHBMLI. Intelligent algorithms were used to solve the proposed objective function. Reinforcement learning (RL) algorithm taking advantage of a nonlinear reward function and fmincon MATLAB function are

solvers of the proposed function. In addition, a new EMS based on fuzzy logic has been developed to dispatch power between BESs.

This topic is worth greater research effort, as there are no published studies that have addressed the study of BES-qZS-CHBMLI with hybrid power plants integrating WT and PV systems that combine RL and novel control strategies based on the BES efficiency. Regarding the system topology, few studies have addressed the dynamics of AC microgrid with hybrid power plants, BESS and an optimizer-EMS connected to the grid. In most studies, DC/DC converters have been used to implement the MPPT strategy for PV and WT power sources, and a voltage-source inverter (VSI) was commonly used for DC/AC conversion. The topology proposed herein is based on ES-qZS-CHBMLI, without an additional DC/DC converter. Moreover, all these previous studies have used a configuration of a power plant based on a BES-qZS-CHBMLI integrating the same PV systems and BESs into each module in series and integrating PV or WT sources with different nominal power in each module has not been sought. Finally, the evaluation of grid performance in terms of active and reactive power at the sight of the grid operator was neglected in these previous studies. Regarding the EMS, previous studies have executed an EMS based on distributing the power among the BES according to their state-of-charge (SOC), where the BES efficiency has been overlooked because the EMS focused only on the SOC values and demanded power.

This research developed new solutions to improve the control and operation modes of hybrid power plants with WT, PV systems and ESS by using more efficient inverters and control strategies based on intelligent control algorithms.

Table of contents

Resumen i
Abstract iii
Table of contents v
List of figures ix
List of tables xi
List of acronyms xiii
1. Introduction 3
2. Objectives and Hypotheses of the thesis 11
2.1. Objectives of the thesis 11
2.2. Hypotheses of the thesis 12
3. Review of the background – State of the Art 19
3.1. PV panels technologies 21
3.2. Wind turbines 22
3.3. Energy storage technologies 23
3.4. High voltage converter technologies 27
3.4.1. High voltage source converters 27
3.4.1.1. *Series/parallel-connected switch cells* 27
3.4.1.2. *Cascaded (H-bridge) multilevel voltage source converters.* 28
3.4.1.3. *Capacitor -clamped multilevel voltage source converters.* 28
3.4.1.4. *Diode-clamped multilevel voltage source inverters.* 29
3.4.2. High voltage impedance source multilevel converters 30
3.4.2.1. *Dc-link peak voltage controls.* 31
3.4.2.2. *Power control.* 32
3.4.2.3. *MPPT techniques.* 32
3.4.2.4. *Modulation techniques.* 34
3.4.2.5. *Energy management systems.* 34
4. Description of the configurations under study 49
4.1. Modelling of the RES 49
4.1.1. Wind turbine. 49
4.1.2. Photovoltaic (PV) system 52
4.2. Modelling of the Quasi Z-source network 53
4.3. Modelling of the Battery 55
4.4. Converter modulation technique 56
4.5. AC grid model 58

4.6. Modelling of the hybrid configurations 58
4.7. Reinforcement learning algorithm 60
4.7.1. Number of neural network neurons 64
4.7.2. Reducing Effort 64
4.7.3. Hyperparameters 64
4.7.4. Designing reward 65
4.7.5. Random initializations 66
4.7.6. Is down function 66
5. Control objectives 49
5.1. Independent MPPT algorithm and pitch angle control 49
5.1.1. Case study 1: MPPT for wind turbines and pitch angle controller 49
5.1.1.1. Adaptive PID controller 49
5.1.1.2. Gain scheduled recurrent ANFIS type-2 with passive RL 51
5.1.2. Case study 2: MPPT for hybrid cascaded RES system 57
5.2. Power control 58
5.3. Energy management system 61
5.3.1. Proportional SOC Energy Management System (SOC-EMS) 61
5.3.2. Fuzzy Logic Energy Management System (FLC-EMS) 62
5.3.3. Model Predictive Control Energy Management System (MPC-EMS) 64
5.3.4. Fmincon Function Energy Management System (OPT-EMS) 66
5.3.5. Reinforcement Learning Algorithm Energy Management System (RL-EMS) 68
6. Results and discussion 91
6.1. EMS comparison 91
6.1.1. Case 1: PV plants – EMS: fmincon function (OPT) 91
6.1.2. Case 2. A. Simulation results: Hybrid PV and WT power sources – EMS: OPT- SOC – MPC 95
6.1.3. Case 2. B. Experimental Results: Hybrid PV and WT power sources – EMS: OPT-SOC - MPC 102
6.1.4. Case 3. Hybrid PV and WT power sources – EMS: FLC- OPT- SOC 104
6.1.5. Case 4. PV power plants – EMS: Multiagent RL 108
6.1.6. Case 5. A. PV power plants – EMS: Single-Agent RL- Training 112
6.1.7. Case 5.B. Hybrid PV and WT power sources – EMS: Single-Agent RL Algorithm-Testing 115
6.1.8. Case 6. Single WT power source – Adaptive MPPT and passive reinforcement learning algorithm for pitch angle control 117
6.1.8.1. Step wind speed test 118

6.1.8.2. Random wind speed test 121
6.1.8.3. Longer simulation for comparative study and load analysis 125
6.2. Comparison of EMSs 128
7. Conclusions, contributions and future works 145
7.1. Conclusions 145
7.2. Main contributions of the thesis 146
7.3. Future works 148
References 153
List of publications III

List of figures

Fig. 3.1. Benefits of RES [6]. 19
Fig. 3.2. Renewable power generation cost for the last 12 years [6]. 20
Fig. 3.3. Renewable power generation share by 2050 [6]. 20
Fig. 3.4. Worldwide solar PV capacity installations [6]. 21
Fig. 3.5. Worldwide wind capacity installations [6]. 23
Fig. 3.6. Schematic diagram of multimode VSC composed of n two-level VSC modules [50]. 27
Fig. 3.7. Schematic diagram of a wye-connected, H-bridge-based, multilevel VSC [50]. 28
Fig. 3.8. One-leg five level capacitor-clamped multilevel VSC [53]. 29
Fig. 3.9. Conceptual representation of an n-level diode-clamped multilevel VSC [55]. 30
Fig. 3.10. Topology of n-layer grid-tie PV system (a) ZS-CMI based (b) qZS-CMI based [64]. 31
Fig. 4.1. Operating regions of a variable speed WT. 50
Fig. 4.2. *The qZSI* topology and operating modes. 54
Fig. 4.3. Equivalent circuit for the shoot-through state and non-shoot-through state [65] chapter.12. 57
Fig. 4.4. Modulation scheme used for each BES-qZSI module. 57
Fig. 4.5. Grid-connected ES-qZS-CHBMLI with PV power generation under study. 59
Fig. 4.6. Hybrid power plant under study based on BES-qZS-CHBMLI and RES (PV power plants and WT) and control system. 60
Fig. 4.7. Actor neural network architectures. 62
Fig. 4.8. Critic neural network architectures. 63
Fig. 4.9. Picking up a policy by an agent. 63
Fig. 4.10. ε-greedy procedure. 65
Fig. 5.1. Passive RL structure based PSO for recurrent type-2 fuzzy logic pitch agent. 52
Fig. 5.2. Simplified scheme of the passive RL structure. 56
Fig. 5.3. Block diagram of the proposed controller implemented for the CART3. 57
Fig. 5.4. MPPT control strategy. 58
Fig. 5.5. Control schemes of each qZSI module. 59
Fig. 5.6. Active and reactive power control strategy. 61
Fig. 5.7. Fuzzy-EMS structure. 63
Fig. 5.8. Overall MPC-EMS [139]. 66
Fig. 5.9. OPT-EMS structure. 68
Fig. 5.10. An insight to a neural network of a TD3 agent. 71
Fig. 5.11. Multiagent RL EMS. 72
Fig. 6.1. Case 1. BES powers. 92
Fig. 6.2. Case 1. BES SOC: BES1, BES2, and BES3. 93
Fig. 6.3. Case 1. Grid active and reactive power. 93
Fig. 6.4. Case 1. a) Seven-level output voltage of the ES-qZS-CHBMLI. (b) Grid voltage and current. 94
Fig. 6.5. Case 1. Grid active and reactive power. 94
Fig. 6.6. Case.2. A. (a) PV1 irradiance, (b) PV1 output power, (c) PV2 irradiance, (d) PV2 power plant, (e) wind speed, (f) WT output power. 96
Fig. 6.7. Case.2. A. Grid active and reactive power. 97
Fig. 6.8. Case.2. A. BES power for OPT-EMS, SOC-EMS, and MPC-EMS: (a) BES1, (b) BES2, and (c) BES3. 98
Fig. 6.9. Case.2. A. BES SOC: (a) BES1, (b) BES2, and (c) BES3. 99

Fig. 6.10. Case.2. A. BES efficiency found by EMSs..... 100
Fig. 6.11. Case.2. A. (a) Seven-level output voltage of the BES-qZS-CHBMLI, and (b) Grid voltage and current..... 101
Fig. 6.12. Case.2. B Experimental setup with OPAL-RT- real-time simulator OP4510..... 102
Fig. 6.13. Case.2. B. Experimental results for: (a) OPT-EMS grid active and reactive power, (b) OPT-EMS grid voltage and current, and Seven-level output voltage of the BES-qZS-CHBMLI. 103
Fig. 6.14. Case.2. B. Experimental results for BES power: (a) OPT-EMS, (b) SOC-EMS, and (c) MPC-EMS..... 103
Fig. 6.15. Case.3. Results for BES power: (a) OPT-EMS, (b) SOC-EMS, and (c) FLC-EMS. 105
Fig. 6.16. Case.3. BES SOC: (a) BES1, (b) BES2, and (c) BES3..... 105
Fig. 6.17. Case.3. Grid active and reactive power..... 106
Fig. 6.18. Case.3. BES efficiency..... 106
Fig. 6.19. Case.3. EMSs' errors analysis 107
Fig. 6.20. Case.4. (a). PV1 irradiance, (b) PV1 output power, (c) PV2 irradiance, (d) PV2 power plant, (e) PV3 irradiance, (f) PV3 output power..... 109
Fig. 6.21. Case.4. Grid active and reactive power..... 109
Fig. 6.22 Case.4. BES power 110
Fig. 6.23. Case.4. BES SOC: (a) BES1, (b) BES2, and (c) BES3..... 110
Fig. 6.24. Case.4. (a) Seven-level output voltage of the ES-qZS-CHBMLI. (b) Grid voltage and current..... 111
Fig. 6.25. Case.5. A. Reward plot for TD3 agent 112
Fig. 6.26. Case.5. A. PVs irradiance (a). IRR. 1, (b). IRR. 2, and (c). IRR. 3..... 113
Fig. 6.27. Case.5. A. Output BESs power..... 113
Fig. 6.28. Case.5. A. BESs SOC: (a). BES1, (b). BES2, and (c). BES3..... 114
Fig. 6.29. Case.5. A. Grid active and reactive power 114
Fig. 6.30. Case.5. B. Output BESs power..... 115
Fig. 6.31. Case.5. B. BESs SOC: (a). BES1, (b). BES2, and (c). BES3..... 116
Fig. 6.32. Case.5. B. Grid active and reactive power 116
Fig. 6.33. Case. 6. Dynamic response comparison under one step raise: (a) control input acceleration; (b) rotor speed 119
Fig. 6.34. Case.6. Dynamic response comparison of the controllers under different pace steps 120
Fig. 6.35. Case.6. Turbulent wind pattern 121
Fig. 6.36. Case.6. Time and frequency responses for speed error acceleration..... 122
Fig. 6.37. Case.6. Time and frequency domain responses for pitch angle acceleration 123
Fig. 6.38. Case.6. Results obtained for the CART3: (a) generator power (kW); (b) generator speed (rpm); (c) generator torque (N.m)..... 124
Fig. 6.39. Case.6. Comparison of the speed error acceleration by boxplot and histogram plot 125
Fig. 6.40. Case.6. Results for 4000 s simulation (a). Wind pattern (b). Pitch angle curve..... 126
Fig. 6.41 Case.6. Moment variations on blade I, tower and rotor as a function of time and frequency; blue line (GS-RL-RANFIST2), red line (GC-PI) 127
Fig. 6.42. Case.6. Normalized DEL values of the selected load variables for CART3 128

List of tables

Table 3.1. BES features and typical values [44]. 26
Table 4.1. RL agent types and features. 61
Table 5.1. Fuzzy rules base table. 64
Table 6.1. Case 1. Parameters of BES1. 91
Table 6.2. Case 1. Parameters of BES2. 91
Table 6.3. Case 1. Parameters of BES3. 91
Table 6.4. Case 2.A. Parameters of BESs. 95
Table 6.5. Case 2.A. Parameters of grid references. 96
Table 6.6. Case.2. A. Parameters of the simulation setup. 97
Table 6.7. Case.2. A: Comparison of EMSs 101
Table 6.8. Case.3: Comparison of EMSs 108
Table 6.9. Case.4: Parameters of BES 108
Table 6.10. Case.6: Parameters of CART3 117
Table 6.11. Case.6: Comparison of the control strategies 127

List of acronyms[1]

AC – Alternate current
BES – Battery energy storage
CHBMLI – cascaded H-bridge multilevel inverter
DAB – Dual active bridge
DC – Direct current
DFIG – Doubly-fed induction generator
EMS – Energy management system
ESS – Energy storage system
GS – Grid side
HVDC – High-voltage direct current
IGBT – Insulated-gate bipolar transistor
JCR – Journal citation report
MPC – Model predictive control
MPPT – Maximum power point tracking
PCC – Point of common coupling
PEM – Proton exchange membrane
PMSG – Permanent-magnet synchronous generator
PWM – Pulse-width modulation
PV – Photo voltaic
qZSIs – quasi-Z-source inverters
BES-qZS-CHBMLI – Battery energy stored quasi-Z-source cascaded H-bridge multilevel inverter
RES – Renewable energy sources
RL – Reinforcement learning
SCIE – Science citation index expanded
SCS – Supervisory control system
SOC – State-of-charge
STATCOM – Static synchronous compensator
T&D – Transmission and distribution
VSC – Voltage source converter
WECS – Wind energy conversion system
WT – Wind turbine
ZSIs – Z-source inverters

[1] The use of an ‘s’ after any of these acronyms refers to the plural.

CHAPTER ONE

CAPÍTULO UNO

1

1. Introduction

Although traditional power systems have satisfied energy demand for a long time, they will not be able to meet the current challenges alone, as fossil fuels are predicted to run out soon. In the last couple of decades, there has been great interest in using RES worldwide owing to the increase in energy demand and the reduction of environmental pollution. The integration of RES into power systems can be attributed to environmental, economic, and social benefits. Driven by these benefits, future power systems are predicted to be entirely RES. Therefore, modern power systems combine non-conventional resources to provide sustainable power systems capable of meeting the significant increase in demand.

Among the RES, WT and PV technologies are currently the most common ones owing to their exceptional benefits they provide. Nowadays, application of these sources for the large-scale power systems is increasing, starting to reach a significant share in the RES market. However, many factors must be taken into account if hybrid power sources are inserted to the power network. In this regard, power electronic converters, energy storage system, advanced control techniques, and energy management systems are relevant aspects to be taken into account in order to alleviate the existing issues.

The first issue is finding an appropriate topology for application of RES in large-scale power systems. Among different suggested topologies, multilevel inverters have shown growing interest in power system applications. One proposed multilevel configuration is a cascaded H-bridge multilevel VSC that is assembled by connecting multiple single-phase full-bridges or H-bridges in series. Using more IGBT switches and passive elements is not economical, however, inserting RES as the clean power sources makes the multilevel configuration very practical and util for large power systems. Each module could be controlled independently, and the modules can support output requirements all together.

The second issue is intermittent characteristics that exist in the nature of RES. Lack of natural energy leads to less power production by RES and therefore the requirements of the grid may not be satisfied. Hence, ESS must be inserted to back up the energy production or to save the available energy having been not requested by the demand. Among ESS, the electromechanical batteries are commonly used as they are more economically and environmentally friendly.

Another factor is the way of inserting ESS to the configuration. Using a DC-DC converter as a bridge for connecting ESS to the power system has been suggested more in the previous studies. However, it is not economical to add additional converter for every ESS. For this reason, instead of conventional multilevel inverter/converters, impedance-based sources, also called Z-source inverters (ZSIs), are receiving a great deal of attention because they provide interesting characteristics that make them suitable for RES applications combined with ESS. Using this network allows to insert ESS to the system without any connectors. The ESS can mitigate the intermittent nature of solar generation and make the PV installation able to operate even during the absence of sunlight for a certain period. Also, the ESS can smooth the PV and WT power outputs and contribute to voltage and frequency regulation. The use of different BES, combining different storage nominal and initial components, could have advantages for large hybrid penetration, covering a wide range of power and energy requirements.

The last important issue is that the use of ESS requires local controllers and also energy dispatching by a suitable supervisory control of the energy sources. From a broad perspective, studying the control systems for RES generation is important to achieve an efficient power conversion with energy storage and satisfy the power quality requirements. There are numerous control techniques. Among them, PI/PID controller is extensively found in the literature, but the need for more robust control systems leads to the use of intelligent control techniques. In this work, the aim is to design a control system based on advanced control techniques for different control variables, and the main goal is introducing proper EMS based on multi objective purposes such as the state of charge (SOC) of the BESS, efficiency of the BESS, voltage, or reactive power, among others, in order to improve the efficiency and operation of the energy sources.

This thesis studies of a hybrid power system combining quasi-Z source converter inverter (qZSI) technology, RES (WT and PV power plants) and BES to provide enhanced solutions for controlling the operating variables of energy sources (RES and BES). However, the integration of RES such as WT and PV in the main grid or connecting them to local loads requires precise actions and monitoring owing to the intermittency and fluctuation of these sources. Thus, it is necessary to find solutions by advanced control and operation techniques to maximize RES power utilization while maintaining the system reliability.

In the previous paragraphs, the expected relevance of intermittent renewable energy sources, particularly of WT and PV, in the electric power systems has been stressed. Furthermore, the availability of various battery storage systems, based on dissimilar operating principles, and different nominal operations, has been presented. As seen, there exist a vast number of alternatives regarding the technology, operation and topology of hybrid systems comprising wind and solar power generations supported by energy storage as an auxiliary source. Therefore, it is interesting to study these options to make reasonable and informed decisions in terms of these parameters.

The scenario described above advances the framework of this thesis. The main topology contribution of this work is the evaluation of diverse hybrid system configurations consisting of wind and PV power generations as the main power source, and electrochemical energy storage as an auxiliary element. Regarding the system topology, few studies have addressed the dynamics of AC microgrid with hybrid power plants, BES and an optimizer-EMS connected to the grid. In most studies, a DC/DC converter was used to implement the MPPT strategy for PV and WT power sources, and a VSI was commonly used for DC/AC conversion. The topology proposed herein is based on ES-qZS-CHBMLI, without an additional DC/DC converter. Moreover, all these previous papers have used a configuration of a power plant based on a BES-qZS-CHBMLI integrating the same PV systems and BESs into each module in series and integrating PV or WT sources with different nominal power in each module haven't been sought. Finally, the evaluation of grid performance in terms of active and reactive powers at the sight of the grid operator was neglected in these previous works. Regarding the EMS, the referred works have executed an EMS based on distributing the power among the BES according to their SOC, where the BES efficiency was overlooked because the EMS focused only on the SOC values and demanded power.

To cover the mentioned gaps of previous studies, this thesis studies a hybrid power plant based on a BES-qZS-CHBMLI but integrating hybrid RES (WT and PV systems, and not only PV power plants), and different BES (and not the same BES) into each module connected in series; while operator power requests are considered in controllers design and evaluated in experimental results. On top of that, the development of an optimal EMS is suggested to satisfy

the power demand while dispatching energy among the BES to optimize their efficiency. The alternatives were studied under various configurations, regarding the location of the ESS or the storage technology. Moreover, several control strategies have been designed and implemented on the modelled systems. The evaluation and comparison of the control strategies have also been carried out. The results obtained from the simulations completed have been discussed in the corresponding sections. These outcomes provided crucial information on the performance and adequacy of the configuration, storage device, or control strategy, under the operating conditions imposed on the simulations. From the observation of the results obtained, conclusions have been drawn in every analysis.

This thesis has been developed under the "**8215 – *Ingeniería Energética y Sostenible (Sustainable and Energy Engineering)***" Doctorate Programme of the **University of Cádiz**. This work has been carried out in the ***Sustainable and Renewable Electrical Technologies* (PAIDI-TEP023)** Research Group, led by Dr. Luis M. Fernández Ramírez, supervisor of this thesis. Furthermore, this work has been funded by the Regional Ministry of Economic Transformation, Industry, Knowledge and Universities of Junta de Andalucía under **Grant PY20_00317**. The University of Cádiz also funded a research stay at the **Chair of Power Electronics**, at Kiel University (Kiel, Germany), under the supervision of Prof. Marco Liserre (Chair Director) and Dr. Jun (Senior Lecturer), carried out during the research process of this thesis. As a result of the research works carried out during the progress of this thesis, **one** journal paper already published and another journal paper under review and **three** conference papers, all of them with blind peer-review process, have been published presenting the main advances and contributions. The journal paper has been published in scientific journals indexed in the *Science Citation Index Expanded* edition of the *Journal Citation Reports* (**JCR-SCIE**), and the proceedings of three of the conference papers have been published at the *IEEE Xplore Digital Library*.

The rest of this document is organised as follows. After this introduction, chapter 2 presents the objectives and hypotheses of the thesis. A thorough review of the backgrounds is carried out in chapter 3. The configurations under study are described in chapter 4. The proposed intelligent control and EMS systems are presented in chapter 5. The simulations and experimental results are shown and discussed in chapter 6. Finally, chapter 7 draws the main conclusions of the thesis, presents its main contributions, and proposes several future research works that can give continuity to this study.

CHAPTER TWO

CAPÍTULO DOS

2

2. Objectives and Hypotheses of the thesis

This section presents the main objectives of this work. Furthermore, the hypotheses to be evaluated throughout this study are stated.

2.1. Objectives of the thesis

The fundamental objective of this thesis is the study of the configuration, control, energy management and operation of a hybrid power plant integrating RES and BES into a configuration based on qZS-CHBMLIs, to generate new knowledge in the topic, and propose innovative solutions that favour its viability and contribute to its development. To fully comprehend the operation of such schemes, dynamic modelling and simulation are valuable tools to analyse their response under various working conditions. Taking this into account, the specific objectives of this thesis are:

• Determination of the hybrid power under study: Definition of the parameters and characteristics of the hybrid power plant under study.

The first step is finding a useful topology of multilevel inverters with hybrid RES sources and ESS. Besides that, PV and WT initializing parameters must be evaluated. Balancing RES output power with grid demand (summation of output power of modules with grid operator needs) is also important to have a stable condition. Defining appropriate ESSs type and their nominal parameters is another subtask. One of the contributions of this thesis is using BESs with different nominal and under study parameters.

• Dynamic modelling of the main components: Modelling of the elements of the hybrid power plant (PV power plants, WT, BES and qZS-CHBMLIs), and evaluation of their operation.

Designing model is a fundamental objective for further tasks. Implementing impedance network with suitable active and passive elements, displacement of ESS parallel with qZS, switching bridge type and modulation technique are studied.

• Design and evaluation of the control systems for the energy sources of the hybrid power plant.

Designing control systems for active and reactive powers, and voltage levels in the hybrid system is another objective. Parameters such as active and reactive power, as well as voltage at the DC link and the grid are of particular interest. These variables determine how the hybrid system interacts with the power system where it is connected. In order to achieve a satisfactory integration of these hybrid arrangements in larger networks, it is crucial to develop adequate control strategies for the previously stated magnitudes.

• Design of the supervisory control system for EMS considering different EMSs

Beyond all the mentioned-fundamental objectives, EMS is the main contribution of this thesis. For storing energy or supporting the RES with the BES, SOC and MPC as conventional EMSs methods, and optimization algorithms based on fmincon Matlab function, fuzzy logic, and machine learning algorithms like RL are exploited.

• Evaluation and comparison of the different solutions proposed in order to increase BESSs total efficiency.

Due to the distinctive performance of every EMS, it is interesting to evaluate and compare the response of efficiency attained by each EMS. This can be achieved by introducing different range of batteries output power. In other words, during designing EMS is appreciated to think about the amount of each ESS outpower and SOC values simultaneously (and not only SOC values).

• Developing and analysing experimental results by real time simulators.

The designs can be implemented, assessed, and validated experimentally in laboratory through an OPAL RT 4510 HIL system (a compact, extremely powerful HIL). Finding real time results assures the practical usage of the proposed topology and control algorithm.

• Analysing critically and comparing the configurations under study.

After the modelling and simulation stages, it is essential to undertake a thorough and critical observation of the results obtained. A correct interpretation allows drawing conclusions on the strengths and weaknesses of different topologies and/or storage devices to develop successfully certain applications.

2.2. Hypotheses of the thesis

Growing interest in using intelligent algorithms in different aspects of control systems is inevitable and power converters are no exceptions. Meanwhile, the integration of RES into the main grid is expected to yield more efficient and reliable systems, which will support the development and implementation of sophisticated converters for the interconnection between RES and grid. Therefore, it is crucial to design intelligent control algorithms for RES control and optimization and to execute all actions that can potentially improve the integration of multilevel inverters to hybrid power systems. In this regard, this thesis addresses the study of the hypotheses stated below:

• The incorporation of a grid connected CHBMLI with hybrid RES can improve the output power level, making that applicable for large-scale power systems.

The grid connection of large-scale RES can deal a great amount of demand. Taking advantage of energy diversity from nature, cascading the output levels attained by sources, and using ESS implies a more accurate balance between actual electricity production and a pre-established demand.

• Using qZSI into the CHBMLI improves output response and system efficiency and raise open/short circuit immunity. Moreover, ESS could be paralleled with impedance network which omits the need for a DC-DC converter.

Using cascaded modules in multilevel inverters, the integration of ESS through DC-DC converter imposes a huge number of moneys for investment market, especially when the

number of modules increases significantly. Hence, using qZSI is totally economically as the values of its passive elements are small.

• The incorporation of ESS will secure the generation during the lack of sun and wind energies. In other words, storing and producing energy by ESS covers intermittent characteristic of RES.

Coupled operation of ESSs and RES allows obtaining a controlled electric power output from the hybrid system. Regardless of the characteristics of the incoming PV irradiance and temperature and wind profile, sufficient power flows toward grid when ESS are used. Furthermore, unexpected fluctuations in both demand and generation can be smoothed through a proper control of the ESS.

• The proposed solution will allow the integration of hybrid RES (WT and PV systems, and not only PV power plants), and different BES (and not the same BESs) into each module connected in series.

In the configurations evaluated in this work, the interest in applying different sources and batteries parameters has been taken into account. Hence, each module has its own input source parameters and nominal batteries parameters that makes this topology more practical.

• The optimal EMSs to be developed will allow to satisfy the power demand while dispatching energy among the BESs to optimize their efficiency.

EMSs proposed in this thesis have multi functions. The proposed objective function introduces a term of efficiency in ESSs productions and limits the SOC values through the proposed constrains. Moreover, the EMSs have never forgotten their main task of satisfying grid operator requests.

• The use of intelligent algorithms and optimizers in the energy management of the system under study increases the energy efficiency, and well power tracking.

Saving potential energy or producing sufficient one is an important task that whatever the EMS acts better, more energy can be saved and therefore, the system efficiency increases greatly.

• The hybrid configurations considered allow managing the reactive power exchange with the grid. Apart from active power, the reactive power flows within the elements of the hybrid systems, and more importantly the exchange with the grid, are also observed.

To evaluate these hypotheses, the main components comprising the grid connected CHBMLI have been modelled and simulated through the Matlab/Simulink software and some of its toolboxes. Recent versions of Matlab/Simulink include an RL toolbox and a fmincon Matlab function allowing the implimintation of EMSs in Simulink. Several modifications and examples have been added on the RL detailed toolbox available in the SimPowerSystems library. The most relevant changes are targeted towards the agents' details.

To validate the Simulation results, OPAL RT 4510 HIL system is used that allows modelling and simulating in real-time the components of ESS, power converters and grids, and testing power electronics controllers in a wide range of applications.

Acknowledged models have also been used for the energy storage devices. Furthermore, data and technical features of commercially available equipment provided by manufacturers have been used when possible, in the design and sizing processes, in order to increase the accuracy of the ESS models and resemble the behaviour of actual devices.

At the end, simulations of various operating conditions have been carried out in the simulation software Matlab/Simulink. The hybrid systems modelled have been evaluated under irradiance changes, fluctuating wind speed, variable grid active and reactive power demands. Analysing the results obtained from these simulations allows highlighting the most significant differences among the configurations considered, thus illustrating the main benefits of each alternative according to the target application.

CHAPTER 3

CAPÍTULO TRES

3. Review of the background – State of the Art

Sustainable and environmentally friendly renewable energy sources (RES) and energy savings are gaining more penetration in power systems as clean alternatives [1]. In fact, around 70% of the new electricity generation units are projected to be low-carbon technologies, raising the total share of these sources to nearly 45% of the total generation in 2030 [2]. Inevitably, renewable sources have a key role to play here. For instance, estimations of a 4,000% and a 1,000% growth in the total final energy consumption share of solar PV and wind power respectively are reported in [3].

Nonetheless, the benefits of a higher participation of renewable energies transcend the climate indicators. Furthermore, it is frequently considered as a whole industry, with technological, economic, political and social implications added to the environmental benefits [4]. Such indirect effects of renewable energies are often studied thoroughly, and the figures are promising. Solar PV and wind manufacture and installation, as well as bioenergy feedstock harvesting and hydropower, are expected to be the main drivers of employment growth in RES sectors. This plan also estimates employment reduction and stabilization in the fossil fuels and nuclear sectors respectively, however obtaining a net increase in the global energy industry [5]. Fig. **3.1** shows the pressing needs and attractive opportunities driven by the ongoing energy transformation.

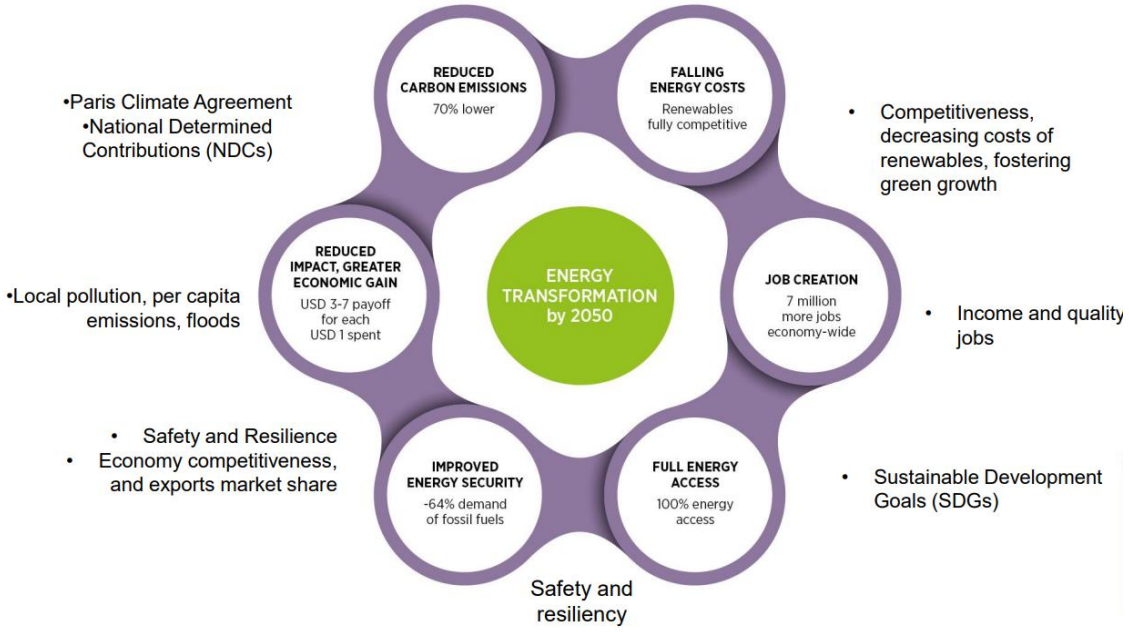

Fig. 3.1. Benefits of RES [6].

Fig. **3.2** presents international renewable energy agency (IRENA) costing database of 15,000 large scale RES power projects and 1.5 million rooftop PV systems covering half of all existing and planned RES capacity.

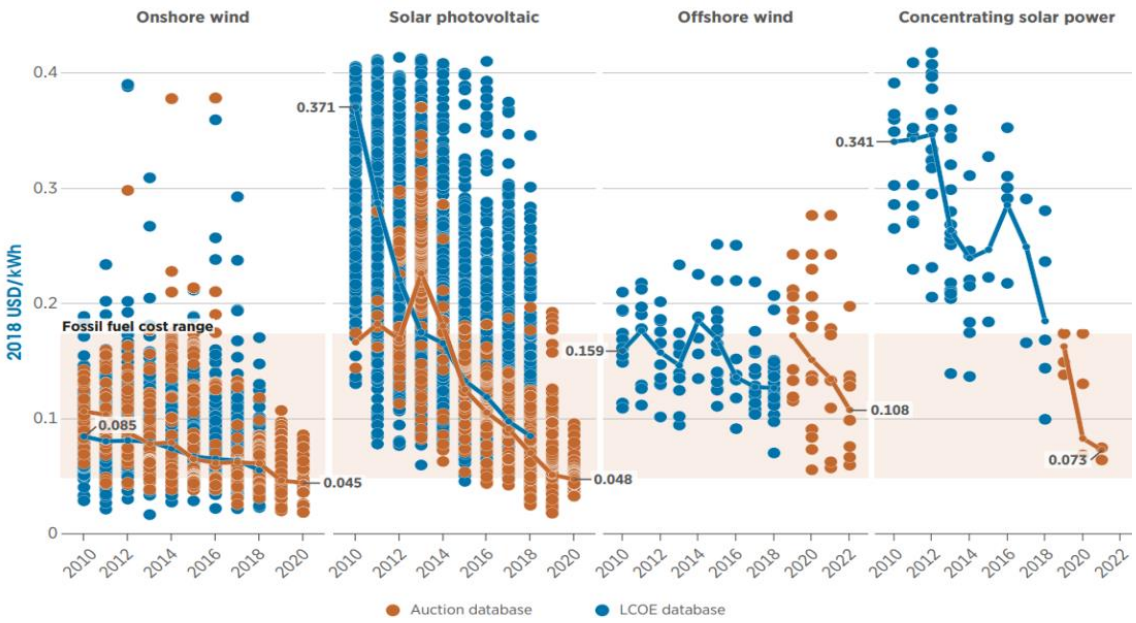

Fig. 3.2. Renewable power generation cost for the last 12 years [6].

Currently, wind turbine (WT) and photovoltaic (PV) systems are the most promising RES, because they provide a large unlimited volume of energy without emissions and other benefits such as global availability, high rate of technological development, no moving parts (in the case of PV generation), high reliability, no emissions, and more competitive costs with respect to other generating technologies [7-9]. However, the intermittent characteristics of these sources and their dependency on environmental conditions negatively affect consumer needs [10]. Therefore, to cover this stochastic nature of WT and PV sources, energy storage systems (ESS) are being applied to compensate the power demand that RES cannot satisfy or to store power not requested [11]. Fig. **3.3** provides that wind and solar PV would be prominent generation sources by 2050. Wind power supply would need to increase from 6% in 2018 to 35% of total electricity needs by 2050. It shows that recently wind power supply would need to increase from 6% to 35% of total electricity needs by 2050 and solar PV generation share would need to increase from 2% to 25% by the same year.

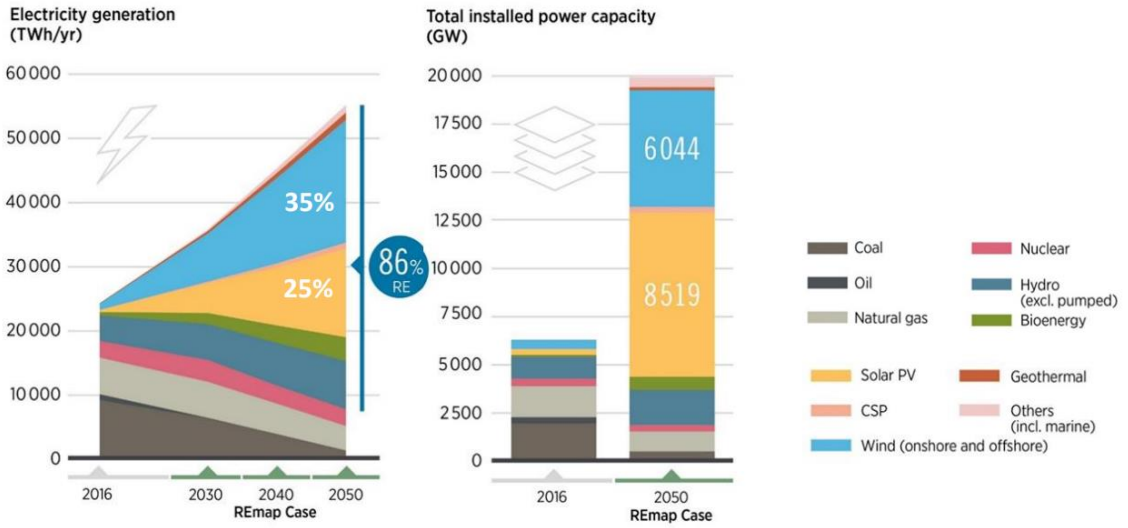

Fig. 3.3. Renewable power generation share by 2050 [6].

This section deals with a review of the most relevant research published in the field of hybrid power systems comprising WT, PV and ESS as a means of improving grid integration of RES. In this regard, WT, PV power sources, ESS technologies, high power converter topologies, and control algorithms and EMS applied for hybrid cascaded multilevel inverters will be discussed. It is divided in five subsections. First, the most applicable RES are discussed. Second, ESS types and applications are reviewed. Third, the use of RES in high power systems through high power converters are presented. Then, impedance network inverter types are reviewed and the application of them in hybrid RES is discussed. At the end, various energy management systems, control strategies and modulation techniques of cascaded multilevel qZSI hybrid RES based are reviewed are discussed in the literature, also examining their performance and principal characteristics.

3.1. PV panels technologies

Fig. 3.4 represents the share of each continent in solar PV capacity installations. Asia is poised to dominate the solar PV installations, with more than half of global installations by 2050, followed by North America (20%) and Europe (10%). Even though installed capacity may remain highest in Asia, North America and Europe, market growth seems likely to shift to other regions, with large markets also expected to emerge in South America and Africa.

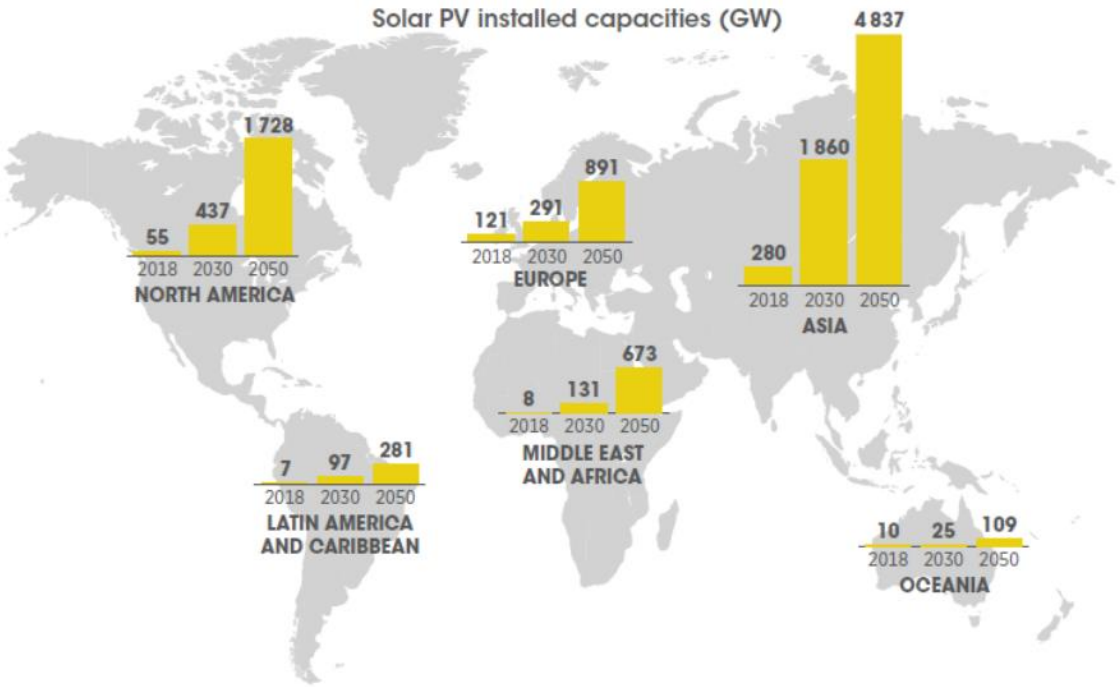

Fig. 3.4. Worldwide solar PV capacity installations [6].

In RES power system marketing the technology used in the manufacture of PV cells is a priority, since efficiency is a factor that influences the performance and the costs of the plant. In 2013, the highest efficiency of a cell reached 18.8% However, the maximum commercial efficiency is 15%, and the most frequently found values are in a range between 9% and 12% [12]. Nowadays, various materials are used to manufacture PV panels.

The most used material is silicon, due to its high efficiency and maturity [13] and the availability as the second most abundant raw material [14]. Practically, crystalline semiconductors of mono-crystalline silicon and GaAs have shown a better performance. Highly expensive, GaAs manufacturing and raw materials are mainly used in PV concentrators and in space technology, due to greater resistance to high temperatures and being lighter [8]. To make this technology more economical, poly-crystalline or amorphous organic and inorganic materials have been introduced as the examples of silicon-based but less pure materials called mono-crystalline silicon. The most commercialized one is poly-crystalline nowadays [15].

Another technology that has excellent potential due to its low weight, high flexibility, and low cost, is thin-film despite its low efficiency [16]. Amorphous silicon is the most popular technology compared to other materials like CIS, CIGS and CdS, CdTe, and despite being the most common and occupying the first position in the market among thin-film technology, it is more prone to degradation [13].

Polymer PV cells are another relatively new technology that are based on organic macromolecules derived from petrochemicals. Manufacturing is much cheaper, cells are lighter and less fragile, compared than mineral semiconductors cells. Their flexible nature makes them very suitable for integration into flexible materials or organic polymers or silicones, even textile fibres. However, it suffers of limited lifetime due to the degradation of polymers when exposed to sunlight [14,15, 17].

Other less popular PV technologies have also been introduced. Based on the combination of crystalline and non-crystalline silicon the hybrid solar cell has been introduced [12] that suffer of manufacturing complexity. The Graetzel solar cell, also known as a dye-sensitized solar cell, is a relatively new technology that is being studied as an alternative to problems of efficiency, cost, and environmental issues [18]. low-cost, very easy creating, semi-flexible, semi-transparent, or even totally transparent in those recently designed are the advantage of this technology. However, lower energy conversion efficiency compared than that of silicon-based, and wear of the electrolyte or the anode in use at certain environmental conditions are disadvantages of this technology [18].

Based on [19], crystalline silicon is the predominant material today and will continue for years. However, in the long term (2030 and beyond) silicon will be progressively reduced. For the authors, many technologies will coexist, and the efficiencies will be slightly different from today's values. Moreover, it is mentioned that these technologies can be divided into two types: (i) Cells with ultra-low-cost, with efficiencies varying from medium to low, highlighting the concept of dye-sensitized cells; and (ii) cells with ultra-high efficiency, highlighting the third generation in PV cells (such as the multijunction made of amorphous Silicon or Gallium Arsenide) [lais thesis]. Razykov et al. In reference [20] it is expected that thin-film photovoltaic technologies to play an important role in the future global PV market. It is stated that further research and development will be conducted to increase the effectiveness of Copper Indium Gallium Selenide (CIGS) thin films, CdTe, Si, and multijunction cells and nano PV devices.

3.2. Wind turbines

Nowadays, wind turbines play a crucial rule worldwide in electricity production and they are considered prominent options. According to different prospective scenarios, wind power

generation will be able to provide up to 18% of the global electricity demand by 2050, preventing up to 4.8 Gt of CO2 from being released to the atmosphere annually [20]. In its annual report for 2012, the IEA said that the global wind power capacity now operating in 100 countries can provide more than 3% of the world's electricity demand. Fig. **3.5** is worldwide wind capacity installations showing that Asia (mostly China, India, Iran) would largely drive the pace of wind capacity installations, with more than half of global installations by 2050, followed by North America (23%) and Europe (10%). For offshore wind, Asia would take the lead in the coming decades with more than 60% of global installations by 2050, followed by Europe (22%) and North America (16%). Another potentially a game-changing wind turbine technology is floating offshore that multiplies the global offshore wind potential covering 5-15% of global offshore capacities by 2050.

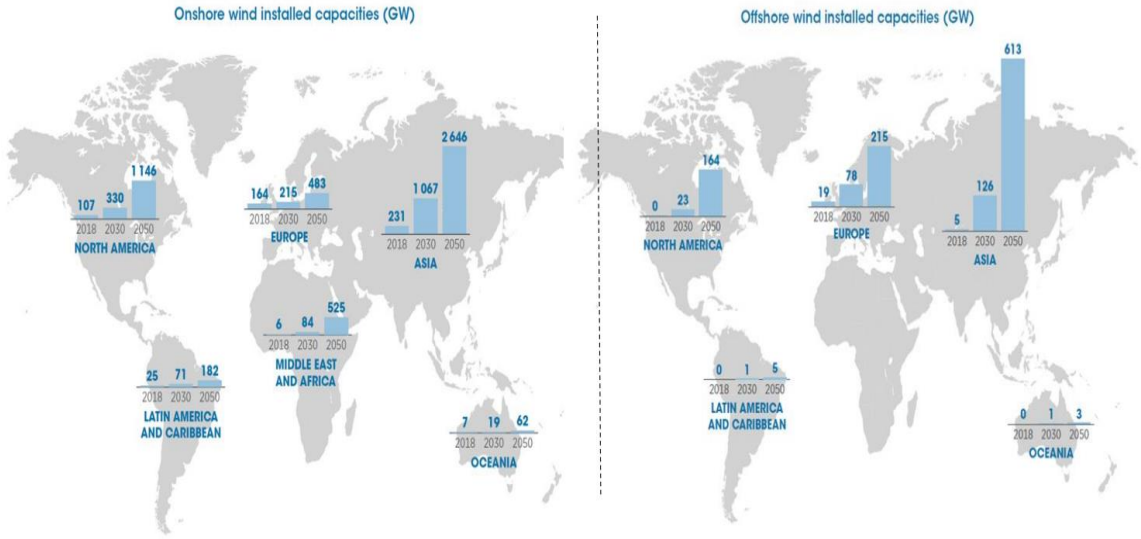

Fig. 3.5. Worldwide wind capacity installations [6].

There is a huge word wide effort to increase participation of WT in future power systems. It is expected to come true by 2030 to reach from 964 GW to 1,933 GW of wind power capacity and from 1,684 GW to 4,042 GW in 2050 [21].

The wind turbines are classified as Horizontal Axis Wind Turbine (HAWT) and Vertical Axis Wind Turbine (VAWT) [22]. The first used wind turbine was VAWT but researchers suggest that it can only be used economically for small wind projects like residential applications and HAWT can be used to generate bulk amount of electricity. Traditional windmills generally used to work on thrust principle, at that time they were employed for grinding grains and pumping water. In modern wind turbines, aerodynamic principle is adopted for rotating the blades. Aerodynamic structure of blades uses lifting force of air for rotation of prime mover. In olden days, wind turbines were used to work in constant speed irrespective of wind velocity. But these wind turbines suffer from mechanical stress due to high wind speed.

3.3. Energy storage technologies

Inserting energy storage system into Hybrid RES power plants allows the excess energy generated to be stored for a later use when necessary. Energy storage can help power grids withstand peak demand, allowing transmission and distribution grids to function efficiently. In

shorter periods, storage can be effective in smoothing short peaks and distortion in voltage [21]. ESS in electric power grids is inserted to fulfil power quality, bridging power, and energy management. To maintain the power quality, batteries must intervene rapidly to satisfy the reference parameters in a short time [23-25]. Switching from one generator to another takes several minutes that in this interval BESs have the duty of suppling power, this process is known as bridging power [25-27]. Energy management system that is the main contribution of this thesis, involves sorting or producing energy in various operational conditions.

Traditionally, grid operators were responsible for monitoring and operating electric power systems to maintain the power balance between consumption and generation instantaneously. Due to the fact that both sides can experience variations in time horizons ranging from seconds to days, seasons or years [28–31], this task is a certainly hard. Moreover, the operator rarely can modify the demand patterns. Beyond all, with a larger penetration of RES in the power systems, there is always uncertainty on the production side, which in turn arise new challenges for the grid operator to manage the intermittency and uncertainty of RES productions.

Nowadays, a wide variety of energy storages designed based on different physical principles that can be used in applications with renewable energies. Battery energy storages are more common in RES power system applications, especially in PV cases. In fact, ESS can develop several tasks in hybrid applications with renewable sources, such as load levelling and voltage or frequency regulation. Moreover, the ESS can manage the intermittency and fluctuations of the renewable generation, allowing a controlled output from a natural resource [32,33]. Each of these operations requires a particular behaviour of the ESS. Some demand a fast response with a short duration energy boost, while others need a long-term energy supply with little variation. Moreover, the ESS can combine with the main power source through different topologies, by using the power conversion technology available. Hence, it is worth mentioning and summarising the storage technologies suitable for the purpose of this thesis.

Currently, Energy storage technologies can be classified as electrical, electrochemical, chemical, thermal, and mechanical, which are based on various concepts and physical principles. The main features and performance of ESS is behind on physics of them, and a superiority comparison is not possible [34–36]. Electrochemical batteries are typically used as ESS because of their low cost and non–toxic materials [37].

Electrochemical batteries are based on chemical reactions and have the double function of storing and releasing electricity, alternating the charging and discharging phases, without noise or emissions [38]. There is a wide range of technologies used in the manufacture of these storages, such as lithium-ion, lead-acid, sodium-sulfur, nickel-cadmium, nickel-metal, nickel-iron, hydride, zinc-air, lithium–polymer, iron–air, etc. It has been noted that their main advantages are their high energy density and the maturity of some of these technologies. And their main drawback is the relatively low durability for high amplitude cycles [38]. According to [28], large-scale storage was rare until recently and some batteries contain toxic material, and therefore, the environmental impact of discarding these batteries must be considered. Based on [29] batteries that are potentially suitable or more practical for large-scale storage are lead-acid, nickel-cadmium, sodium-sulfur, sodium nickel chloride, and lithium-ion.

Lead-acid batteries are the oldest and the most frequently used rechargeable type that working based on lead dioxide (cathode) and lead (anode) chemical reactions and sulfuric acid that acts as an electrolyte [30]. Their advantages are highly energy-efficient (between 85 and

90%), easy-installing, low level of maintenance, and low investment cost [21]. Regarding the disadvantages, they provide competitive costs and relatively limited lifetime, low energy density, and can cause a large environmental impact [29].

In Nickel Cadmium batteries, nickel hydroxide is used in the positive electrode, while cadmium hydroxide is used in the negative. The electrolyte is an aqueous solution of potassium hydroxide with some lithium hydroxide. NiCd batteries have a high energy density (50-75 Wh/kg), robust reliability, and very low maintenance requirements, but a relatively short cycle life (2000-2500) [31]. The main disadvantages of these batteries are a relatively high cost due to the expensive manufacturing process, and the fact that cadmium is a toxic heavy metal, and therefore poses problems associated with the disposal of NiCd batteries [33]

In Lithium-ion (Li-ion) batteries, a pair of graphite (anode) and lithium metal oxide (cathode) plates filled with dissolved lithium salts in organic carbonates [28]. The main feathers of them are high energy density, cycle life and efficiency, very low self-discharging rate, with a maximum of 5% per month, and almost 1500 life cycles [39]. However, the battery life is highly depended on temperature that can be severely shortened by deep discharges. Other disadvantages are in the structure of them as they need a protection circuit to maintain safe operation of this fragile battery types. The protection circuit is built into each battery pack to limit the maximum cell charge voltage and prevent the cell voltage from shrinking discharges [21].

Sodium sulphur batteries compose of a positive-negative molten sulphur- sodium electrode that are separated by a sodium beta-alumina ceramic electrolyte [40]. A high temperature, typically in the range of 300-350 ºC, are used to keep sulphur and sodium in a liquid state [41]. This battery type for a full depth of discharge (DOD) has an expected 2.500 cycles operational duration of 15 years. The energy density is higher than the lead-acid battery. Beyond that, except sodium, this battery type is 98% material-recycling [42].

Vanadium redox flow batteries are using redox technology that offer significant advantages, such as the absence of self-discharge and degradation for deep discharge [21]. Depends on the number of cells in a battery stack the power is rated, while the energy is a function of the volume of electrolyte stored in the tanks. It offers a high energy density (compared to lead-acid batteries) and long life. The variety of the application of this battery type like applications in electric utilities and industrial end-users makes them valuable in marketing as well as almost 85% cell efficiency [28] that is considered high.

Metal-air batteries, usually composed of aluminium or zinc, are a promising and the cheaper technology in comparison to other technology types [28]. The lithium-air battery has received more interests among the various metal-air batteries. These batteries have shown a limited operating temperature range during different tests [21]. Needless to say, that high reactivity of lithium with humidity and air can cause a fire, which is a high safety risk. Additionally, low life cycle for these batteries has been reported [43].

Based on the competence application of BES, some features can be reviewed. A brief review of the most relevant characteristics and typical values is presented in Table **3.1** produced with data obtained from [44].

Table 3.1. BES features and typical values [44].

	Pb-ac	Li-ion (MWh)	NaS	Redox-flow	Metal-air
Power rating (MW)	<40	0.01 – 0.1 1 – 100 (demo)	0.05 – 34	0.03 – 3	<0.01
Storage capacity	<40	0.02 – 10	0.4 – 250	2 – 60	
Discharge time	s – h	m – h	s – h	s – 10 h	s – +24 h
Response time	Fast (ms)	Fast (ms)	Fast (ms)	Very fast	
Storage duration	m – da	m – da	s – h	h – mo	h – mo
Power density (W/kg)	75 – 300	50 – 2,000	90 – 230	<170	
Energy density (Wh/kg)	25 – 50	75 – 350	100 – 250	10 – 50	150 – 3,000
Efficiency (%)	65 – 90	75 – 99	70 – 90	60 – 85	<50
Lifetime (years)	5 – 15	5 – 15	10 – 20	5 – 20	5 – 20
Cycle life (10^3)	0.2 – 2	1 – 20	2.5 – 4.5	10 – 13	0.1 – 0.3
Self-discharge (%/day)	0.1 – 0.3	0.1 – 5	20	small	very small
Capital cost (€/kW)	2,100	2,500	2,250	1,400	1,400
Capital cost (€/kWh)	450	550	350	300	275
Maturity	Mature	Demonstration	Commercial	Demonstration	Demonstration
Environmental impact	Negative	Negative	Negative	Negative	Small

(A) **Power rating:** The nominal amount of MW discharging or charging power that a storage device can have.

(B) **Storage capacity:** The amount of available energy in the ESS after a complete charge cycle [47].

(C) **Discharge time:** The range of time that the ESS can keep releasing energy continuously. They are considered as a long-term storage or short-term technologies.

(D) **Response time:** The needed time for an ESS to start sorting or releasing energy on demand [47,84]. For the electrochemical batteries milliseconds respond time is considered to rapidly changes on the energy demand.

(E) **Efficiency:** The electric energy output-input ratio during a complete charge and discharge cycle. This term for batteries is around 90% of the inputted energy and batteries are considered as high efficiencies technologies. This term is evaluated in this thesis for different EMS and compared in varies control algorithms to find the way of increasing that.

(F) **Lifetime:** The expected time in years that each ESS can remain in operation. For batteries it can be almost a decade.

As it has been previously stated, due to the intermittent and uncontrollable nature of RES, a large penetration of PV and WT sources into electric power systems might introduce stability, reliability and power quality issues that threaten the proper operation of the grid, other suppliers and consumers.

3.4. High voltage converter technologies

The energy produced by the RES is always in fluctuation and converting it to an appropriate AC voltage and frequency power is crucial. The interface between the sources and stand-alone load or grid is fulfilled by using power converters to transfer reliable and efficient energy toward the consumer side [45]. A converter is considered as a desirable bridge if the factors such as good regulation of the output voltage and frequency, high efficiency and reliability, protection against short circuits, and safety are fulfilled [46]. DC-AC converters, called inverters, has the duty to provide an alternating current with identical features like frequency of grid network that is being connected. Current-source inverter (CSI) and Voltage-source inverter (VSI) by two-level have been applied for energy conversion in industry, however its usage is limited in high-voltage, high-power systems by switching ranges due to semiconductor manufacturing technology of silicon carbide or gallium nitride [47, 48]. Hence, other inverter topologies have been suggested and in the following are reviewed.

3.4.1. High voltage source converters

3.4.1.1. *Series/parallel-connected switch cells*

Connected switch cells and multilevel converters have been introduced for high-power applications to take advantage of fulfilling synthesized output voltage level and improving harmonic performance. In [49] series/parallel-connected switch cells have been proposed for high-voltage, high-power converters. Fig. **3.6** shows a schematic diagram of an n-module VSC by *n* identical two-level VSC modules are connected in series and parallel, respectively, at their AC and DC ports. In the AC-side to achieve the desired voltage level and waveform, corresponding open-winding transformers are used. The modularity feature of this inverter type that reduces manufacturing costs, facilitates maintenance, and permits provisions for spare parts makes them a desired topology [50].

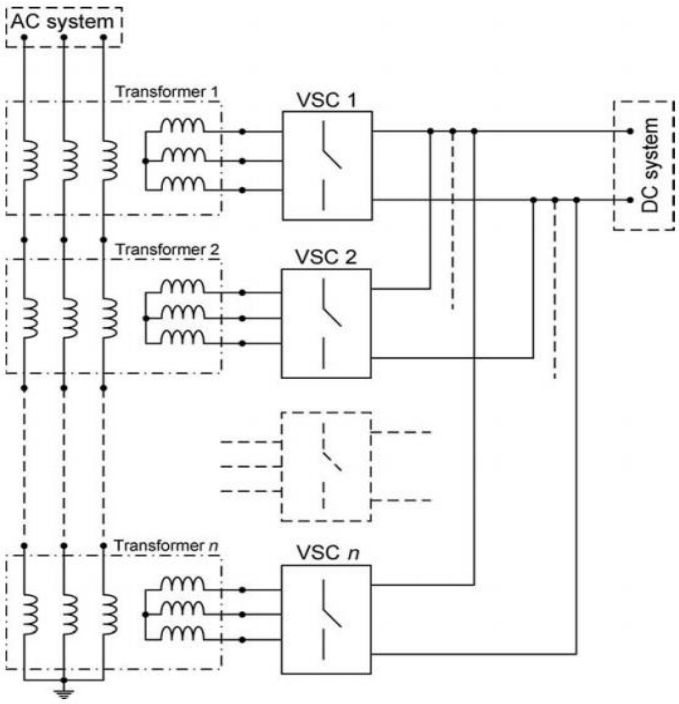

Fig. 3.6. Schematic diagram of multimode VSC composed of n two-level VSC modules [50].

Also, an alternative configuration has been suggested that VSC modules are connected in series at both the AC and DC sides. However, because of various practical limitations, the number of series-connected switch cells is limited and cannot be constructed for any voltage level.

3.4.1.2. *Cascaded (H-bridge) multilevel voltage source converters.*

Multilevel configurations have been introduced as another option for high-power application system to accommodate their voltage requirements [51]. One proposed multilevel configuration is a cascaded H-bridge multilevel VSI that is assembled by connecting multiple single-phase full-bridges or H-bridges in series. Fig. **3.7** shows the topology of this converter type. The necessity of multiple isolated DC sources in each module makes this topology expensive (if RES is not used), while it is attractive for reactive-power exchange, as in static synchronous compensator (STATCOM) applications. Furthermore, to achieve the desired voltage level, corresponding open-winding transformers are used in the AC-side connection.

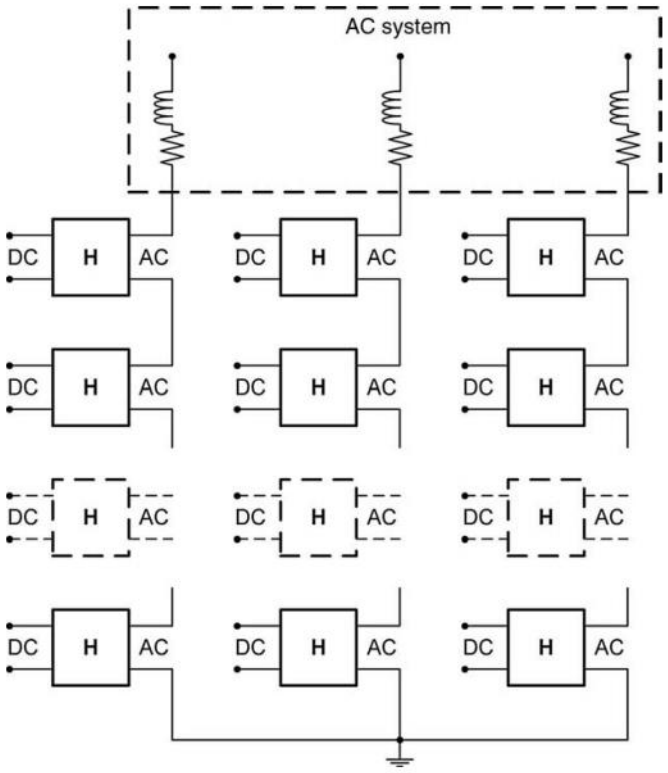

Fig. 3.7. Schematic diagram of a wye-connected, H-bridge-based, multilevel VSC [50].

3.4.1.3. *Capacitor -clamped multilevel voltage source converters.*

Another class of multilevel converters is the capacitor-clamped multilevel VSC that also is known as flying capacitor multilevel VSC (FC-VSC) [52]. Fig. **3.8** illustrates the topology of this converter type. Dispatching voltage is reached by floating additional capacitors, not clamped diode. The gap among two capacitors corresponds to the nominal voltage of the devices, defines capacitors voltages.

This converter type has not been used widely in practice as a large number of relatively large-size capacitors must be used, and therefore, the regulation of the capacitor voltages is challenging.

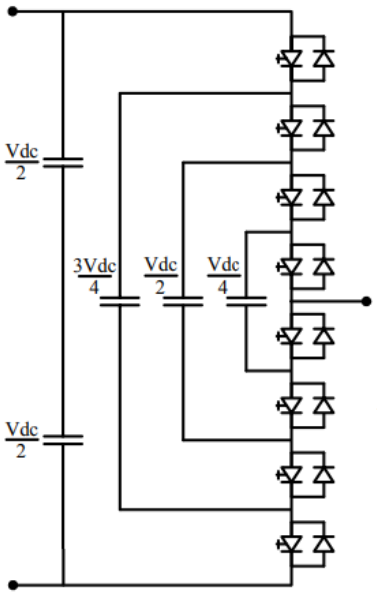

Fig. 3.8. One-leg five level capacitor-clamped multilevel VSC [53].

3.4.1.4. *Diode-clamped multilevel voltage source inverters.*

To avoid the drawbacks of the aforementioned multilevel converter class, a diode clamped multilevel VSI has been realized for different voltage levels [54]. **Fig. 3.9** shows a conceptual diagram of an n-level Diode-clamped multilevel converter in which the AC side consists of legs represented by a fictitious n-tuple-through switch, and the DC bus consists of n − 1 nominally identical capacitors C1 to Cn−1. In this topology dynamic and static overvoltage for switching devices is limited using clamping diodes connected in series. Different voltage levels are generated for output voltage in the ranging between half value of positive and negative of V_{DC}. Hence, it becomes necessary to consider several diodes in series to find the required voltage. In contrast to main devices, the nominal voltage of the clamping diodes is higher than the voltage of one level. The number of clamping diodes is increased based on the level number of inverter legs if rated voltage of a clamping diode equals rate voltage of the main switching devices. Although this inverter offers lower switching losses and stress and a less distorted synthesized AC voltage, it requires a multimodule structure for high- voltage applications and the number of levels should be limited to seven or nine levels maximum. Moreover, in practice, more diodes are needed that makes more practical problems such as parasitic inductances or package difficulties [55].

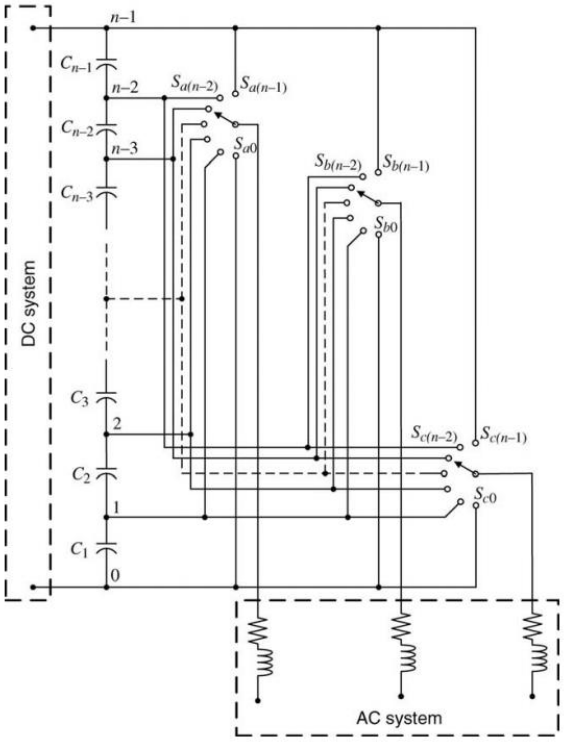

Fig. 3.9. Conceptual representation of an n-level diode-clamped multilevel VSC [55].

3.4.2. High voltage impedance source multilevel converters.

For the mentioned cons of conventional multilevel inverter/converters, impedance-based sources, also called Z-source inverters (ZSIs), are receiving a great deal of attention because they provide interesting characteristics that make them suitable for RES applications combined with ESS [56] , [57,58]. It takes advantage of an impedance network in the input of inverter for voltage balancing. The impedance network has passive and active elements makes it capable for this purpose. Offering a shoot-through (ST) state during the zero-state interval makes this inverter type capable of boosting the input voltage, which improves inverter reliability and enlarges its application fields. To improve some characteristics of the usual impedance inverter, many configurations have been suggested such as: high-performance improved ZSI (HP-IZSI) [59], Quasi-resonant soft-switching Z-source inverter (QRSSZSI) [60], neutral point ZSI (NPZSI) [61].

The quasi-ZSI (qZSI) has been suggested as a topology modification that could be used for energy conversion purposes in multilevel cascaded structures [62]. Several qZSIs can be arranged to build a cascaded H-bridge multilevel inverter (CHBMLI) and easily scaled by adding more cascaded modules without the need for a voltage transformer at the inverter output. In this case, the output filter is smaller than that of other multilevel configurations [63]. Fig. **3.10** illustrates the n-layer of the (a) ZSI-CHBMLI (b) qZSI-CHBMLI for grid connected PV power applications.

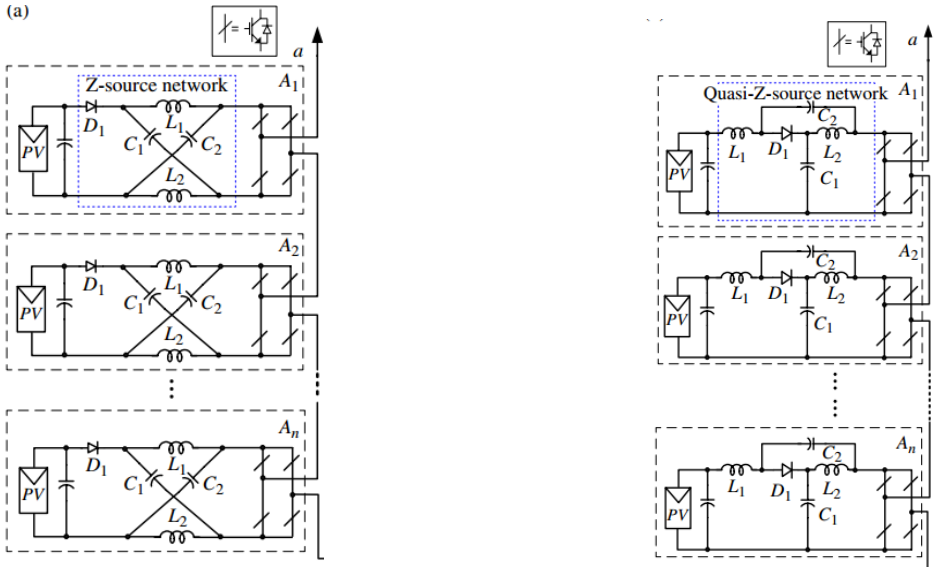

Fig. 3.10. Topology of n-layer grid-tie PV system (a) ZS-CMI based (b) qZS-CMI based [64].

The qZSI-CHBMLI balances the dc-link peak voltage in each module to achieves voltage step-up/down function during dc to ac single-stage power conversion. Hence, the distributed maximum power point tracking (MPPT) is achieved independently in each module. Moreover, due to allowing shoot-through states, the system shows high reliability and low cost due to saving one-third of the modules when compared to conventional multilevel converters [65].

Independent dc-link peak voltage controls of all modules, modulation type, MPPT algorithm based on ST duty cycle, grid-tie power control are basements of designing the qZSI-CHBMLI based grid-tie PV system. Not many, some works have executed in these four control parts. In [65] the qZS-CMI' advantages over the conventional CMI in terms of reliability, cost, and efficiency have been studied when applied to MW-scale PV power systems. For PV applications, [66] worked on efficiency evaluation of GaN switches-based qZSI-CHBMLI. References [67-69, 64] suggested control methods for both single-phase and three-phase qZSI-CHBMLI based PV power system. If ESS is used in this configuration, an appropriate EMS is necessary to dispatch power between storages. In the following the control and modulation techniques used for qZSI-CHBMLI are reviewed.

3.4.2.1. *Dc-link peak voltage controls.*

For each module in each phase the dc-link peak voltage control must be included. Dc-link voltage vary between zero and the peak value, but the peak voltage value of DC-link must be controlled in a constant value. In [56] suggested a proportional (P) regulator of the inductor current closed loop and a PI regulator of dc-link peak voltage closed loop employed to ensure zero-error tracking and improve the dynamic response, respectively. The shoot-through duty cycle and voltage of capacitor C_1 used to calculate the actual dc-link peak voltage. To achieve the balanced dc-link voltage in three phases, the dc-link peak voltages of all modules set to the same desired value.

Independently control scheme was suggested in [70] for a three layers qZSI-CHBMLI system. The peak voltage value of DC-link was made of the sum of V_{C1} and V_{C2} of impedance

network. Hence, V_{C1} and V_{C2} were added together to produce the peak value. In this paper, the output power reference was adjusted by a PI controller to build the peak value. The output power reference was different according to each PV string output power.

3.4.2.2. *Power control.*

The grid-tie current control to reach demanded power level is another issue to be considered in designing qZSI-CHBMLI. All the studies have the same idea of using two-phase stationary αβ frame through two-phase transformation, that can be fulfilled through sensing the phase angle of grid voltage by the phase-lock loop (PLL) ensuring unity power factor operation. Reference [56] came with a bright idea for three-phase model in which the grid-tie current peak value references are the outputs of the total PV voltage controllers. A proportional and resonant (PR) regulator was used in grid-tie current control to track the zero-error sinusoidal references.

In [71] controlling active and reactive powers were sought in a three-level neutral-point-clamped qZSI-CHBMLI topology connected to a single-phase grid. Two paralleled control loops were used that were regulated by PI controllers: the internal control loops for adjusting the amplitude of the reference signal and the external control loops for adjusting the phase of the reference signal. The internal control loop regulates the error of the d component of the grid current by acting over d and q component of the inverter reference voltage. The external control loop regulates the error of the q component of the grid current and acts just over q component of the inverter reference voltage.

In [70] qZSI-CHBMLI topology with three modules connected to a single-phase grid, the sum of each PV string output power defined the total power injected to the grid. The grid-injected current drawing from each module is the same as the modules are in the series connection. As each module provides different power level, references [72,73] introduced a proportionality factor calculated by sharing each module power per total output power. The grid-tie current closed-loop control is fulfilled in the mentioned papers and give the idea in this work to design appropriate controllers.

3.4.2.3. *MPPT techniques.*

To maximizes power output from RES various MPPT techniques are presented till date. In this part the perturb and observe (P&O) and fuzzy logic control algorithms are briefly reviewed.

P&O MPPT is widely used in wind and solar energy systems based on perturbing a control parameter in small step-size and observing the changes in a target function, until the slope becomes zero [22]. In the other words, a mathematical optimization function is used to search for the local maximum points of the function to get the optimal operating point that maximizes the extracted energy. If the operating point is to the left of the peak point, the controller must move the operating point to the right to be closer for the maximum point, and vice versa.

In [74,75] author proposed flow chart of Perturb & Observe to find reference power and speed in WT systems connecting to constant load. In [76] experimental test on P&O for PMSG WT suggested for a variable load. Where, based on the deviation of generator voltage per power, the operating point executed to shift towards its MPP (toward or reverses perturbation direction).

In [77], P&O algorithm were proposed for a hybrid system comprising of wind, solar and fuel cell. [78] suggested an adaptive P&O to reduce the effect of mechanical stress on generator caused by unwanted torque. P&O step size was replaced by a ramp signal and the MPP on the curve was tracked by using the normal flow of P&O. [79-82] suggested P&O algorithm for wind turbine maximum power extraction based on different generator parameters.

For WT applications, conventional analytical methods can be used to reach the appropriate blade pitch angle for above rated wind speeds [83] but using actual formulas and practical results needs linear approximations that are unrealistic assumptions. A common pitch angle control method for variable speed WT is to use rotor speed as a function of wind speed. However, rotor speed, torque, and system dynamic vary with changes in the wind pattern, and this dependence is problematic. So, other controllers like PI, sliding mode, adaptive and robust controllers have been implemented to reduce this sensitivity [84,85]. The linear PI with fixed gains covers only a specific range of operating points [86]. Most of the sliding mode control methods increase the chattering phenomena and putting high mechanical stress on WT system [87]. Adaptive controllers have difficult tuning based on linearized model at specific operating points and in robust controllers, controller operation changes constantly. For the mentioned drawbacks of classical controllers, intelligent pitch control methods capable of getting arbitrary non-linear relationship between the input and output, have become more appealing in recent years [88-90].

Among these methods, fuzzy logic because of the simplicity and effectiveness has become more known and used [91]. Fuzzy logic is an effective way to control WTs pitch angle due to the capacity of being planned for every moment and designed despite the lack of system information. In [92] mechanical power variations and their derivatives were added with wind speed factor as fuzzy inputs. For omitting the needs of wind speed data and anemometer, a fuzzy pitch controller was designed in [93] for a permanent magnet synchronous generator WT with the replacement of rotor speed for wind speed in the controller input. Mechanical power, the derivative of mechanical power, and rotor speed were considered as inputs of fuzzy systems. In fuzzy control, parameters fix in their terms, which is the main drawback of such type controllers. Continuous and sudden changes in the wind speed makes the fuzzy controller dependent on learning methods or an online optimizer. A fuzzy-neural controller was used in [94] to adjust the angle between the incoming wind direction and chord line of the blades. The main advantage of this approach is that, in the case of new changes, the fuzzy-neural adaptive networks can obtain new learning methods and adapt themselves to the new data. This controller achieved a more reliable performance in the response of rotor speed and generator output power. A pitch angle control strategy based on the actor-critic RL algorithm for a WT was proposed in [95]. The effectiveness of the RL on tracking the pitch angle proved its online performance, however, the radial basis function (RBF) neural network, which was used to process continuous input and output space, was not satisfied for such complex system. A neural network based on MLP and RBF was applied in [96] for controlling the blade angle. The angular velocity and generator output power were limited subject to different wind conditions. It was observed that the performance of the controller caused magnetic fluctuations in low frequencies under rapid wind changes. An ANFIS control algorithm was proposed in [97] to estimate the WT power coefficient as a function of tip-speed ratio and pitch angle. However, there exist nonlinear modes in WT system that ANFIS is not capable to orient itself with uncertainties. An interval fuzzy type 2 controller was suggested in [98] for blade pitch angle control, where the dependency of the controller on human experience is inevitable.

3.4.2.4. *Modulation techniques.*

For qZSI topology, several modulation strategies based on pulse width modulation (PWM) have been used for the control of the duty ratio. Typical modulation techniques applied to the qZSI are the simple boost control (SBC) [99], the maximum boost control (MBC) [100], the maximum constant boost control (MCBC) [101], and the ZSVM. According to the switching pattern, several options appear for the latter, such as ZSVM6, ZSVM4, ZSVM2, and ZSVM1. These ZSVM techniques are described in detail in [102].

Regarding modulation technics for qZS-CHBMLI, three types of techniques have been suggested in papers. 1) phase-shifted PWM (PS-PWM) were suggested in [67] got the idea from conventional CMI, 2) phase-shifted pulse-width-amplitude modulation has been suggested in [103] to reduce the switching number and loss PS-PWAM (PS-PWAM), and 3) modular multilevel space vector modulation (MM-SVM) has been suggested in [104] for a 3-phase system to enhance the voltage utilization ratio and simplify the modulation implementation. These modulation techniques were implemented for PV application in a three layers multilevel inverter.

3.4.2.5. *Energy management systems.*

qZS-CHBMLIs have been applied to PV power plants in [105-107]. qZS-CHBMLI integrating an ESS, mainly BES (BES-qZS-CHBMLI), is an interesting option for PV power plants, because it cannot operate at night without PV power input. Integration of ESS into the impedance network of a qZS-CHBMLI eliminates the need for a DC-DC converter to connect and operate the ESS [108], allowing the support of the PV power plant.

However, the use of ESS for supporting renewable energy sources or storing produced renewable energy requires an appropriate energy management system (EMS) to achieve the proper operation of the entire system. A 24-hours energy management algorithm for a BES-qZS-CHBMLI with PV systems was proposed in [109] to share the power among BESs covering the difference between the generation and consumption according to the state-of-charge (SOC) of each BES. The same EMS for PV systems and BES integrated into a BES-qZS-CHBMLI was used in [110,111] to balance the BES SOCs of all modules, independently of the variations in the irradiances. This control strategy ensured the safe operation of all BESs with the same SOC, while tracking the grid power reference. Another EMS based on distributing the power depending on the BES SOC for a BES-qZS-CHBMLI with PV systems was suggested in [112]. The proposed EMS was based on limiting the SOCs between the minimum and maximum safety values and dispatching the maximum charge or discharge power to its nominal power. In [113], an EMS based on model predictive control (MPC) was applied for a BES-qZS-CHBMLI with PV systems. The proposed EMS, where less computational effort was needed in the design of the MPC, achieved to mitigate the double line-frequency ripple in the BES current.

CHAPTER FOUR

CAPÍTULO CUATRO

4

4. Description of the configurations under study

In this section, the configuration of the hybrid power plant with cascaded modules consisting of WT and PV power sources, ESS, and impedance network have been analysed and were modelled using FAST tools, Matlab/Simulink, and OPAL-RT4510 real time simulator. Various scenarios are considered to evaluate all aspect of the control and system performances. All the configurations considered are reviewed, providing a concise vision of their most relevant features.

4.1. Modelling of the RES

This subsection describes the modelling of RES used as the sources of the cascaded modules connected to the grid by impedance-base multilevel inverter, and the single WT source model used to feed the requested power by grid.

4.1.1. Wind turbine.

In this work, the wind power generator is modelled as in [114] when proposing the new pitch angle controller, and is modelled as a source function based on wind speed in hybrid cascaded application. The practical application of the proposed pitch controller in the next chapter, is evaluated by using FAST8 for a real experimental 600 kW WT equipped with a synchronous generator with a full-size power converter (Controls Advanced Research Turbine, CART3, located at National Renewable Energy Laboratory, NREL). The CART3 is a conventional three-bladed upwind variable-speed variable blade-pitch-to-feather-controlled WT. This WT is modelled using a two-mass model and a validated aero-elastic simulator called FAST8 (Fatigue, Aerodynamics, Structures, and Turbulence) [115]. FAST8 tool allows to implement an accurate model of the WT in different aero-dynamical and environmental conditions.

Regarding cascaded modules of RES consisting WT source, the WT modelled by the SimPowerSystems library [116], and it has been modified in order to allow the connection and control of the ESS in the corresponding hybrid systems.

WT is usually represented by mathematical models. In transient stability studies, the two-mass model is usually used for modelling the connection between the mechanical and electrical systems of WT. In this model, the control algorithm for generator torque in below rated region is expressed as follows [117]:

$$T \quad = K\omega^2 = \frac{0.5\rho\pi R^5 C_P(\lambda,\beta)}{\lambda^3} \times \omega^2 \tag{4.1}$$

where ρ is the air density (kg/m^3), *R* is the radius of rotor (m), $\lambda$is the tip speed ratio, $\omega$is the rotor speed, C_p is the power coefficient, and β is the blade pitch angle.

$$C_p(\lambda,\beta) = 0.22(\frac{116}{\lambda_i} - 0.4\beta \quad - 5)e^{-\frac{12.5}{\lambda_i}} \tag{4.2}$$

$$\lambda_i = (\frac{1}{\lambda+0.08\beta} - \frac{0.035}{\beta^3+1})^{-1} \tag{4.3}$$

$$\lambda = \frac{\omega R}{v_\omega} \tag{4.4}$$

In this thesis, v_ω is the wind speed and the power coefficient is expressed by the following equation [118]:

As can be seen in Fig. 4.1, there are different operating regions in a variable speed WT. In Region 2, the blade pitch angle is kept constant at zero to maximize the power extracted from the wind, and the generator torque control is used to vary the turbine rotational speed to maintain the optimal tip speed ratio (corresponding to the maximum power coefficient), and thus, maximize the energy capture.

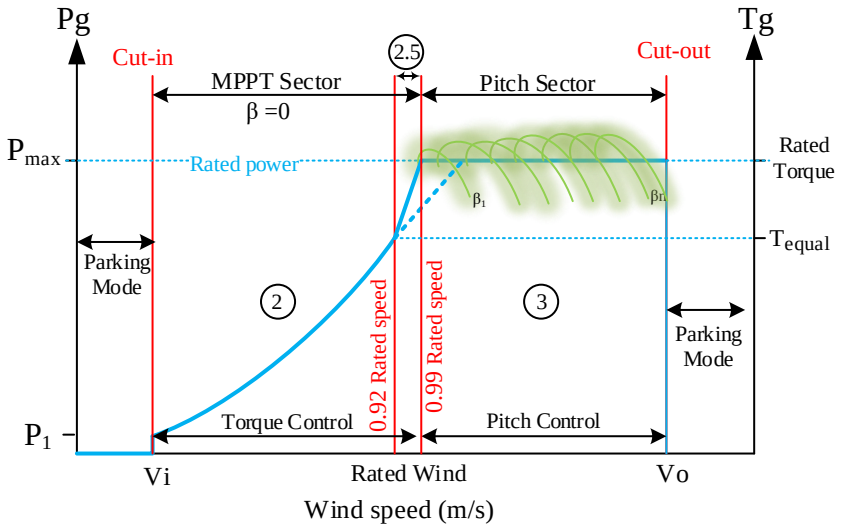

Fig. 4.1. Operating regions of a variable speed WT.

Considering equation (4.4), it can be seen that in certain wind speed, there is just a unique rotational speed that causes the maximum power point tracking (MPPT) in region 2. Using the derivative of the (2), the extreme points of C_p as a function of λ can be found [119]:

$$\lambda_{OPT} = \left(\frac{14.28 + 0.4\beta}{116} + \frac{0.035}{\beta^3}\right)^{-1} - 0.8\beta \tag{4.5}$$

Using equation (4.5), the ratio between the blade tip speed and the wind speed can be obtained for different β. For input to the simulation code FAST, ω must be in units rpm and the generator torque on the HSS side of the gearbox. Therefore, the torque gain K in equation (4.1) must then be multiplied by considering the effect of gearbox as below:

$$K_{NEW} = K \times \frac{1}{N_{gear}^3}\left(\frac{\pi}{30}\right)^2 \tag{4.6}$$

where N_{gear} is the high-speed to low-speed gearbox ratio. In region denoted as 2.5 in Fig. 4.1 it is assued that the torque vary linearly with the rotor speed from Region 2 to Region 3, where the rated torque is achieved at the rated rotor speed. The torque control in different regions is discussed in [120], which, its equation is wraped up in equation (4.7) and used in this simulation part of this thesis.

$$T_g = \begin{cases} 0 & (\omega_{\text{hss}} < 10 \times N_{gear}) \quad region\ 1 \\ \dfrac{K}{N_{gear}^3}\left(\omega_{hss} \times \dfrac{\pi}{30}\right)^2 & region\ 2 \\ (\text{T}_{\text{gmax}}/(\omega_{\text{rate}} \times 0.05)) \times (\omega_{\text{hss}} - \omega_{\text{rate}} \times 0.92) & region\ 2.5 \\ T_{g\,\max} & (T_g > T_{g\,\max}\ \&\ \omega_{\text{hss}} > 0.99 \times \omega_{\text{rate}}) \quad region\ 3 \end{cases} \tag{4.7}$$

where ω_{hss} is the high-speed shaft rotational speed and the constant values are defined by NREL [120].

For designing WT model in Simulink in the cascaded modules of RES consisting of WT source, a simple model is considered to reduce the simulation complexity and time. The out power of the WT model is found by:

$$P_{WT} = \frac{1}{2} \cdot \rho \cdot A \cdot C_p(\lambda, \theta) \cdot v^3 \tag{4.8}$$

Regardless of the generator type, in this simulation part, the mechanical torque developed by the wind turbine is obtained dividing the mechanical power P_{WT} by the rotating speed of the wind turbine.

The electrical equations, expressed in the direct-quadrature (*dq*) reference frame rotating at synchronous speed ω_s, are given by equations (4.9) -(4.12), where *u* denotes voltage, *i* denotes current, φ represents magnetic flux, *R* denotes resistance and *L* inductance, indexes *d* and *q* stand for the direct and quadrature components, and indexes *s* and *r* refer to stator and rotor respectively.

$$u_{ds} = R_s \cdot i_{ds} + \frac{d}{dt}\varphi_{ds} - \omega_s \cdot \varphi_{qs} \tag{4.9}$$

$$u_{qs} = R_s \cdot i_{qs} + \frac{d}{dt}\varphi_{qs} + \omega_s \cdot \varphi_{ds} \tag{4.10}$$

$$u_{dr} = R_r \cdot i_{dr} + \frac{d}{dt}\varphi_{dr} - (\omega_s - \omega_r) \cdot \varphi_{qr} \tag{4.11}$$

$$u_{qr} = R_r \cdot i_{qr} + \frac{d}{dt}\varphi_{qr} + (\omega_s - \omega_r) \cdot \varphi_{dr} \tag{4.12}$$

The flux linkages are expressed as in equations (4.13) -(4.16), where index *m* denotes magnetizing.

$$\varphi_{ds} = L_s \cdot i_{ds} + L_m \cdot i_{dr} \tag{4.13}$$

$$\varphi_{qs} = L_s \cdot i_{qs} + L_m \cdot i_{qr} \tag{4.14}$$

$$\varphi_{dr} = L_r \cdot i_{dr} + L_m \cdot i_{ds} \tag{4.15}$$

$$\varphi_{qr} = L_r \cdot i_{qr} + L_m \cdot i_{qs} \tag{4.16}$$

The generator electromechanical torque is calculated as in equation (4.17), where *p* is the number of pair poles.

$$T_e = 1.5 \cdot p \cdot \left(\varphi_{ds} \cdot i_{qs} - \varphi_{qs} \cdot i_{ds}\right) \tag{4.17}$$

P&O algorithm and the pitch angle controller are designed to make sure the maximum power point tracking (MPPT) operating and efficient utilization of WT, respectively. By adjusting the blade pitch angle, the power coefficient is reduced, and thus the power extracted from the wind decreases when the rotational speed increases above the rated speed. In the contrary, in less than the generator rated speed the pitch angle controller maintain optimum power efficiency. In this way, when the wind turbine operates above the rated value, the produced power must be limited by limiting the rotational speed to the rated speed. Therefore, the blade pitch angle controller acts as a rotational speed limiter in any operating conditions.

4.1.2. Photovoltaic (PV) system

PV array which is composed of modules connected in series or parallel is considered as the fundamental power conversion unit of a PV generator system depending mainly on the incident irradiance and temperature of the cell surface [121]. The PV array has nonlinear characteristics, and it is quite expensive and takes much time to get the operating curves of PV array under varying operating conditions [122]. In the following a step-by-step procedure for the simulation of PV cells/modules/ arrays in Matlab/Simulink is presented.

A diode, a controlled current source, a series resistor, and a shunt resistor constitute the model to represent the behaviour of the PV panels, being a model widely accepted and used by many research papers in the literature [121]. The current source I_{ph} represents the cell photocurrent. R_{sh} and R_s are the intrinsic shunt and series resistances of the cell, respectively.

Practically, PV cells are grouped in larger units called PV modules and these modules are connected in series or parallel to create PV arrays which are used to generate electricity in PV generation systems. The mathematical model is given by equations (4.18 – 4.21), where the I-V characteristics are outputted that are calculated by irradiance and temperature.

$$I_O = I_{rs}\left[\frac{T}{T_r}\right]^3 exp\left[\frac{q \times E_{g0}}{nk}\left(\frac{1}{T} - \frac{1}{T_r}\right)\right] \tag{4.18}$$

where, is the module saturation current output current varying with the cell temperature, T_r is nominal temperature, E_{g0} is band gap energy of the semiconductor, I_{rs} is module reverse saturation current, T is operating temperature, n is the diode ideal constant, and the Boltzmann constant is represented by k.

The current output of PV module is calculated by:

$$I = N_p \times I_{ph} - N_p \times I_o \times \left[exp\left(\frac{\frac{V}{N_s} + I \times \frac{R_s}{N_p}}{n \times V_t} \right) - 1 \right] - I_{sh} \quad (4.19)$$

$$V_t = \frac{K \times T}{q} \quad (4.20)$$

$$I_{sh} = \frac{V \times N_p/N_S + I \times R_s}{R_{sh}} \quad (4.21)$$

where, Np is the number of PV modules connected in parallel, Vt is the diode thermal voltage (V), and q is the electron charge.

In order to simplify the models of solar panel, various models have been developed and integrated to many engineering software including Matlab/Simulink. These models are adequate for application involving hybrid energy system if they are provide a flexible tuning of some parameters in the system.

4.2. Modelling of the Quasi Z-source network

ZSI is an emerging topology for power electronic converters with interesting properties, such as buck-boost characteristics and single-stage conversion [123]. In the following section, qZSI topology in detailed model is discussed and will be used in the simulation part.

A two-port network, composed of two capacitors and two inductors connected in an X shape, is employed to provide an impedance source (Z-source) network. ZSI advantageously uses the shoot-through (ST) state to boost the input voltage, which improves converter reliability and enlarges its application fields. Compared with other power electronics converters, it provides an attractive single-stage DC–AC conversion with buck-boost capability, reduced cost, reduced volume, and higher efficiency owing to a lower component number. For emerging power-generation technologies, such as fuel cells, PV arrays, and WT, and new power electronic applications, such as electric and hybrid vehicles, ZSI is a very promising and competitive topology [124].

As mentioned in the previous review chapter, to overcome the drawbacks of the basic ZSI topology, there have been many structural modifications. Among them, qZSI is one of the best options, since it presents several advantages over the basic ZSI, such as a lower component rating than the basic ZSI topology (for example, Z-network capacitors voltages); soft-start capability to suppress resonant current at startup due to the inherent current path at startup in the basic ZSI topology; and the joint earthing of the input power source and the DC link reduces the common-mode noise in the system [125]. The qZSI is driven from the basic ZSI topology by exchanging the positions of the inverter bridge and input diode and inversing their connection directions. The elements are identical to those in the basic ZSI topology.

The capacitance C and inductance L are the main components to be designed in the qZSI. According to [126], the capacitance C (here, the voltage ripple r_v is set to 1%) and the inductance L (here, the voltage ripple r_i is set to 20%) of the Z network can be calculated as:

$$L = \frac{1}{2} \times T_{0max} \times \frac{M_{min} v_{in}}{r_i I_{in}} \tag{4.22}$$

$$C = 2T_{0max} \times \frac{I_{in}}{r_v \hat{v}_{dc}} = \frac{2T_{0max} I_{in}(1 - 2D_{max})}{r_v v_{in}} \tag{4.23}$$

where T_0 is the shoot-through period found by the switching frequency fs:

$$T_{0max} = \frac{2 - \sqrt{3} M_{min}}{2 r f_s} \tag{4.24}$$

where M_{min} is the minimum modulation index found by modulation technique. The maximum duty ratio D_{max} is obtained from:

$$D_{max} = 1 - \frac{3\sqrt{3}\, M_{min}}{2\pi} \tag{4.25}$$

Fig. 4.2 illustrates the impedance network elements and the operation principles of this network. The qZSI allows two possible operation states, called the shoot-through and the non-shoot-trough states. In the shoot-through state, both switches of a leg are active simultaneously, thus short-circuiting the DC side of the converter. On the other hand, in the non-shoot-trough state, the qZSI allows the two zero states and the six active states of a conventional VSI (i.e., at least one of the switches open in each leg) [126].

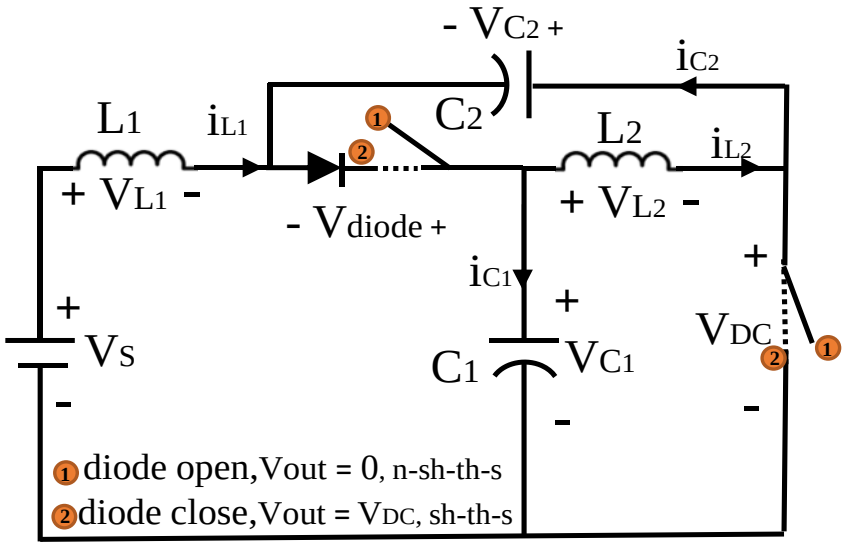

Fig. 4.2. *The qZSI* topology and operating modes.

Now, the relationship between input and output of network is presented. The relationship between the input voltage (V_S) and the voltage across the capacitor C_1 (V_{C1}) is calculated through shoot-through duty cycle D as the following equation.

$$V_{c1} = \frac{1 - D}{1 - 2D} \times V_s \tag{4.26}$$

The relation between V_S and the output voltage of the impedance network (V_{DC}) is:

$$V_{DC} = \frac{1}{1-2D} \times V_S = B \times V_S \tag{4.27}$$

D in this thesis is found by MPPT algorithm in order to intervene RES power effect to the inverter output power level. The modulation signal (M) is found in the control loops stated in chapter 5 section 5.2. M and D with a carrier signal are used as the modulation process inputs.

4.3. Modelling of the Battery

The BES that used in various simulation configurations in this thesis, is connected in parallel with the upper capacitor of the impedance network. These are modelled according to the battery model included in the SimPowerSystems library in Matlab/Simulink [116]. In this thesis, the Lithium-Ion electrochemical battery is modelled as a secondary energy source to back up the intermittent RES generations.

Under mask of the battery block, there is a controlled voltage source in series with an equivalent internal resistance. This bock model calculates the terminal instantaneous battery voltage (V_{batt}) from following equation:

$$V_{batt} = E_{batt} - R_i \cdot i_{batt} \tag{4.28}$$

where E_{batt} is the no-load voltage, i is the battery current, and R_i is the internal resistance of the battery, which is assumed constant during the charge and discharge cycles. There is another parameter in this block as open-circuit voltage that depends on the charge and discharge state of the battery. The open-circuit voltage during charge and discharge can be calculated as in equations (4.29) and (4.30), respectively [44].

$$E_{batt\_char} = E_0 - K \cdot \frac{Q}{|i_t| + 0.1 \cdot Q} \cdot i^* - K \cdot \frac{Q}{Q - i_t} \cdot i_t + f_{hyst\_char}(i) \tag{4.29}$$

$$E_{batt\_disch} = E_0 - K \cdot \frac{Q}{Q - i_t} \cdot i^* - K \cdot \frac{Q}{Q - i_t} \cdot i_t + f_{hyst\_disch}(i) \tag{4.30}$$

where K is the polarization constant or polarization resistance, E_0 is the constant component of the no-load voltage, i_t is the extracted capacity, and i^* denotes the low-frequency current dynamics. As it can be received from these equations, E_{batt} is a function of the instantaneous battery current, the extracted capacity and hysteresis phenomena of the battery during the charge and discharge cycles. Moreover, Q is the maximum battery capacity, and $f_{hyst\ char}(i)$ and $f_{hyst\ disch}(i)$ are functions of the battery current which represent the hysteresis phenomena of the battery during the charge and discharge cycles.

A parameter considered for battery lifetime and maintenance issues is the state of charge (SOC), that monitoring this parameter allows adequate operation and preservation of this device. This task is often developed by supervisory controllers in the configurations considered herein. If the initial SOC state is considered as SOC_0 and Q as the battery capacity (Ah), then SOC is found by:

$$SOC(\%) = SOC_0(\%) - 100\left(\frac{\int i_{batt} dt}{Q}\right) \tag{4.31}$$

There are some other issues mas be taken into consideration during the simulation designing. For instance, the parameters of the model are determined from discharge curves and assumed the same for the charge process. Moreover, the internal resistance of the battery is

considered constant during the charging and discharging processes, the model does not include aging or temperature effects, and the self-discharge of the battery is not considered.

Beyond all, in this work the initial and nominal BESs parameters for every module are considered different. The main advantage of using different BESs is executing a simulation environment closer to practical and real conditions.

4.4. Converter modulation technique

To transfer the energy available in the RES and BES to the grid, the IGBT switches of the inverter are controlled by a modulation technique. The main objective of the modulation techniques is to provide a minimum harmonic distortion and maximum fundamental component in the output.

However, for the impedance multilevel inverters three modulation methods – phase-shifted sinusoidal PWM (PS-SPWM), phase-shifted pulse-width-amplitude modulation (PS-PWAM), and modular multilevel space vector modulation (MM-SVM) – were proposed for the qZS-CMI based PV power system in [67, 103, 104], respectively.

The PS-PWAM was proposed to reduce the switching number and loss. The MM-SVM was introduced for the three-phase qZS-CMI to simplify the modulation implementation and enhance the voltage utilization ratio. The PS-SPWM shown in Fig. 4.3 is a basic method derived from the conventional CMI. As Fig. 4.3 shows, each qZS-HBI module of the qZS-CMI is controlled by the unipolar PWM with the shoot-through references 1−Dn and Dn−1; the m_n are the modulation signals of qZS-HBI modules; the carriers of upper and lower switches for one module are at 180° phase shift. When the carrier is higher than the top shoot-through reference 1−Dn, or lower than the bottom shoot-through reference Dn−1, a shoot-through state is produced. The step-like multilevel voltage waveform is achieved by a π/n phase shift between the adjacent cascaded modules. When compared with the traditional CMI, there are additional shoot-through switching actions in each module of the qZS-CMI, which results in extra switching losses.

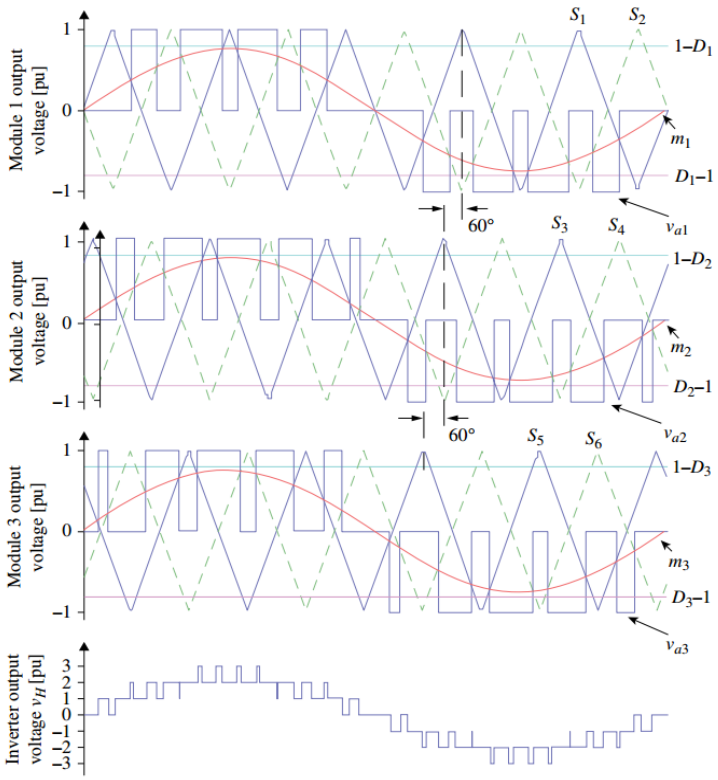

Fig. 4.3. Equivalent circuit for the shoot-through state and non-shoot-through state [65] chapter.12.

The difference of the modulation in this thesis came from using two modulation indexes and one carrier reference. As shown in Fig. 4.4, this modulation method uses for each BES-qZSI module (i[th]module): 1) two signals dependent on the shoot-through duty cycle D_i ($1 - D_i$ and $D_i - 1$), which is obtained from the maximum power point tracking (MPPT) control of the RES (Section 5.1.2); 2) two signals dependent on the modulation index M_i (M_i and $-M_i$), which is obtained from the grid active and reactive power control (Section 5.2); and 3) the carrier signal, which is shifted (180º)/n for each module, where n is the number of modules in series (n=3, in this thesis).

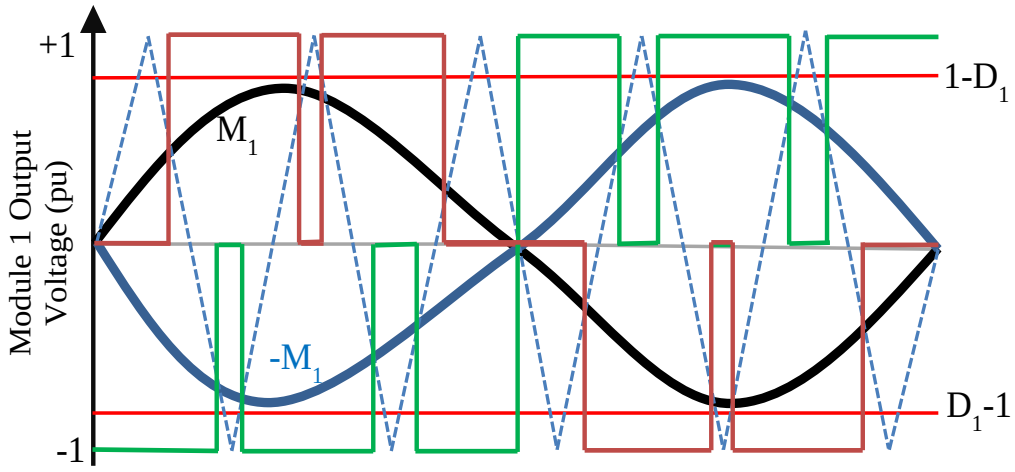

Fig. 4.4. Modulation scheme used for each BES-qZSI module.

4.5. AC grid model

The hybrid configurations evaluated in this thesis are connected to the power system. Single-phase AC grids are modelled as ideal single-phase voltage sources, and for controlling WT pitch angle a three-phase AC grids is considered. The amplitude and frequency of these voltage sources remain constant throughout the modelling of the hybrid and single WT configurations; however, active and reactive power refences are requested by an operator grid to vary along with the simulation.

4.6. Modelling of the hybrid configurations

In this section the modelling of all the hybrid configurations under consideration in this study is detailed. Three separated modules with their own elements are modelled and the structure is shown in Fig. 4.5. In the first case, three PV power sources are used as the RES that can work under different environmental conditions. It consists of three modules connected in series to a single-phase grid. In each module, a PV plant with a terminal voltage stabilizer capacitor is considered as the power source, and a BES is connected to the qZSI impedance network to support the PV plant. Finally, the energy available in the output of impedance network is injected into the grid through a single-phase inverter with IGBT switches in H-bridge topology and modulated by the phase-shift pulse-width modulation (PS-PWM) method. The traditional way of connecting a BES to a RES is using a DC/DC power converter. In the case of qZSI, the BES can be integrated into the impedance network without an additional DC/DC power converter, which is an important advantage over traditional converters [127]. The best place to connect a BES into a qZSI is in parallel to the capacitor C2, making charging and discharging feasible by controlling the switching pulses of the qZSI.

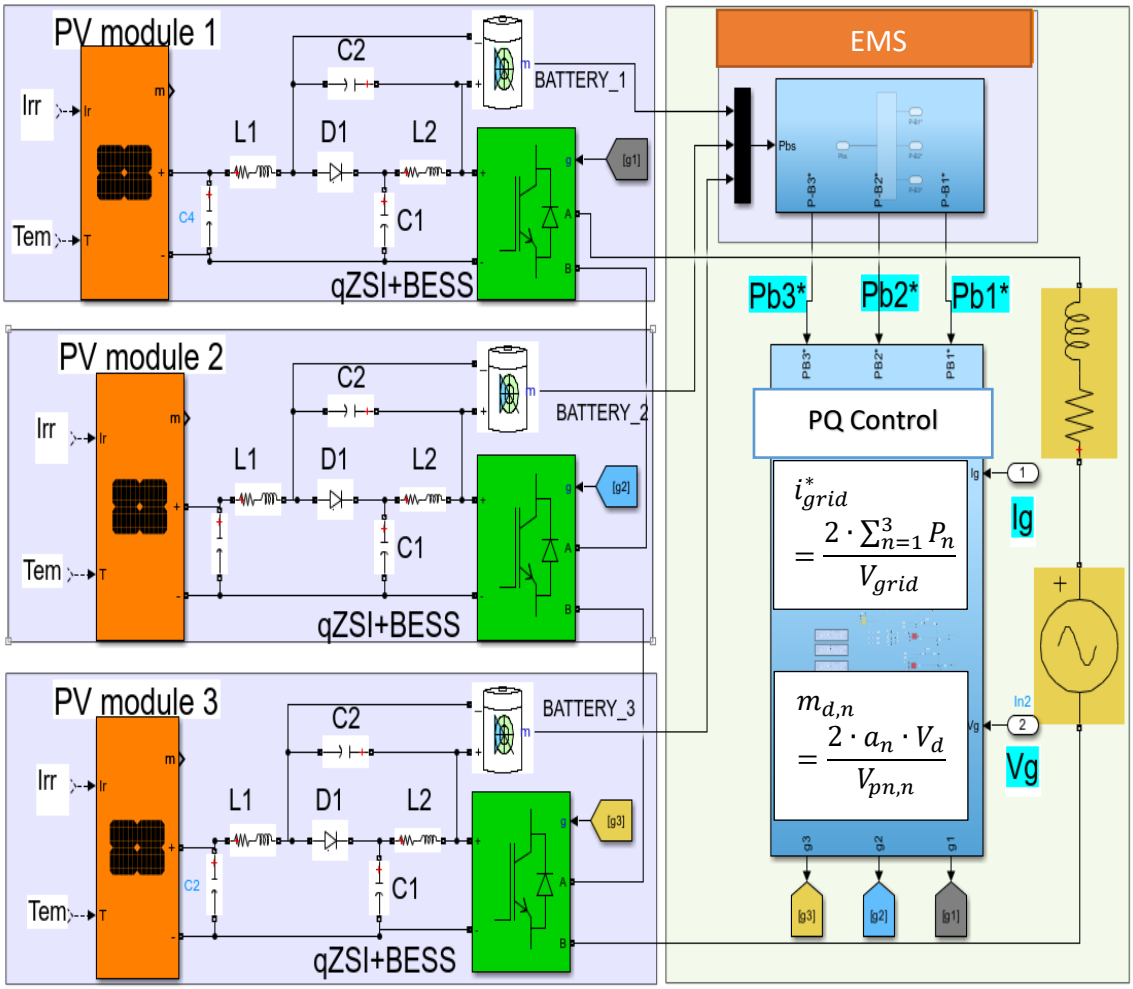

Fig. 4.5. Grid-connected ES-qZS-CHBMLI with PV power generation under study.

Another configuration that is sought in this thesis is considering wind power source in one module of cascaded multilevel inverter. The hybrid power plant under study is composed of three BES-qZSI modules connected in series (BES-qZS-CHBMLI) to a single-phase grid. The first two BES-qZSI modules are fed by independent PV power plants and the third module is fed by a WT. In each module, a different BES is connected in parallel to capacitor C2 of the impedance network to support and store the renewable energy generated from the PV power plant or WT connected to the input of each module. Fig. 4.6 illustrates the hybrid power plant under study and the control system. The independent MPPT control for the PV power plants and the WT is also included in the control designing and is discussed in the next chapter. Each module uses a qZSI, which is composed of a single-phase voltage source inverter with IGBT switches in H-bridge topology and an impedance network with two capacitors (C_1 and C_2) and two inductors (L_1 and L_2).

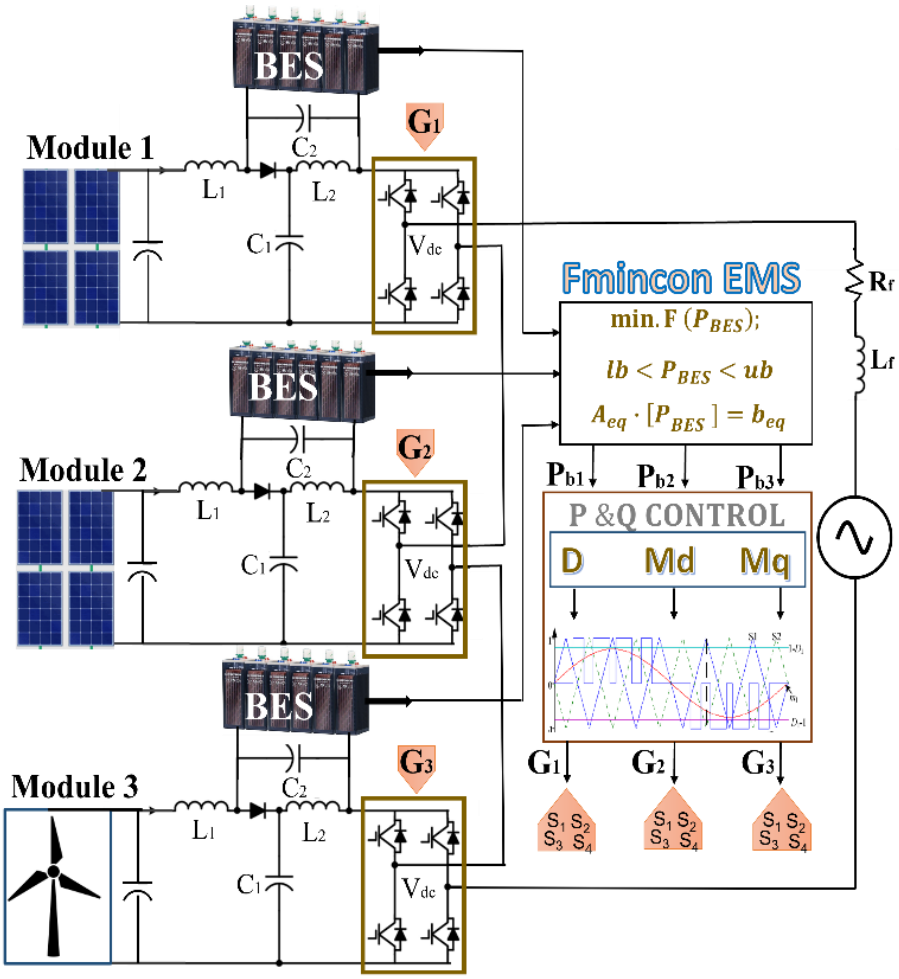

Fig. 4.6. Hybrid power plant under study based on BES-qZS-CHBMLI and RES (PV power plants and WT) and control system.

To give the first perspective of control and EMS parts, in the Fig. **4.6** fmincon EMS is presented as an example of EMSs that will be discussed in the next chapter. Where, the batteries' powers are sensed and entered into the EMS process, in this way the reference batteries power are obtained and inserted to control part. In the control part crucial components are found to be introduced in modulation process and the founded gate signals command the IGBT switches.

4.7. Reinforcement learning algorithm

An EMS is essential for the proper operation of power generation systems. Different energy management algorithms for sharing power between BES depending on the generated PV power and energy consumption were suggested for application in qZS-CHBMLI. RL algorithms can be a good option as they do not need any prior knowledge or transfer function of control parts. Moreover, RL can be executed as a MPPT algorithm to find optimal utilization of RES. In this part, RL agents and types are studied to find the best agent for the case of study in this work.

A reinforcement learning agent interacts with the environment by choosing actions based on observations. How the environment reacts to the agent's actions is typically simulated using

a Simulink model of the environment's dynamics. The agent, the environment, the observations, and the actions are all represented in MATLAB as variables.

To implement RL algorithm both MATLAB code and mixture of code-Simulink options are possible. The Simulink RL toolbox is available that helps to make the implementation easier and more visible and to see agent training progress. The *RL Agent* block requires three pieces of information from the environment: the observations, the reward, and whether the episode has reached a terminal state, which are often interrelated. Depending on the control objectives, the observations and reward function must be defined, and the episode termination is set based on a very bad action or reaching the goal. The reward depends on the state as well as whether either terminal condition was reached. Using the *rlSimulinkEnv* function allows to define an environment variable from a Simulink model. The inputs to the *rlSimulinkEnv* function are the name of the Simulink model, and the variables that define the observation and action specifications.

There are various agents based on the structure and type, that are presented in the Table 4.1. Based on the application of an agent in a control algorithm, like action type, the agent must be selected. For example, for a modulation task the agent must be discrete and for EMS (that actions are continues) the agent must be continuous.

Table 4.1. RL agent types and features.

Agent	Action	Type	Representation
Q-Learning	Discrete	Critic	rlQValueRepresentation
SARSA	Discrete	Critic	rlQValueRepresentation
Deep Q-Network	Discrete	Critic	rlQValueRepresentation
Policy Gradient	Discrete Continuous	Actor Actor-Critic	rlStochasticActorRepresntation (Actor) rlValueRepresentation (Critic)
Actor- Critic	Discrete Continuous	Actor-Critic	rlStochasticActorRepresntation (Actor) rlValueRepresentation (Critic)
DDPG	Continuous	Actor-Critic	rlDeterministicActorRepresntation (Actor) rlQValueRepresentation (Critic)
Proximal Policy Optimization	Discrete Continuous	Actor-Critic	rlStochasticActorRepresntation (Actor) rlValueRepresentation (Critic)
TD3	Continuous	Actor-Critic	rlDeterministicActorRepresntation (Actor) rlQValueRepresentation (Critic)

An agent needs a way to represent its policy, and therefore an agent is made up of one or more representations of actors or critics. To create agents, it is needed to create neural networks

to represent agent representations of actors and critics. A neural network is represented in MATLAB as an array, where each element of the array is a variable that represents a layer of the network. It can use various functions to create different kinds of layers. These networks are built by specifying the layers that comprise them. A deep neural network is made up of multiple layers. Each layer receives input from the previous layer, performs an operation on the input, and passes the output to the next layer. For actor or critic networks, typically the inner (or "hidden") layers are fully connected layers or activation function layers that consists of a number of neurons. Each neuron is a mathematical operation: multiply the input by a constant (called the weight) and add another constant (called the bias). The resulting value is then passed to the next layer. In a fully connected layer, each neuron takes input from every neuron in the previous layer and passes the output to every neuron in the next layer. This means that each neuron has many weights. In between fully connected layers, there are typically activation function layers that apply a function to introduce nonlinearity. Two commonly used activation functions are: (1) the rectified linear unit (or "ReLU"), which leaves positive inputs unchanged and sets negative inputs to zero. (2) the hyperbolic tangent, which smoothly maps all inputs into the range [-1 1]. Fig. 4.7 and Fig. 4.8 represent deterministic and stochastic actor neural network architectures and value, Q-value critic neural network architectures, respectively.

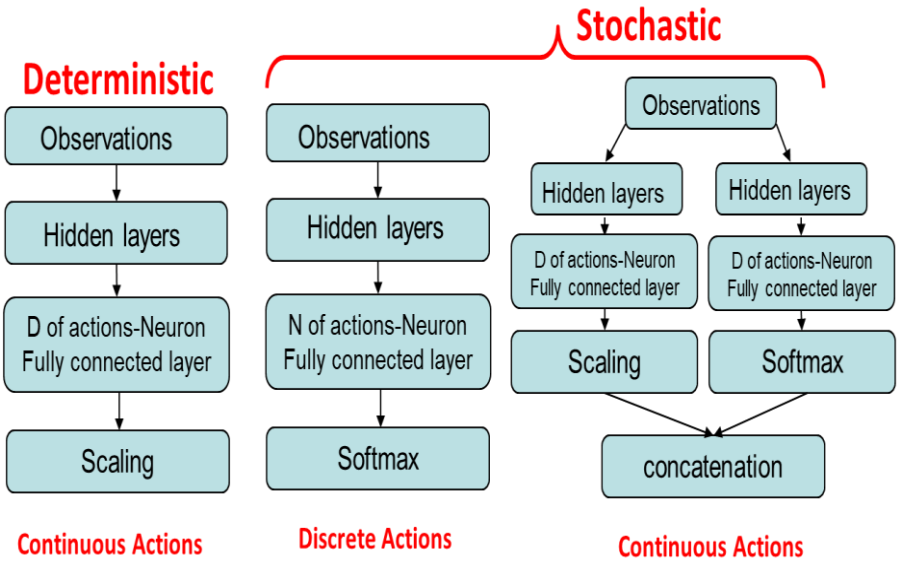

Fig. 4.7. Actor neural network architectures.

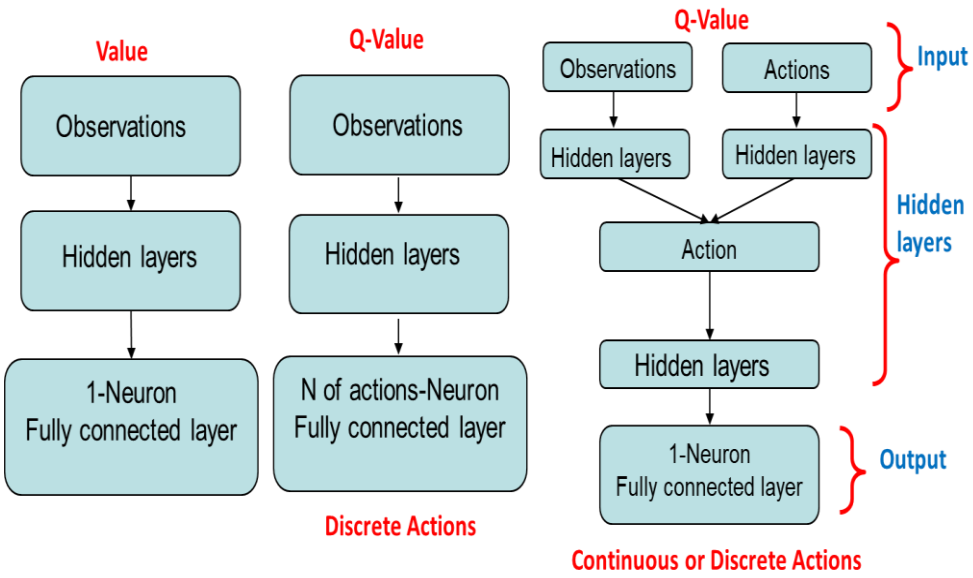

Fig. 4.8. Critic neural network architectures.

However, the policy that the agent picks the actions must be defined. Strategies to pick an action in a given state are: (A). always pick the next action at random, (B). always pick the next state that gives the highest known reward. (C). take chances and explore new states in the hope of finding a better path. (D). Always play it safe and avoid the chance of a negative reward. These policies are divided to Deterministic and Statistic ones. For Deterministic type, agent always chooses the same fixed action when it reaches a particular state, and for Statistic one, agent varies the actions it chooses for a state, based on some probability for each action (suitable for games- not to be predictable). Considering the total accumulated reward over all time-steps of each episode (r) as Return= r_0+ r_1+ r_2. Therefore, among many possible policies, the agent must select one that maximizes its Return. The Fig. 4.9 gives a better understanding of this fact.

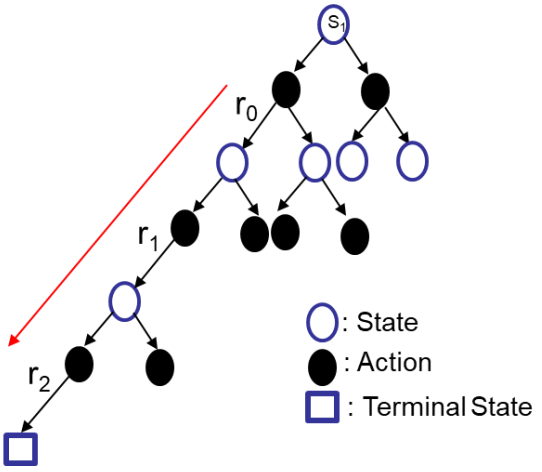

Fig. 4.9. Picking up a policy by an agent.

Some agents work better than others for a given problem. Between continues agents, TD3 showed better results in the case under study as it takes advantage of a gradient in actor representors. To create an agent one of the *rlAgent* functions can be used, and one of the *rlRepresentation* functions can be used to create a representation for an agent.

Reinforcement Learning is challenging, and successful training often requires many iterations, adjusting options and hyperparameters. The environment must be well- defined if the agent is going to learn well to accomplish its objectives. Some precautions and suggestions are presented in the following to improve the training process.

4.7.1. Number of neural network neurons

With enough neurons, a network can represent an extremely complicated function. It is said more neurons can help training to learn better, however, more neurons mean more parameters, and therefore more training. It is suggested to start with a simple-default network and check the training progress. If the agent doesn't seem to be able to learn, no matter what the other tries, increasing the number of hidden-layer neurons in the networks sometimes is helpful.

4.7.2. Reducing Effort

It is common to look for a strategy that achieves a goal with as little effort as possible. It is more necessary in practice that cost very single action, and this process is going to repeat hundreds of times. Therefore, discouraging unnecessary actions will reduce the learning period in simulation, and cost in practice. To include this issue in the training, the actions that agent execute them that makes the system unstable or leads it to the worst place, must be punished significantly and the episode stop immediately. It is common to add discrete rewards or penalties as *''is done''* for achieving a goal or violating a constraint.

4.7.3. Hyperparameters

The training and agent hyperparameters define the details of algorithm process that are essential to be defined well. The main parameters are presented in the following.

A.) **ε-greedy:** This parameter seeks the balance between the Exploration and Exploitation terms. This is a rate at which the agent chooses random moves, to promote strategy exploration to ensure the agent meets the whole environment. A larger value of epsilon means that the agent randomly explores the action space at a higher rate. Regarding Exploration term, it randomly tries different actions and observe the rewards by ε rate. The ε is the rate at which the agent chooses random moves, to promote strategy exploration to ensure the agent meet the whole environment. And Exploitation term picks the best actions which will yield the maximum return. Fig. 4.10 shows the curve of following these two terms as the training progresses. By using an epsilon decay term, the number of explorations can decrease. There is also a term called epsilon-min (ε_{min}) that agent should explore at least this amount.

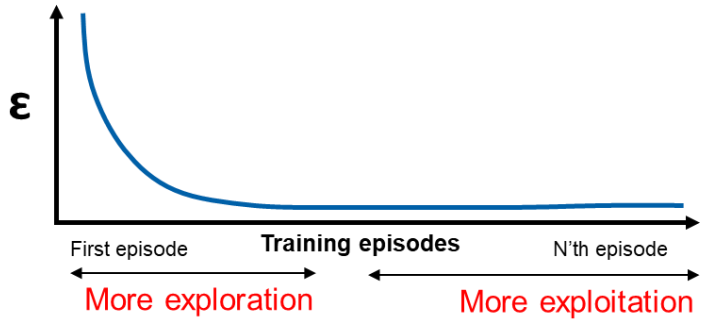

Fig. 4.10. ε-greedy procedure.

At the end of each training time step, if epsilon is greater than epsilon min, then it is updated using the following formula:

$$\varepsilon_{max} * \varepsilon_{decay}^{n^{th\ episode}} = \varepsilon_{current} \tag{4.32}$$

Exploration is critically important that if the agent doesn't explore enough, it will settle on a poor policy. If the agent seems to have stopped learning, experimenting with the exploration options to promote better exploration is suggested.

B.) **number of episodes:** It presents the number of games the agent will play. The reward plot should be monitored continuedly to see if the number of episodes is enough or should be changed for further training.

C.) **learning rate (α):** It is related to the neural network learning parameters. It must not be too low that slows down the learning process and not too much that may not converge. It is said to use as large a learning rate as possible, but if the agent's policy seems to be changing randomly without any improvement to the average reward, the learning rate may be too high.

D.) **Gamma (γ):** This is the decay or discount rate that encourages the agent to care more about the immediate reward compared to later rewards. It weights later rewards over time as: $r_0 + \gamma\, r_1 + \gamma^2\, r_2 + \ldots + \gamma^n\, r_n$

E.) **Experience buffer length:** This is a term to store the experience (state-action-reward S,A,R,S') in the experience buffer.

F.) Stop training: Training an RL algorithm takes time. Agents can go through periods of better and worse performance as they try different policies. Even if the agent is not yet performing well, unless it's clearly no longer learning anything useful, it must keep training. If the maximum number of training episodes is reached while the agent is still making progress, the number of episodes must be increased.

4.7.4. Designing reward

The agent's learning is dictated by the reward function. Then it is crucial to check the agent isn't learning to exploit a "loophole" in the reward, such as producing more than enough batteries power, or avoiding penalty by producing zero batteries power outputs, or the agent choose the worst actions to terminate the episode early by *"Is down"* gate to avoid negative rewards. It is recommended to shape the reward function to guide the agent towards desirable

states and not only relying on sparse rewards that can make training difficult as the agent may never achieve the reward through random exploration.

Another thing that must be taken into account in defining reward function, is considering a negative coefficient to prevent agent to stuck in a position that have been received to accumulating positive reward rather than reaching the goal (which terminates the episode). This small penalty is imposed by feedbacking actions to the reward function by unit delay block.

Visualizing the reward through time can give an idea of the agent's performance that gives a measure of how well the agent is progressing towards its goal. However, the agent receives a significant positive reward for reaching the goal and a penalty for errors. If the coefficient of rewards or penalties makes the reward function gathers a large value, changing the y-axis limits using either the interactive plot tools or ylim ([ymin ymax]) helps to make it easy to see the variation in the reward before the final state.

4.7.5. Random initializations

A good controller can perform well under a variety of circumstances. Using different initial states and parameters is another trick to have an adaptive RL algorithm that works not only for the predefined environment conditions, but also for more simulation times and varying conditions. Therefore, a local function is suggested to randomly choose different set points, reference values, or initial values of a particular system. For example, in the case of study here, initializing different irradiance values, different grid power reference, varying wind speed or… in every episode could makes the Rl adaptive enough to every conditions.

4.7.6. Is down function

Using this function reduces the training time significantly. It is a logical function that when the value 1 enters the gate, makes it activated and stops the current episode. When some events happen that terminate the episode, the reward should be large enough to offset the potential minimum or maximum possible rewards that could be achieved if the episode had not terminated. For example, the agent collects small negative rewards at each time step without a penalty for its errors, the agent could learn to go to the worst condition as quickly as possible to terminate the episode. Therefore, a huge penalty must be considered for the worst condition avoid agent making interest to this path.

CHAPTER

CAPÍTULO

FIVE

CINCO

5

5. Control objectives

Beside the pitch angle controller for a single WT connected to the grid, the control objectives associated with the hybrid power plant under study are: 1) maximum power point tracking (MPPT) for power sources, 2) a control subsystem for the active and reactive power injected to the grid, and 3) energy management system (EMS). Several control architectures and MPPT algorithms have been proposed to achieve these requirements. Advanced control strategies for anti-islanding protection, low-voltage ride-through, reactive power injection, and improving the resilience of power distribution systems.

To be more specific in our case of study, there exist numerous control techniques and EMS to implement for BES-qZS-CHBMLI that can be used depending on the desired application. Researchers have studied the control methods, control schemes, and modulation techniques for different applications of this type of inverter [128]. Moreover, supervisory control is another main purpose of this study. Therefore, novel approaches for supervisory control are discussed and compared with conventional EMS.

qZS-CHBMLIs have been applied to PV power plants in [129, 130]. qZS-CHBMLI integrating an ESS, mainly BES (BES-qZS-CHBMLI), is an interesting option for PV power plants, because it cannot operate at night as there is no PV power input. Integration of ESS into the impedance network of a qZS-CHBMLI eliminates the need for a DC-DC converter to connect and operate the ESS, allowing the support of the PV power plant.

5.1. Independent MPPT algorithm and pitch angle control

The MPPT control subsystem is responsible for achieving the maximum power of the RES according to the incident radiation and temperature in the PV panels and the wind speed in the WT.

5.1.1. Case study 1: MPPT for wind turbines and pitch angle controller

In this subsection, two adaptive controllers are suggested for MPPT, and pitch angle control of WT designed for CART3 wind turbine US national laboratory by Fast toolbox. First an adaptive PID controller is designed and then a passive RL based transfer learning is suggested.

5.1.1.1. *Adaptive PID controller*

In Region 3 (Chapter.4, Fig. 4.1), with above rated wind speeds, the goal is to maintain the rated power. In this case, the rotor speed is kept at rated speed (ω_{rate}) so that control the pitch angle, and as this signal control orders, the pitch blades actuators command to change the power extracted from the wind. The torque is kept constant at the rated value and only the pitch angle is controlled according to the difference between the rated speed and the current rotational speed. When the rotational speed exceeds its nominal value, the pitch angle control system increases the pitch angle to reduce the power extracted from the wind [131]. Based on a linear model system at an operating point, classical PID controllers are typically used to design the blade pitch controller due to their simplicity and easy implementation. A linear model of PID pitch angle control was described in [132], where the pitch perturbation ($\Delta\ \beta$) is expressed as

the summation of proportional (k_P), integral (k_I) and derivative (k_D) terms of the perturbed rotational speed ($\Delta\omega$, difference between the rated speed and the current rotational speed):

$$\Delta\beta(t) = k_P\Delta\omega(t) + k_I\int \Delta\omega(t)dt + k_D\dot{\Delta\omega}(t) \tag{5.1}$$

To determine the appropriate gains of the PID controller, a Laplace transform of the closed-loop system is obtained as follows:

$$\Delta\beta(s) = k_P\Delta\omega(s) + k_I\frac{1}{s}\Delta\omega(s) + k_D s\Delta\omega(s) \tag{5.2}$$

A linear model for controller design is suggest by A.D. Wright in [132], which has the following form:

$$\dot{\Delta\omega} = A\Delta\omega + B\Delta\beta + B_d\Delta v \tag{5.3}$$

where A, B, B_d are the parameters related to the turbine aerodynamic and v is the hub-height uniform wind speed disturbance across the rotor disk.

By Laplace transforming both sides of equation (5.3) and replacing Δβ by equation (5.2), the closed-loop transfer function $T_c(s)$ between the measured output (Δω) and the disturbance input (Δv) is determined by the following equation [132]:

$$T_c(s) = \frac{B_d(s)}{(1 - Bk_D)s^2 + (-A - Bk_P)s + (-Bk_I)} \tag{5.4}$$

To achieve the closed-loop system stability and obtain appropriate gains for the PI, the roots of equation (5.4) must have negative real parts. To calculate the roots, the denominator is put equal to zero.

$$(1 - Bk_D)s^2 + (-A - Bk_P)s + (-Bk_I) = 0 \tag{5.5}$$

So,

$$(1 - Bk_D) > 0, (-A - Bk_P) > 0, (-Bk_I) > 0$$

By comparing equation (5.5) with a standard form of a second order system ($s^2 + 2\delta\omega s + \omega^2 = 0$) and choosing K_D=0 (PI controller), the K_I and K_P can be obtained:

$$2\delta\omega = \frac{-A - BK_P}{1 - BK_D} \Rightarrow K_P = \frac{-(A + 2\delta\omega(1 - BK_D))}{B} \tag{5.6}$$

$$\omega^2 = \frac{-BK_I}{1 - BK_D} \Rightarrow K_I = \frac{-\omega^2(1 - BK_D)}{B} \tag{5.7}$$

where, the ω and δ are desired natural frequency and damping ratio from which Kp and Ki can be calculated.

5.1.1.2. *Gain scheduled recurrent ANFIS type-2 with passive RL*

This subpart proposes an innovative intelligent structure based on RL for the pitch angle control in order to improve the WT response. In the proposed control structure, the controller gains are adjusted in a real-time process through GS-RL-RANFIST2. The proposed passive RL differs from other intelligent controllers in that the initial learning process starts by using premier control signals clustered and unsupervised, and the output objective signal is updated by consecutive repetitions. This method is appropriate for all control systems of white box and black box model, and specifically, for new control systems having not studied previously. The subsidiary advantage of the proposed controller is to diminish the number of rules used in type-2 fuzzy logic pitch controllers, which in turn reduces the complexity of the controller design. Moreover, the use of the recurrent structure allows to cover more modes of the system nonlinearity. To reach this adaptive algorithm, first type-2 fuzzy logic systems is reviewed, and the implementation is discussed.

When the weaknesses of type-1 fuzzy logic system came to light, fuzzy type-2 started getting more attention to cover more uncertainties by defining the secondary membership function [22]. To directly handle the membership functions and rule uncertainties, type-2 fuzzy logic system is chosen here instead of type-1 fuzzy logic, as the main basement of the pitch angle controller. The fuzzy type-2 is used to calculate the PI gains in accordance with the variable's variations.

In type-2 fuzzy logic systems (T2FLS), the dimension of the membership function is constant and the interval between the upper $\bar{\mu}_F$ and lower $\underline{\mu}_F$ of membership functions limits the general case. Considering fuzzy rule base consisting of L fuzzy IF-THEN rules as following:

$$Ruls^{(l)}: IF\ x_1\ is\ \tilde{F}_1^l\ and\ x_2\ is\ \tilde{F}_2^l\ THEN\ y\ is\ \tilde{G}^l \quad l = 1, \dots, L.$$

where x_1, x_2 are the input variables, y is the output variable.

$\tilde{F}_1^l$, $\tilde{F}_2^l$, and $\tilde{G}^l$ are type-2 fuzzy sets ($while\ f(u) = 1\ \forall\ u \subseteq [0\ \ 1]$), which are expressed by [133]:

$$\tilde{F}_1^l = \int \mu_{\tilde{F}_1^l}(x_1)\,/x_1 = \int \frac{\int_{u \in J_x} 1/u}{x_1} J_x \subseteq [01] \tag{5.8}$$

$$\tilde{F}_2^l = \int \mu_{\tilde{F}_2^l}(x_2)\,/x_2 = \int \frac{\int_{u \in J_x} 1/u}{x_2} J_x \subseteq [01] \tag{5.9}$$

$$\tilde{G}^l = \int \mu_{\tilde{G}^l}(y)\,/y = \int \frac{\int_{u \in J} 1/u}{y} J \subseteq [01] \tag{5.10}$$

where u and J_x is referred to as the primary membership of x.

The type-reducer converts the interval type-2 fuzzy set to a type-1 fuzzy set. With the center-of-sets type reduction a type-1 output fuzzy set is obtained as follows:

$$y = \frac{\sum_{l=1}^{L} f^l y^l}{\sum_{l=1}^{L} f^l} which f^l \in F^l = \left[\underline{f}^l \overline{f}^l\right], \begin{cases} \underline{f}^l = \underline{\mu}_{F_1^l}(x_1) \times \underline{\mu}_{F_2^l}(x_2) \\ \overline{f}^l = \overline{\mu}_{F_1^l}(x_1) \times \overline{\mu}_{F_2^l}(x_2) \end{cases} \tag{5.11}$$

where $y^l = \left[y_L^l \quad y_R^l\right]$ is the centroid of the type-2 fuzzy set $\tilde{G}^l$, and y_L and y_R are obtained as follows:

$$y_L = \frac{\sum_{l=1}^{p} \overline{f}^l y_L{}^l + \sum_{l=p+1}^{L} \underline{f}^l y_L{}^l}{\sum_{l=1}^{p} \overline{f}^l + \sum_{l=p+1}^{L} \underline{f}^l} \qquad y_R = \frac{\sum_{l=1}^{q} \overline{f}^l y_R{}^l + \sum_{l=q+1}^{L} \underline{f}^l y_R{}^l}{\sum_{l=1}^{q} \overline{f}^l + \sum_{l=q+1}^{L} \underline{f}^l} \tag{5.12}$$

where *p* and *q* could be obtained through a Karnik–Mendel algorithm iterative algorithm. Here, the Takagi-Sugeno-Kang (TSK) fuzzy set is chosen to implement an ANFIS structure, which $y=Y^l = \left[\underline{y}^l \overline{y}^l\right]$ (upper and lower of consequent MFs). Here linear functions are prefered to crisp ones as follows [133]:

$$\overline{y}^l = \overline{a}_1^l x_1 + \ldots + \overline{a}_I^l x_I + \overline{d}^l \tag{5.13}$$

$$\underline{y}^l = \underline{a}_1^l x_1 + \cdots + \underline{a}_I^l x_I + \underline{d}^l \tag{5.14}$$

where $a_1,\ldots a_I$ are weight coefficients of the output membership functions and *d* is constant value.

Fig. 5.1 shows the model-based computation of the reward function in the purposed environment and proposed agent. The initial neuro-fuzzy structure consists of 3 memberships for each input and 3 rules, as shown.

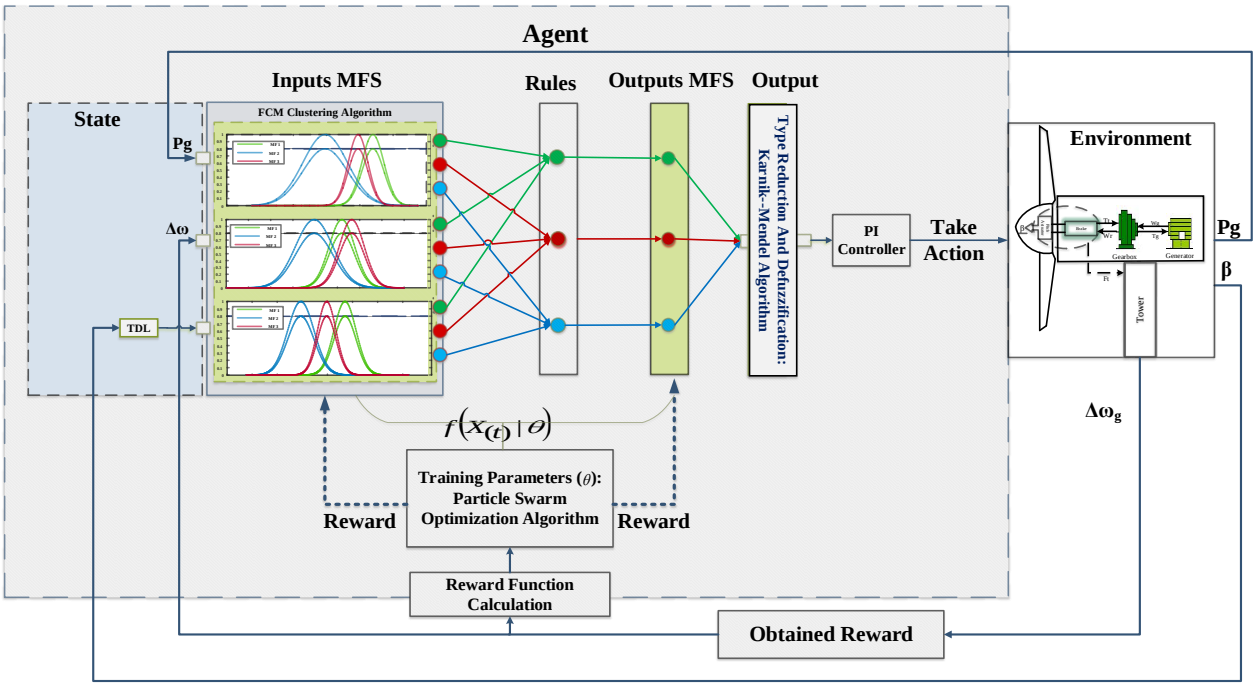

Fig. 5.1. Passive RL structure based PSO for recurrent type-2 fuzzy logic pitch agent.

The proposed pitch angle controller is designed to control the rotational speed, and thus, limit the power extracted from the wind. In this case, the control objective is to keep the rotor speed at its rated value while smoothing the output power and the performance of the pitch angle system. In the first stage, the necessary data including the pitch angle, rotor speed error (or power error) and its deviation are received from the PI controller. The structure of reaching suitable PI parameters is discussed in subsection 5.1.1.1 and its control variables are defined by equations (5.6, 5.7). Receiving such appropriate data is essential for building an initial fuzzy

inference system (FIS) structure through the unsupervised clustering fuzzy c-means (FCM) algorithm.

FCM is a data clustering method used here to reduce the extra repetitive rules in fuzzy structure, which in turn would reduce the complexity of neuro-fuzzy network with maximizing efficiency [134]. Every data given in the former stage belongs to a cluster (A1, A2, …, Aj) with one degree of membership. The FCM process begins with one initial guess for the clusters' centers and determines the membership degree for each one of the clusters, which are on a constant replacement to find their proper spot based on minimizing the objective function. The internal objective function represents the distance of every node in relation to the cluster center and it is defined as follows:

$$O.F. = \frac{1}{n}\sum D(x_i, c_j(i))^2 \tag{5.15}$$

where x is the type of the data, and Cj is jth cluster center, both of which constitute the general statement, and n is the number of data.

xi can become a Aj cluster member if its distance to Aj cluster center in relation to the distance of xi to all other cluster centers is the lowest. The data distances are minimized in relation to the cluster center through the objective function. Now, a basic FIS is generated for recurrent ANFIS including Sugeno rules and input-output membership functions.

There exist nonlinear modes in WT system that ANFIS is not capable to orient itself with these modes. For designing orientated controller in line with the nonlinear nature of the system and converging more nonlinear modes of the system, RANFIS is suggested. To achieve a recurrent structure, the output feedback is applied as the input. In this regard, delay of the recurrent collected pitch angle is applied as a controller input (β(t-1)), together with the rotational speed error (Δ(t)) and mechanical power (P(t)). The correlation between inputs vectors and the output vector is estimated through the function f̂ as follows:

$$\beta_{(t)} = \hat{f}\left[P_{(t)}, \Delta\omega_{(t)}, \beta_{(t-1)}\right] \tag{5.16}$$

In order to search for optimal solutions and reach the objective signals, passive RL is translated into optimization tasks. RL, as an independent method relying on its own experience through a lot of trial error, is widely used in artificial intelligence fields and has penetrated in industrial control systems.

The learning algorithm is a sequence of state, action, and reward and the purpose is to maximize the total cumulative reward, based on the reward function. It makes agent (here, RANFIS) capable of learning in an interactive environment (here, WT system), either with the white box or without the mathematical model and the prior knowledge (black box). The superiority of the proposed RL is to exploit the PI data, which means the training algorithm starts with a basic paradigm. Through the reward signal, RL takes advantage of evaluating positive and negative behaviour of the learning model. The reward function is defined by generator speed error (e_t):

$$E = \frac{1}{N}\sum_{t=1}^{T} e_t^2 \tag{5.17}$$

By considering the generated FIS (in the former stage) as the S_0 state, the agent takes action (A_0) and goes a step forward. Environment transfers to a new state (S_1) and gives a reward (R_1) to the agent. Base a policy, the reward function evaluates the reward and decides when planning actions further and further into the future further. Because of the reward assumption, the best behaviour would be achieved by maximizing the total cumulative reward, which could be written in each step *t* and *k* time steps as [135]:

$$G_t = \sum_{k=0}^{T} R_{t+k+1} \tag{5.18}$$

To sure that the agent does not choose R_1 (the more predictable reward), a discount rate between [0 1) is added to the total cumulative reward:

$$G_t = \sum_{k=0}^{\infty} \gamma^k R_{t+k+1} \tag{5.19}$$

Now, a PSO algorithm is used to solve the particles to move through the search space of action sequences. Because of the complex RL problem, the performances vary notably depending on the chosen partitions of the state space. Furthermore, to get good quality control and adapt to the environment, the agent must search for new states and maximize reward simultaneously. To find such optimal control action sequences PSO algorithm is used. The PSO algorithm does not require a priori assumptions about problem-specific policy representations because it directly optimizes action sequences [136].

Individuals of the population in PSO, named particles, adjusts its position according to its own experience and neighbouring particle, making use of the best position encountered by itself and its neighbour. In the implemented PSO algorithm, the velocity of each particle and its position are calculated as follows [137]:

$$\mathrm{V_i(k+1)} = \phi(\mathrm{k})\mathrm{V_i(k)} + \alpha_1\left[\gamma_{1\mathrm{i}}\left(\mathrm{p_i} - \mathrm{x_i(k)}\right)\right] + \alpha_2\left[\gamma_{2\mathrm{i}}\left(\mathrm{G} - \mathrm{x_i(k)}\right)\right] \tag{5.20}$$

$$\mathrm{x_i(k+1)} = \mathrm{x_i(k)} + \mathrm{V_i(k+1)} \tag{5.21}$$

where *i* is the particle index, *k* is the discrete time index, V_i is the velocity of i^{th} particle, $\varphi(k)$ is the inertia function, and α_1 and α_2 are the acceleration constants, x_i is position of i^{th} particle, p_i is the best position found by i^{th} particle, *G* is the best position found by swarm, and γ_{1i} andγ_{2i} are random numbers in the interval [0,1] applied to i^{th} particle.

After initializing the swarm and randomizing the position and velocity of each particle, the fitness (x_i) is evaluated, and *p* and *G* are initialized by the best position found by particle and swarm. Then the velocity of the particle is updated through a linear decreasing strategy and controlled as follows:

$$\mathrm{V_i(k+1)} = \begin{cases} \mathrm{V_i(k+1)if V_i(k+1)} < \mathrm{V_{max}} \\ \mathrm{Vi(k+1)_{max}}_{\mathrm{max}}\{ \end{cases} \tag{5.22}$$

Finally, based on the new value of fitness function p, *G* is updated as *G = min (p)*. Now, *a* prototype of the RANFIS could be written as below:

$$\text{Output} = \frac{\sum \mathrm{w_i f_i}}{\sum \mathrm{w_i}} = \frac{\sum \mu_{\mathrm{Ai}}(\mathrm{x}).\mu_{\mathrm{Bi}}(\mathrm{y})(\mathrm{a_i x} + \mathrm{b_i y} + \mathrm{c_i})}{\sum \mu_{\mathrm{Ai}}(\mathrm{x}).\mu_{\mathrm{Bi}}(\mathrm{y})} \tag{5.23}$$

where $\{a_i, b_i, c_i\}$ are referred to as the consequent parameters and a fixed node labeled μ [31]:

$$\mu_{Ai}(x) = \frac{1}{1+[(\frac{x-c_i}{\sigma_i})^2]^{b_i}} = \exp\frac{-0.5(x-c_i)^2}{\sigma_i^2} \tag{5.24}$$

where x is the input node i, A_i is linguistic label accompanying the node and b_i, c_i and σ_i are the set of premise parameters.

The last stage is to implement the mentioned training method for RANFIST2. If a_1, b_1, c_1 and d_1 are coefficient of output parameters, the first rule of TSK fuzzy system including three input-one output system could be written as below:

Rule 1: if x_1 is A_1 and x_2 is B_1 and x_3 is C_1, then $Y_1=a_1x_1+b_1x_2+c_1x_3+d_1$.

According to equations (5.11), (5.13), (5.14), and (5.24) and $\underline{y}^l = \overline{y}^l$, the overall pitch angle output (before commanding actuators) is calculated as:

$$\beta_{ref} = \frac{\sum_{l=1}^{L}[\sum_{j=1}^{I}\left(a_j^l x_1 + b_j^l x_2 + c_j^l x_3 + d^l\right) exp(-\frac{1}{2}\sum_{i=1}^{n}\left(\left[\frac{\overline{x_i - c_i}}{\sigma_i}\times\frac{x_i - c_i}{\sigma_i}, \frac{\underline{x_i - c_i}}{\sigma_i}\times\frac{x_i - c_i}{\sigma_i}\right]\right)^2)]}{\sum_{l=1}^{L} exp(-\frac{1}{2}\sum_{i=1}^{n}\left(\left[\frac{\overline{x_i - c_i}}{\sigma_i}\times\frac{x_i - c_i}{\sigma_i}, \frac{\underline{x_i - c_i}}{\sigma_i}\times\frac{x_i - c_i}{\sigma_i}\right]\right)^2)} \tag{5.25}$$

where $\underline{f}^l, \overline{f}^l$ are expanded and x_3 is defined as β_{ref} for having recurrent structure. Fig. 5.2 represents a simplified scheme of the proposed controller.

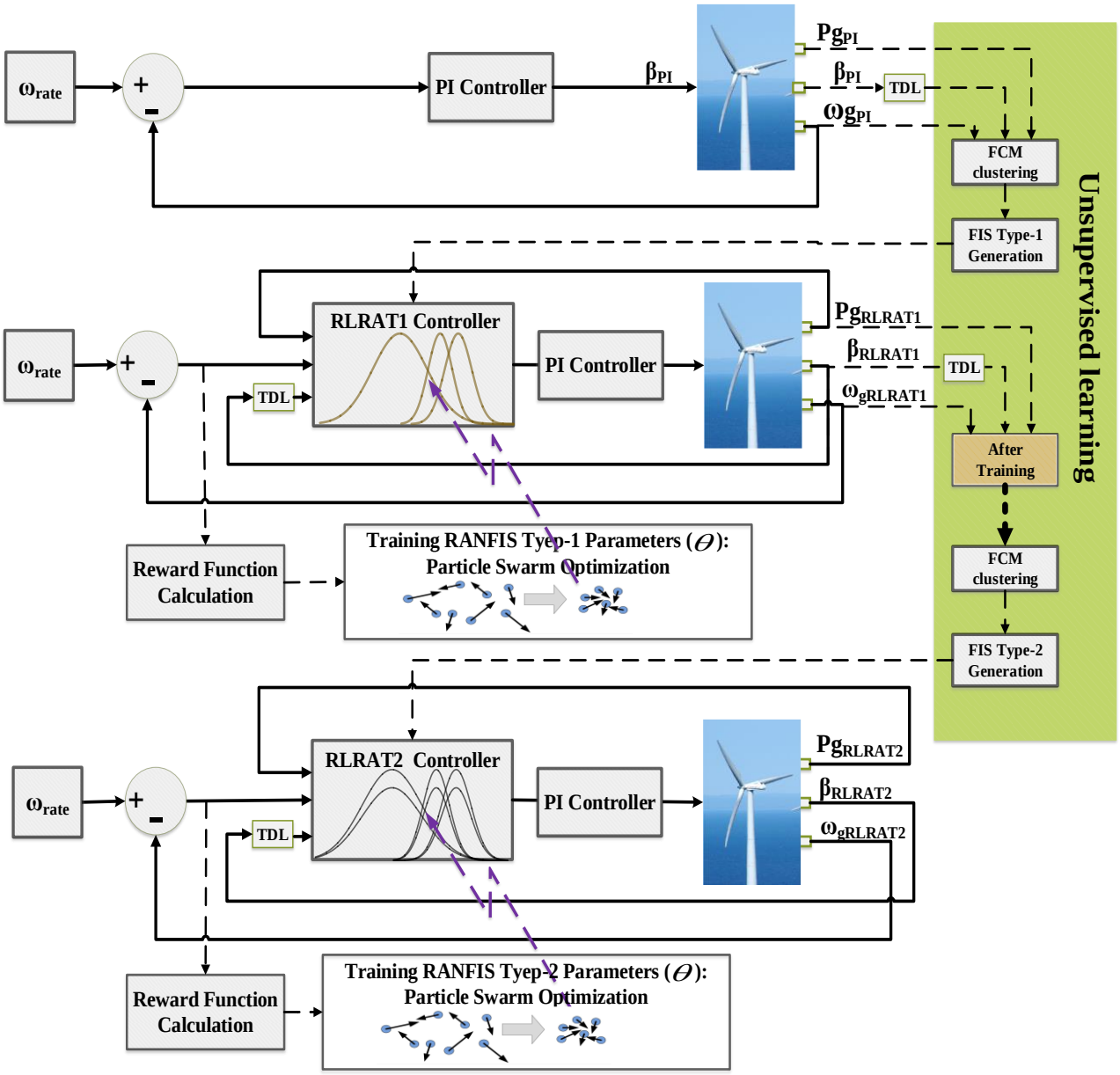

Fig. 5.2. Simplified scheme of the passive RL structure.

The block diagram of the blade pitch angle controller implemented for the CART3 is shown in Fig. 5.3, where the generator speed, generator power, and delay of angle are considered as the inputs of the controller. Because of limitations in the FAST code, the FAST model does not include any blade-pitch actuator dynamic effects. To command a real blade pitch angle, an additional actuator dynamic block is added. The proposed GS-RL-RANFIST2 and GC-PI controllers are tested in the CART3 under step and random wind pattern. The GC-PI controller is an adaptive controller designed and tested by NREL. Hence, the GS-RL-RANFIST2 performance is compared with the proved GC-PI controller.

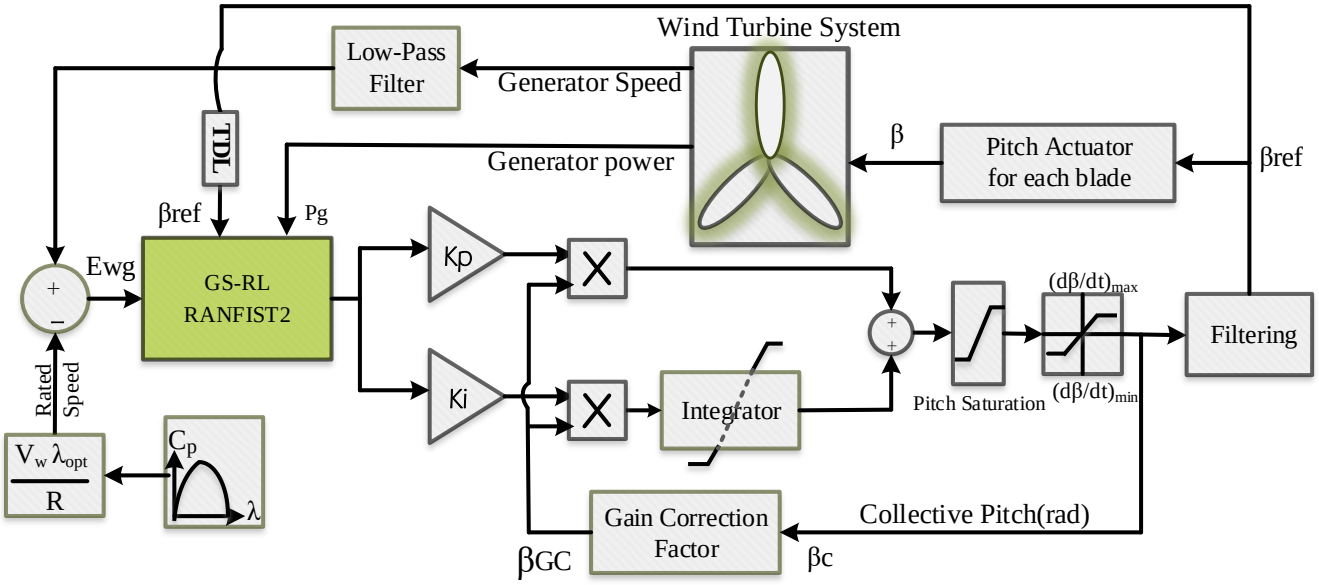

Fig. 5.3. Block diagram of the proposed controller implemented for the CART3.

5.1.2. Case study 2: MPPT for hybrid cascaded RES system

At that point, a PI controller will be used to reach the required reference voltage on the PV panels by adjusting nth shoot-through duty ratio (D). In this case, D_n will also be employed to boost the PV voltage to a higher level. This scheme will allow to obtain an independent MPPT control for each module, which implies obtaining the maximum power for different environmental conditions in different modules. For example, an independent MPPT control of each module of a PV plant is shown in Fig. 5.4. The output voltage and current of each PV string will be detected and inputted to the MPPT controller. The controller will output a reference to the PV close-loop voltage regulator. The PV voltage reference will be refreshed every sample step by using MPPT algorithm. By regulating the shoot-through duty ratio D_n the output voltage of each PV string will be controlled at different values according to the environmental conditions.

The Perturb and Observe (P&O) algorithm is applied to determine the DC voltage of the RES (PV power plant or WT) connected at the input of the qZSI, which allows MPPT to be achieved according to the incident radiation and temperature for the PV power plants and the wind speed for the WT. In each qZSI, D_n is used to control the DC voltage and boost the voltage. The independent MPPT control for the PV power plants and the WT is illustrated in Fig. 5.4.

The DC voltage and current measured for each renewable energy source are used in the MPPT controller to determine the reference DC voltage. A PI controller adjusts D_n to track the reference DC voltage to achieve the RES to operate at MPPT.

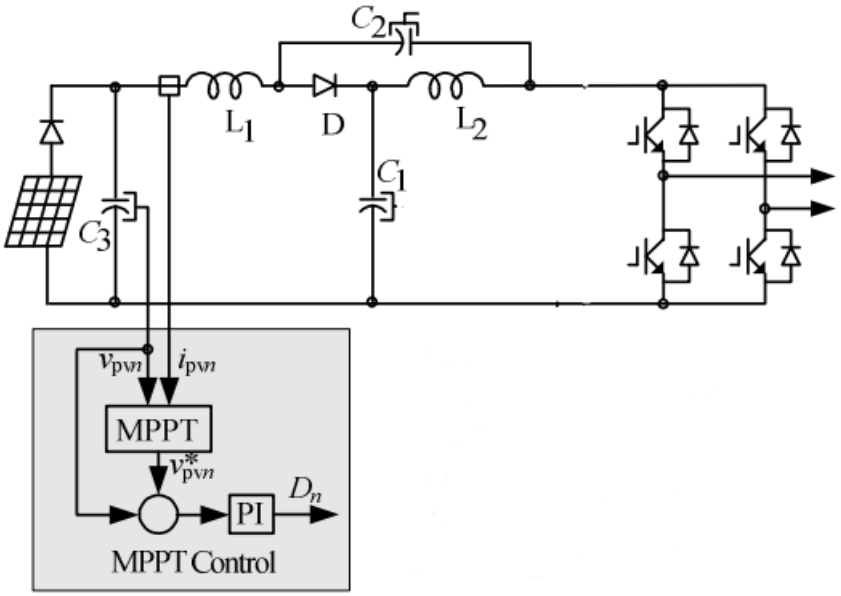

Fig. 5.4. MPPT control strategy.

5.2. Power control

The main objective of the grid power control subsystem is regulating the power injected to the grid according to a set reference as the grid demand. The total power injected to the grid is the sum of each RES output power and ESS. Therefore, the output voltage and current of each module must be controlled accordance with grid parameters. To control the active power (P) and reactive power (*Q*) delivered to the grid, first the phase angle of the grid voltage and current is obtained from a phase locked loop (PLL). The control of P and Q is implemented through separate control loops at a d-q synchronous reference frame, where the d-component is used to control P and *q*-component to control *Q*. In single-phase systems, the voltage and current variables are transformed into orthogonal stationary α-β components, where the imaginary signal β is equal to the real component α but delayed by a ¼ period. The orthogonal α-β components are then converted into a rotation coordinate frame d-q.

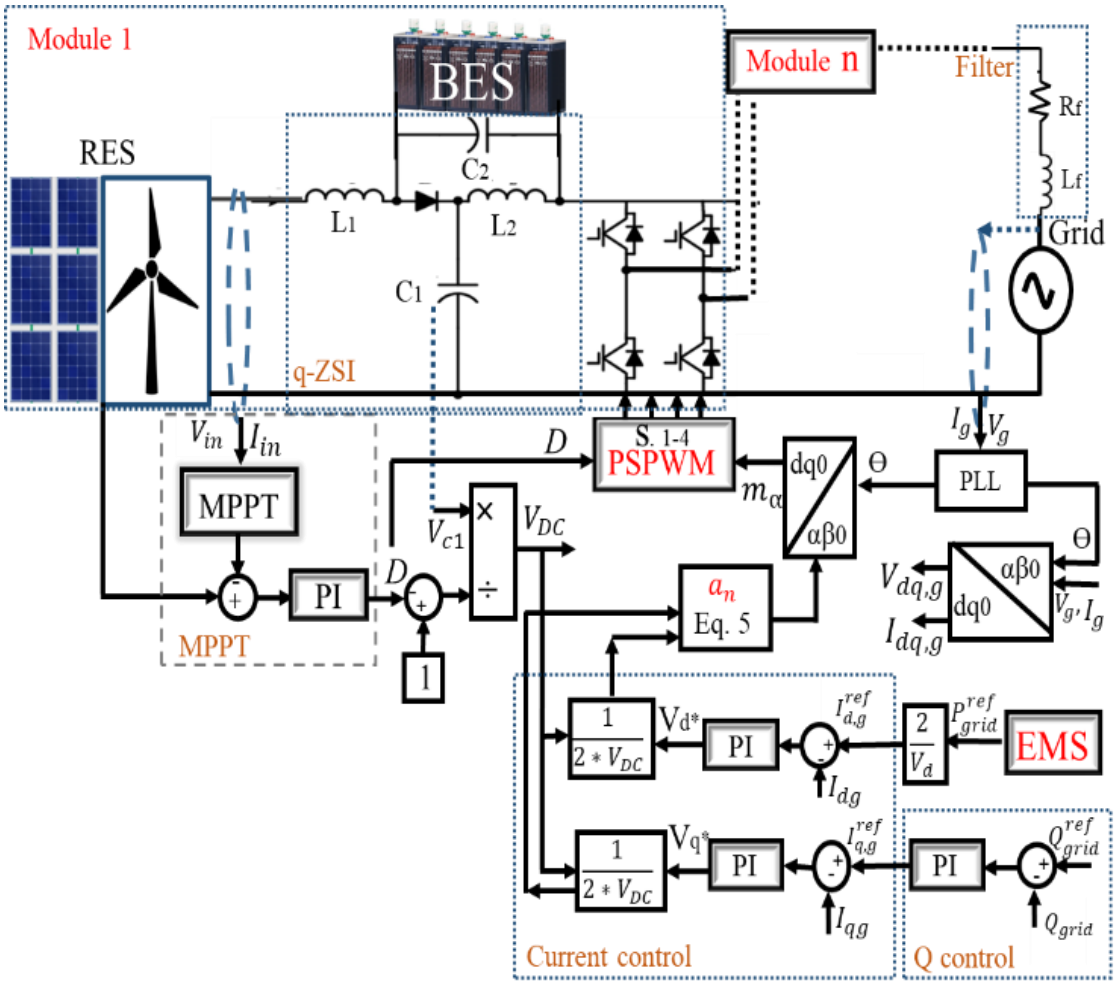

Fig. 5.5. Control schemes of each qZSI module.

Two separate *d-q* control loops are used to control *P* and *Q* delivered to the grid using the modulation index *M*, as shown in Fig. 5.5.

To control *P*, a control loop for the *d*-component current (i_d) is implemented in each qZSI. The total power injected into the grid is the sum power of the RES including the two PV power plants, WT, and BES. Therefore, the total power reference (P_{grid}^{ref}) is calculated as the sum of the power reference for each qZSI (P_i^*) as:

$$P_{grid}^{ref} = \sum_{i=1}^{3} P_i^* \tag{5.26}$$

where i is the number of modules, and P_i^* is calculated by EMS that will be discussed below.

The peak value of the grid current (i_{grid}^*) is calculated by the grid voltage (V_{grid}) and the power reference for each qZSI [112]:

$$i_{grid}^* = \frac{2 \cdot \sum_{i=1}^{3} P_i^*}{V_{grid}} \tag{5.27}$$

Using the phase-shifted-PWM (PS-PWM) method, the *d*-component of the modulation index M_i ($m_{d,i}$) for each module can be calculated by adjusting the *d*-component of the grid voltage (V_d).

$$m_{d,i} = \frac{2 \cdot a_i \cdot V_d}{V_{pn,i}} \tag{5.28}$$

where a_i denotes the power factor of each module, defined as the relationship between the power reference for each qZSI and the total power reference, which can be calculated as follows.

$$a_i = \frac{P_i^*}{P_{grid}^{ref}} \tag{5.29}$$

To control *Q*, a control loop for the *q*-component current (i_q) is implemented in each qZSI (similar to the *P* control scheme) using the *q*-component of M_i ($m_{q,i}$) as the control variable. Once $m_{d,i}, m_{q,i}$ are obtained from the control loops of *P* and *Q*, the *α*-component of the modulation index ($m_{\alpha,i}$) is calculated. Finally, the gate signals for the IGBTs of the ES-qZS-CHBMLI are generated from $m_{\alpha,i}$ and D_i according to the modulation scheme shown in Fig. 4.4.

The phase-lock loop (PLL) determines the phase angle of grid voltage to ensure that the grid current references are in phase with grid voltages. The grid-tie current closed-loop control can be achieved in the two-phase stationary α-β frame using three-phase/two-phase transformation. The practical grid-tie current tracks the sinusoidal references with zero-error using the current controller. Many researchers have developed adaptive controllers in order to get better static and dynamic performances. Some of these controllers are feed-forward controllers, deadbeat (DB) controllers, sliding modes, proportional-resonance (PR) controllers, and repetitive controllers. The PI controller is widely used because it is the easiest controller to implement and for regulating grid active power (P) and reactive power (Q). For this reason, PI regulators are used in this thesis.

Two control loops (a_d and a_q) for the grid control parameters regarding d-q components. The d control loop regulates the error of the d component of the grid current by acting over the inverter reference voltage. This implies that the PI controller adjusts P by modifying the d component of the modulation index (M_d). The q control loop regulates the error of the q component of the grid current and acts just over q component of the inverter reference voltage. This controller adjusts the Q through modifying q component of modulation index (M_q). Once the values of md, mq, and D_n have been attained, the gate signals for the IGBTs of the inverter can be produced from the α -component of the modulation index, shoot-through duty ratio, and the phase angle of the grid voltage. Fig. 5.6 illustrates the power control strategy that is used in this thesis for one of the modules.

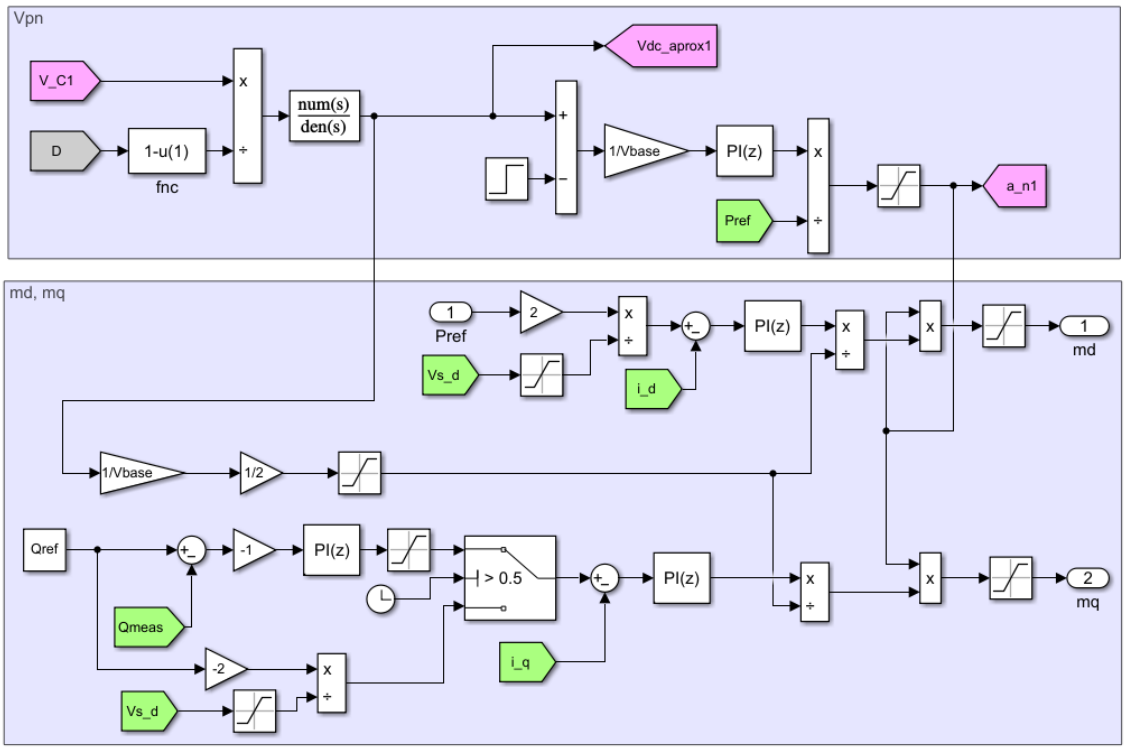

Fig. 5.6. Active and reactive power control strategy.

5.3. Energy management system

In this section, five different EMS control strategies are presented, being applied to the case study presented in the next Chapter. The hybrid system requires a supervisory control system that coordinates the performance of both energy sources (WT, PV, and BESS) and allows a reliable and controlled response. Fuzzy logic controller (FLC), model predictive controller (MPC), optimal EMS (fmincon function optimizer), and reinforcement learning (RL) algorithms have been applied in this thesis and in this section are discussed.

This supervisory control sets the power reference to be provided by/stored in the battery, depending on its SOC and the power mismatching between the power generated by the RESs and the power demanded by the grid. In the other words, the proposed EMSs determine the optimal power of each BES, considering the maximum BES power capacity, limited values of the BES SOC (operation between a maximum and minimum SOC to avoid reducing the BES lifetime), and available power as constraints.

5.3.1. Proportional SOC Energy Management System (SOC-EMS)

This subsection describes an EMS with a proportional sharing algorithm based on the SOC of the BESs (SOC-EMS) [112]. This EMS is executed to dispatch power among the BESs according to their SOC values. The BES with the highest SOC is discharged more than the others, and the BES with the lowest SOC receives more power in the charging mode. Being in charging or discharging mode is defined by the gap between RES power productions and grid demanded power. In this way, the SOC-EMS operates in the charging mode if the total RES power generation is higher than the grid active power reference. On the contrary, if the total PV power

generation is lower than the grid active power reference, the system operates in the discharging mode. The power of the BESs for the charging and discharging modes can be calculated according to equations (5.30) and (5.31) respectively:

$$P_{BES,i}^{char} = \frac{P_{BES,tot} \cdot DOD_i}{\sum DOD_i} \tag{5.30}$$

$$P_{BES,i}^{dischar} = \frac{P_{BES,tot} \cdot SOC_i}{\sum SOC_i} \tag{5.31}$$

where $P_{BES,i}^{char}$ and $P_{BES,i}^{dischar}$ are the power for each BES in the charging and discharging mode, respectively; and $\mathrm{DOD_i}$ denotes the depth of discharge for ith BES.

Considering the battery life factor in designing EMS is common and in [112] two constraints are considered to limit charging or discharging beyond the considered bonds. First, the SOC cannot exceed two thresholds, denoted as $SOClow$ for the discharging mode, and $SOChigh$ for the charging mode. Second, the maximum power that each BES can inject or receive is limited to the rated power of the BES. The different operation conditions of the SOC-EMS are described as: (a). Normal conditions ($SOC_{\mathrm{Min}} < SOC\mathrm{i} < SOC_{\mathrm{Max}}$): Allowing all BESs operate in the discharging or charging mode at the same time according to equations (5.30), (5.31); (b). High SOC value ($SOC_{\mathrm{ni}} \geq SOC_{\mathrm{Max}}$): Avoiding overcharging for the SOC of a certain BES having exceeded the maximum limit if the BESs that are operating in the charging mode. The SOC-EMS decides for that specific BES not to be charged anymore and set its power to zero, and for the rest of BESs the SOC-EMS letting them continue operating in the charging mode until they reach SOC_{Max}; (c). Low SOC value ($SOC_{\mathrm{i}} \leq SOC_{\mathrm{Min}}$): Avoiding overloading for the SOC of a certain BES having exceeded the maximum limit if the BESs that are operating in the discharging mode. The SOC-EMS decides for that specific BES not to be discharged anymore and set its power to zero, and for the rest of BESs the SOC-EMS letting them continue operating in the discharging mode until they reach SOC_{Min}.

5.3.2. Fuzzy Logic Energy Management System (FLC-EMS)

Fuzzy logic control (FLC) is suggested in this thesis as an EMS for the hybrid RES systems that covers a wide range of operating conditions while shows a better dynamic response. The BES power references are defined by the proposed FLC-EMS, taking into account the grid operator requests and the battery SOC values inserted as inputs of FLC. Fig. 5.7 shows the structure of the FLC-EMS, where triangular membership functions are used for representing states of each parameter.

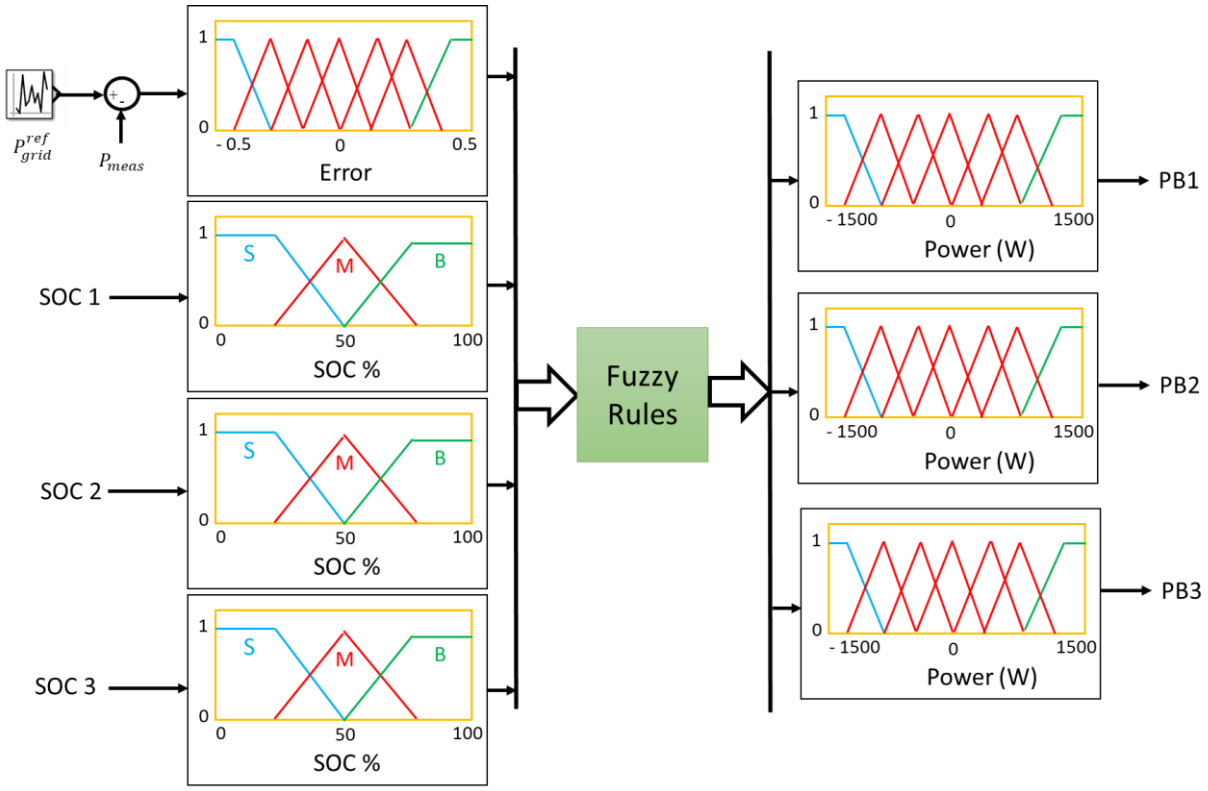

Fig. 5.7. Fuzzy-EMS structure.

The fuzzy controller operates under a list of rules that define the status of the output signals regarding the level of the input signals [138]. Table 5.1 represents the fuzzy rules table including 180 rules to define the output of each battery based on the entered parameters in FLC. Only inequality conditions of SOCs are considered in the rules' table, and the conditions when 2 or 3 BESs have the SOC values are not considered in the table to reduce the complexity of the FLC and simulation time. For the FLC outputs that are batteries reference power (PB1, PB2, PB3), 10 tags are used to represent them as: charge zero (CHZ), charge small (CHS), charge medium (CHM), charge big (CHB), charge very big (CHVB), discharge zero (DZ), discharge zero (DS), discharge medium (DM), discharge big (DB), discharge very big (DVB). For error that is the first fuzzy input, the considered tags are: negative zero (NZ), negative small (NS), negative medium (NM), negative big (NB), negative very big (NVB), positive zero (PZ), positive small (PS), positive medium (PM), positive big (PB), positive very big (PVB).

The ranges of the error (first FLC input) are considered between -1 to 1 to compensate the error more in very specific ranges. And other inputs that are the percentage of SOCs, are defined between 0 to 100 % for the FLC with Mamdani rule-based structure. The ranges of the outputs power to be considered during the membership functions definition are considered between -1500 to 1500 W.

Table 5.1. Fuzzy rules base table.

Param	SOC1 < SOC2 < SOC3 SOC1= S, SOC2=M, SOC3= B			SOC3 < SOC2 < SOC1 SOC1= B, SOC2=M, SOC3= S			SOC1 < SOC3 < SOC2 SOC1= S, SOC2=B, SOC3= M		
PB / Error	PB1	PB2	PB3	PB1	PB2	PB3	PB1	PB2	PB3
NZ	CHS	CHZ	CHZ	CHZ	CHZ	CHS	CHS	CHZ	CHZ
NS	CHM	CHS	CHZ	CHZ	CHS	CHM	CHM	CHZ	CHS
NM	CHB	CHM	CHS	CHS	CHM	CHB	CHB	CHS	CHM
NB	CHVB	CHB	CHM	CHM	CHB	CHVB	CHVB	CHM	CHB
NVB	CHVB	CHVB	CHB	CHB	CHVB	CHVB	CHVB	CHB	CHVB
PZ	DZ	DZ	DS	DS	DZ	DZ	DZ	DS	DZ
PS	DZ	DS	DM	DM	DS	DZ	DZ	DM	DS
PM	DS	DM	DB	DB	DM	DS	DS	DB	DM
PB	DM	DB	DVB	DVB	DB	DM	DM	DVB	DB
PVB	DB	DVB	DVB	DVB	DVB	DB	DB	DVB	DVB
Param	**SOC3 < SOC2 < SOC1 SOC1= M, SOC2=B, SOC3= S**			**SOC2 < SOC1 < SOC3 SOC1= M, SOC2=S, SOC3= B**			**SOC2 < SOC3 < SOC1 SOC1= B, SOC2=S, SOC3= M**		
PB / Error	PB1	PB2	PB3	PB1	PB2	PB3	PB1	PB2	PB3
NZ	CHN	CHN	CHS	CHN	CHS	CHN	CHN	CHS	CHN
NS	CHS	CHN	CHM	CHS	CHM	CHN	CHN	CHM	CHS
NM	CHM	CHS	CHB	CHM	CHB	CHS	CHS	CHB	CHM
NB	CHB	CHM	CHVB	CHB	CHVB	CHM	CHM	CHVB	CHB
NVB	CHVB	CHB	CHVB	CHVB	CHVB	CHB	CHB	CHVB	CHVB
PZ	DP	DS	DP	DP	DP	DS	DS	DP	DP
PS	DS	DM	DP	DS	DP	DM	DM	DP	DS
PM	DM	DB	DS	DM	DS	DB	DB	DS	DM
PB	DB	DVB	DM	DB	DM	DVB	DVB	DM	DB
PVB	DVB	DVB	DB	DVB	DB	DVB	DVB	DB	DVB

5.3.3. Model Predictive Control Energy Management System (MPC-EMS)

This part presents another EMS based on MPC suggested for ES-qZS-CHBMLI in [139] for multi-objective control targets. MPC is a feedback control technique based on a model and an optimization algorithm for multiple-input multiple-output (MIMO) linear time-invariant (LTI) systems. This controller allows weighting each controlled variable according to its importance in the control of the system [139]. It is designed to meet active and reactive grid requested powers with an optimal power distribution among the BESs according to their SOC values and making sure the SOC values don't across the operating values.

BESs SOC levels and total BES power are considered as inputs and three BESs current references as outputs, to allow an optimized tracking of the active and reactive powers delivered to the grid. To dispatch power based on SOC values, constraints are defined to keep the BESs operating between MAX and MIN permission of charging and discharging bands.

The structure of the proposed MPC is shown in Fig. 5.8. MPC works with three types of variables: manipulated, measured and disturbances. The manipulated variables (MV) are the control signals applied to the plant. The measured outputs (MO) are the signals to be controlled in order to track the imposed references. Additionally, perturbations can be considered through the measured or unmeasured disturbances (MD, UD) inputs. The optimization of the cost function is carried out within a prediction horizon (PH). The cost function (J) is given by (15) [139]:

$$J = \sum_{i=1}^{PH} [y(k+i|k) - w(k+i|k)]^2 \lambda_1 + \sum_{i=1}^{N} [\Delta u(k+i-1|k)]^2 \lambda_2 \tag{5.32}$$

This function penalizes the deviation of the measured outputs (y) from their reference values (w) on one hand, and on the other hand, the control effort (Δu) required to track the reference signal. This calculation is carried out each time step (k), for every future instant (i), within a prediction and a control horizon (PH and N, respectively). Moreover, the relative importance of each term is defined through the weighting matrices $\lambda_1$and λ_2. The aim of MPC is to minimize the cost function (J), that is, to achieve an adequate tracking of the reference signals with the minimum control effort. In this sense, MPC uses quadratic programming (QP) to solve the optimization problem. In this work, the matrices composing the MIMO system for the MPC are:

$$y = \begin{bmatrix} SOC_1 \\ SOC_2 \\ SOC_3 \\ P_{BESS,tot} \end{bmatrix} \quad u = \begin{bmatrix} I_{BES,1}^{ref} \\ I_{BES,2}^{ref} \\ I_{BES,3}^{ref} \end{bmatrix} \tag{5.33}$$

$$w = \begin{bmatrix} SOC_1^{ref} \\ SOC_2^{ref} \\ SOC_3^{ref} \\ P_{BESS,tot}^{ref} \end{bmatrix} \quad \lambda_1 = \begin{bmatrix} \tau_1 & 0 & 0 & 0 \\ 0 & \tau_2 & 0 & 0 \\ 0 & 0 & \tau_3 & 0 \\ 0 & 0 & 0 & \tau_4 \end{bmatrix} \lambda_2 = \begin{bmatrix} \gamma_1 & 0 & 0 \\ 0 & \gamma_2 & 0 \\ 0 & 0 & \gamma_3 \end{bmatrix} \tag{5.34}$$

where $P_{BESS,tot}^{ref}$ denotes the reference total power of the BESSs. As shown in Fig. 5.8 the inputs (y) are the SOC and the total power of the BESSs (SOC_n and $P_{BESS,tot}$, respectively). The latter is calculated as the sum of the active power of each BES, as in equations (5.35)–(5.36):

$$P_{BES,n} = V_{BES,n} \cdot I_{BES,n} \tag{5.35}$$

$$P_{BES,tot} = \sum P_{BES,n} \tag{5.36}$$

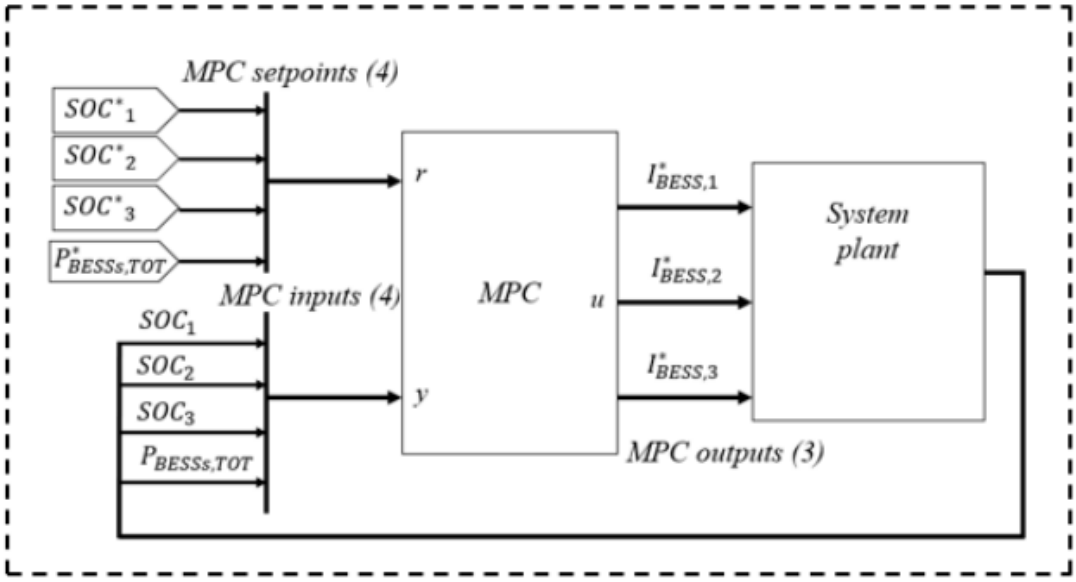

Fig. 5.8. Overall MPC-EMS [139].

The MPC is designed with the Model Predictive Control Toolbox. The first step in the MPC design is to linearize the plant model with the Simulink Control Design Toolbox. The constraints of Max SOC and Min SOC are considered 90% and 15%, respectively. The SOC reference is set to the average value between these thresholds, i.e., SOC_n = 52,5 %. $P_{BESS,tot}^{ref}$ is defined using a PI controller that tracks P_{grid} with P_{grid}*. However, it is necessary to set constraints for the optimization problem. In this case, the BESs currents and $P_{BESS,tot}$ are limited strictly according to their rated values for the charging and discharging modes to ±43.63 A and ± 3600 W, respectively. At the end, a weighting factor of 500 is used for $P_{BESS,tot}$ (high priority), while a weighting factor of 0.1 (below average priority) is set for SOC_n. The next step in the design of the MPC is to establish the weighting factors. The MPC prioritizes the tracking of $P_{BESS,tot}^{ref}$.

5.3.4. Fmincon Function Energy Management System (OPT-EMS)

The aim of the fmincon EMS (here is called (OPT-EMS)) is to define the BES power reference of the BES integrated into the ES-qZS-CHBMLI to optimize the BES efficiency while satisfying the system power balance and providing the active and reactive powers demanded by the grid. Fig. 5.9 illustrates the control scheme implemented in the EMS.

In this EMS, an objective function (equation (5.37)) based on optimizing the global BES efficiency of the hybrid power plant is suggested, and a constrained nonlinear multivariable algorithm, by fmincon Matlab function, is applied to determine the optimal solutions. The constraints defined for fmincon function are based on the maximum BES power capacity, limited values of the BES SOC, and available power (difference between the PV power and grid demand). The global BES efficiency to be maximized (η_{BES}) is calculated from equation (5.38) dividing the input powers of the BES into the output powers and efficiencies of each device:

$$min\,\{OF = 1 - \eta_{BES}\} \tag{5.37}$$

$$\eta_{BES} = \frac{P_{BES,1} + P_{BES,2} + P_{BES,3}}{P_{BES,1}^{in} + P_{BES,2}^{in} + P_{BES,3}^{in}} = \frac{P_{BES,1} + P_{BES,2} + P_{BES,3}}{\left(P_{BES,1}/\eta_{BES,1}\right) + \left(P_{BES,2}/\eta_{BES,2}\right) + \left(P_{BES,3}/\eta_{BES,3}\right)} \tag{5.38}$$

Where $P_{BES,1}$, $P_{BES,2}$, $P_{BES,3}$ are the BES powers, and $\eta_{BES,1}, \eta_{BES,2}, \eta_{BES,3}$ are the BES efficiency for the BES 1, 2 and 3, respectively, and which are calculated by equation (5.39).

$$\eta_{BES,i} = \begin{cases} 0.5.* \left(1 + \sqrt{\dfrac{1 - 4 * R_{BES,i} * P_{BES,i}}{(V_{BES,i})^2}}\right) discharge \\ 2./\left(1 + \sqrt{\dfrac{1 - 4 * R_{BES,i} * P_{BES,i}}{(V_{BES,i})^2}}\right) charge \end{cases} \tag{5.39}$$

where $R_{BES,i}$ is the BES resistance, and $V_{BES,i}$ is the BES voltage.

In the implementation of the optimization problem, the power balance (equality constraint) and power limits (constraint bounds) must be considered.

- *Power balance*:

A linear equality constraint based on the power balance is considered in the EMS to share power among the BES. Based on the nominal power of the BES and BES output power, the power equality constraint limits the output of the algorithm. The sum of the BES powers ($P_{BES,tot}$) must be equal to the reference value obtained as the output from a PI controller, which compares the reference grid power with the measured grid power.

$$P_{BES,tot} = \sum_{i=1}^{3} P_{BES,i} \tag{5.40}$$

Since there are three qZSI in series and each one integrates a BES, the equality constrain is applied as

$$A_{eq} \cdot [P_{BES}] = b_{eq} \tag{5.41}$$

where $A_{eq} = [1\ 1\ 1]$, and $b_{eq} = P_{grid}^{*} - P_{grid}$.

- *Power limits*:

In the charging mode, the BES power can be adjusted to [-$P_{BES,i}^{max,char}$0], whereas, in the discharging mode, the power bounds are [0, $P_{BES,i}^{max,dischar}$]. The maximum powers of the BES are calculated by the following expression:

$$P_{BES,i}^{max,char} = min\left(P_{BES,i}^{nom}, \frac{E_{BES,i}^{nom}}{\Delta t}.\left(\frac{100 - SOC_{BES,i}}{100}\right)\right) \quad (5.42)$$

$$P_{BES,i}^{max,dischar} = min\left(P_{BES,i}^{nom}, \frac{E_{BES,i}^{nom}}{\Delta t}.\left(\frac{SOCmin_{BES,i} - SOC_{BES,i}}{100}\right)\right) \quad (5.43)$$

where $E_{BES,i}^{nom}$ is the nominal energy of the i^{th} BES and $SOCmin_{BES,i}$ is the minimum value of the SOC that the i^{th} BES can have. The minimum SOC and nominal energy of each BES are considered in the optimal EMS as constraints to avoid issues in BESs that can reduce their lifetime.

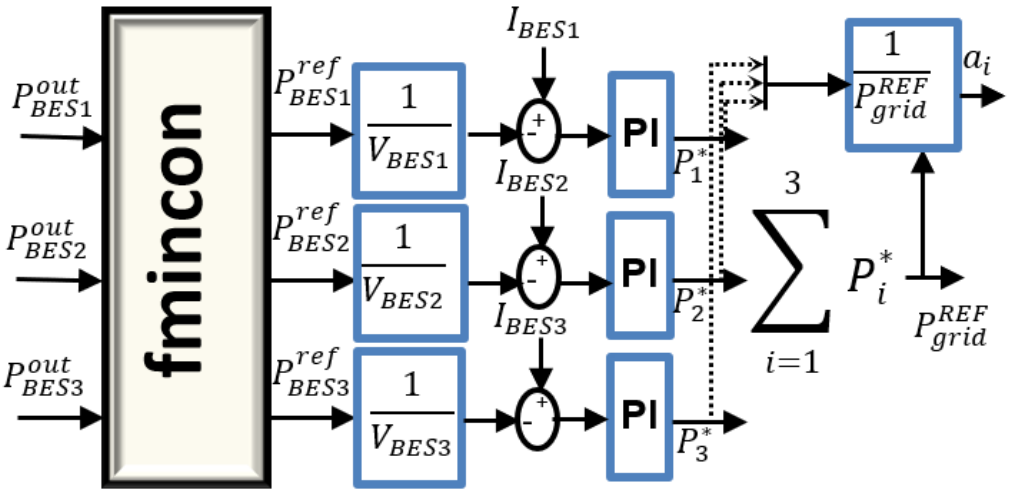

Fig. 5.9. OPT-EMS structure.

5.3.5. Reinforcement Learning Algorithm Energy Management System (RL-EMS)

One of the main contributions of this thesis is implementing an artificial intelligent EMS allowing to optimize the use of the BES integrated into the ES-qZS-CHBMLI associated to each PV power plant. A novel EMS based on RL is proposed for the optimal power balance among the BES used in the ES-qZS-CHBMLI. The RL algorithm is placed on the limit values of the BES SOC, the maximum BES power capacity, and the available power (difference between the PV power and the grid demand). The system to be trained by RL must be defined by the Markov Decision Process (MDP) [140]. To have MDP, three main components must be well defined: environment, including states and actions, agent, and reward function. MDP is based on agent-environment interactions that are executed over a sequence of time-steps taking Actions (A_t) in the given State (S_t), where every S_t and A_t, affect the next state, S_{t+1}. In the following, these three main terms are discussed for the case under study.

- *Environment*:

To create the environment variable, variables must be defined to represent the states and actions. rlSimulinkEnv function is used to create a variable that represents an environment simulated with the Simulink model. Regarding state term, the rlNumericSpec function is used to create a variable to represent numeric observable states (as here the observations are continuous numeric values), with the dimensions of the observations as input.

For multiagent RL, the reference ∑ BES power (∑ BES*), the measured ∑ BES power, the error and the integral error of comparing ∑ BES* and ∑ BES, BES power limits error and its integral, represented in equations (5.44), (5.45), are considered as the state values for both agents. For the other proposed single agent RL algorithm, the states are presented in equations (5.46).

$$S_{t,A} = [\sum BES^*, \sum BES, (\sum BES^* - \sum BES), \int (\sum BES^* - \sum BES), (P_{BES,n}^{maxchar} - P_{BES,n}^{char}), \int (P_{BES,n}^{maxchar} - P_{BES,n}^{char})] \quad (5.44)$$

$$S_{t,B} = [\sum BES^*, \sum BES, (\sum BES^* - \sum BES), \int \left(\sum BES^* - \sum BES\right), (P_{BES,n}^{maxdischar} - P_{BES,n}^{dischar}), \int (P_{BES,n}^{maxdischar} - P_{BES,n}^{dischar})] \quad (5.45)$$

And for a single agent RL

$$S_{t,A} = [\sum BES^*, \sum BES, (\sum BES^* - \sum BES), \int (\sum BES^* - \sum BES), (P_{BES,n}^{max} - P_{BES,n}), \int (P_{BES,n}^{max} - P_{BES,n})] \quad (5.46)$$

The rlNumericSpec function is used to create a variable to represent numeric actions. The actions are considered the BES charging and discharging output power for agent A and agent B, respectively.

$$a_{t,A} = [P_{BES,1}^{char}, P_{BES,2}^{char}, P_{BES,3}^{char}] \quad (5.47)$$

$$a_{t,B} = [P_{BES,1}^{dischar}, P_{BES,2}^{dischar}, P_{BES,3}^{dischar}] \quad (5.48)$$

For a single agent RL the batteries output powers are considered as RL actions, no matter of bien in charging or discharging mode.

$$a_t = [P_{BES,1}, P_{BES,2}, P_{BES,3}] \quad (5.49)$$

Sometimes the actions or observations have physical limits. For the configuration under study, the states are forces normalized to the range [-1 1] and the actions are forces normalized

to the range $[P_{BES,n}^{maxchar} \ 0]$ for charging and $[0 \ P_{BES,n}^{maxdischar}]$ for discharging mode, using the "LowerLimit" and "UpperLimit" options to specify bounds on a numeric variable.

- *Agent*:

Based on the need for continuous actions, two Twin-Delayed deep deterministic (TD3) agents are chosen to generate appropriate BES powers. TD3 is an actor-critic RL agent that is represented by Q-value critic to implement the policy by a function approximator [141]. As TD3 is a state-action value-based agent type, the optimal policy can be derived from founded optimal state-action value, and therefore, it is suitable for control applications. In Q-learning, the value function can be learned based on the Bellman equation [140]. The Bellman equation represents a relationship between the value of a state-action pair (s, a) and the value of the subsequent state-action pair (s´, a´). A discount factor *γ is* considered to weight later rewards over time. It is applied to avoid infinitely growth of cumulative reward (especially for very long episodes) known as an expected total return R, then the Bellman equation is defined as:

$$\mathrm{Q}_{new}^{\pi}(s,a) = \mathrm{Q}_{current}^{\pi}(s,a) + \alpha\,[r(s,a) + \gamma\mathbb{E}[\mathrm{Q}^{\pi}(s',a')] - \mathrm{Q}_{current}^{\pi}(s,a)] \tag{5.50}$$

where α is the learning rate and π is the selected policy. Here, two critic networks $\mathrm{Q}_{\theta 1}$, $\mathrm{Q}_{\theta 2}$ are used, and the training algorithm starts by initializing critics and actor network π_ϕ with random parameters θ_1, θ_2, ϕ. Each target critic and target actor initialize with the same random parameters as $\mathrm{Q}_{\theta 1}(s,a)$, $\mathrm{Q}_{\theta 2}(s,a)$, π_{φ}(s). For each training time step, actions are selected with stochastic noise as $a = \pi_{\varphi}(s) + \epsilon$, ($\epsilon \sim N(0,\sigma)$) and the reward *r* and new states are observed and the experience is stored in the experience buffer *(s,a,r, s´)*. Then, a mini-batch of M transition from the experience buffer is sampled (s_i, a_i, r_i, s_i') and the value function target is set as [141]:

$$y_i = R_i + \gamma * min_{j=1,2}(\mathrm{Q}'_{\theta j}(s'_i, clip(\pi_{\varphi}(s'_i) + \epsilon) \tag{5.51}$$

Equations (5. 51) represents the sum of the experience reward R_i and the minimum discounted future reward from the critics. Next step is updating the critic and actor. The critic is updated through minimizing [141]:

$$L_{j=1,2} = \frac{1}{2M}\sum_{i=1}^{M}(y_i - \mathrm{Q}_{\theta j}(s_i, a_i))^2) \tag{5.52}$$

where, the loss L_j is minimized across all sampled experiences.

The actor is updated through the deterministic policy gradient to maximize the expected discounted reward as follows for observation s_i [141]:

$$\nabla_{\varphi} J(\varphi) = M^{-1}\sum_{i=1}^{M} \nabla_{\varphi}\,\pi_{\varphi}(s_i)\,\nabla_{ai}\mathrm{Q}_{\theta j}(s_i,a)|_{a=\pi_{\varphi}(s_i)} \tag{5.53}$$

where, $\nabla_{\varphi}\,\pi_{\varphi}(s_i)$ is the gradient of the actor output with respect to the actor parameters, and $\nabla_{ai}\mathrm{Q}_{\theta j}(s_i,a)$ is the gradient of the minimum critic output respect to the action find by actor network. Finally, the target network is updated by a smoothing factor.

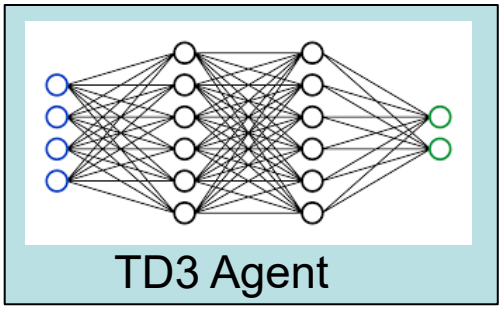

Fig. 5.10. An insight to a neural network of a TD3 agent.

- *Reward Function*:

The index of how well the actions are progressing is defined by the reward (*Rt*) function. The agent follows a policy (strategy to pick actions) that maximizes its total accumulated reward over all time-steps. Different reward function types have been discussed in [142] in Fig. 7 that depicts four reward functions commonly used. Here in our work, the first-order linear function is employed as reward functions to dispatch BES power. First, two BES power limitation terms have been introduced in the last subsection (equations (5.42), (5.43) [143]) to consider SOC safety and BES maintenance issues. In the charging mode, the BES power can be adjusted to [-$P_{BES,i}^{max,char}$0], whereas, in the discharging mode, the power bounds are [0, $P_{BES,i}^{max,dischar}$]. The maximum powers of the BES are calculated by the equations (5.43). The reward function is defined in a way that the agent seeks less penalty to increase accumulated reward. The error of produced ∑ BES power and the reference ∑ BES power, the error of band limitation error for every battery and the measured BES power, and a small penalty for previous actions (for the first 500 episodes), are considered as reward functions.

$$R_{t,A} = \left|\sum P_{BES}^{char^*} - \sum P_{BES}^{char}\right| \times (-1) + \left|P_{BES,n}^{maxchar*} - P_{BES,n}^{maxchar}\right| \times (-0.1) + \left|z^{-1}P_{BES,n}^{char}\right| \times (-0.001) \quad (5.54)$$

$$R_{t,B} = \left|\left(\sum P_{BES}^{dischar^*} - \sum P_{BES}^{dischar}\right)\right| \times (-1) + \left|P_{BES,n}^{maxdischar*} - P_{BES,n}^{maxdischar}\right| \times (-0.1) + z^{-1}P_{BES,n}^{dischar} \times (-0.001) \quad (5.55)$$

Now that all components of MDP are defined, the RL algorithm can be used for the system under study in this thesis. Fig. 5.11 illustrates how two suggested agents are implemented as EMS. One agent is considered for charging and another one for discharging. External actions are used to makes the training easier by distinguishing system modes for agents, where in the charging mode the agent that was considered for discharging modes must produce zero vectors, and vice versa.

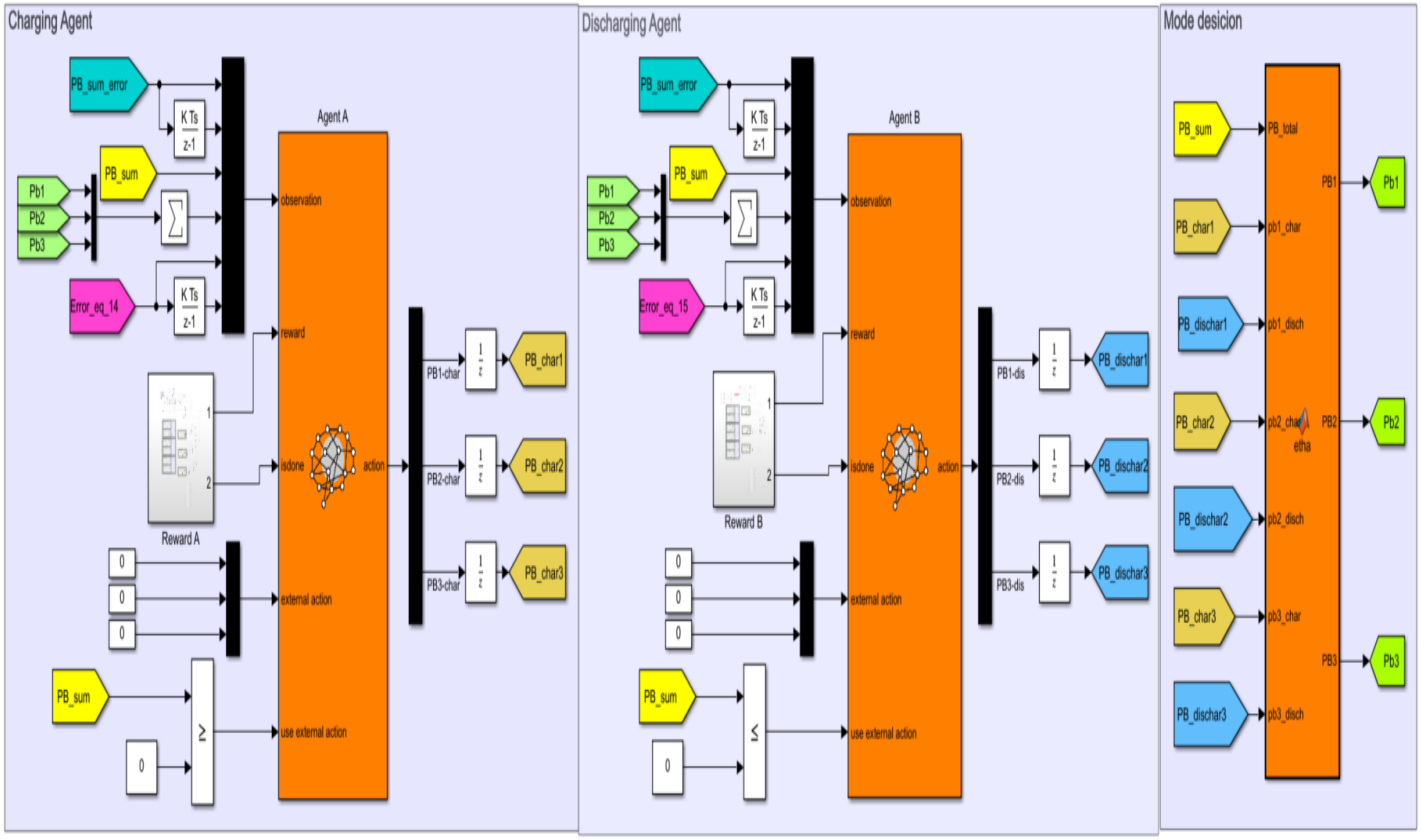

Fig. 5.11. Multiagent RL EMS.

However, using two agents makes learning process much more complicated and time consuming. Even it is so potential that multi agents' usage makes interventions in MDP that doesn't allow agents to learn. Hence, single agent Rl algorithm is more recommended.

CHAPTER 6

CAPÍTULO SEIS

6. Results and discussion

The main results of the simulations carried out to test and compare the configurations proposed in the previous chapter are discussed here. An analogous structure and order is followed in this section.

6.1. EMS comparison

The proposed EMSs in the previous chapter are compared under different working conditions and configurations. Dynamic response of the PV and hybrid RES with BES are presented here. The simulations have been carried out under ramping wind speed and varying irradiance values. In addition, the active and reactive power references also change along the simulation as the grid demand varies. Based on the RES type an EMS, different cases are introduced to be discussed separately. In all cases, the total system power is 14.400 kW, composed of three 4.8 kW independent PV power plants or combination of PV and WT, with a layout of 6 modules in parallel and 2 in series for each PV plant. The main parameters of the impedance network of the qZSI are: $L_1 = L_2 = 0.56mH$, $R_{L1} = R_{L2} = 0.05\ \Omega, C_1 = C_2 = 11mF$. The carrier frequency selected for the inverter technique modulation is $f_c = 3.5\ kHz$.

6.1.1. Case 1: PV plants – EMS: fmincon function (OPT)

In this case, the PV power plants are considered as the sources of each module of the multilevel inverter. The total system power is 14.400 kW, composed of three 4.8 kW independent PV power plants, with a layout of 6 modules in parallel and 2 in series for each PV plant. The BES is a Lithium-Ion BES connected in parallel with the capacitor C_{2_n}, without additional DC/DC converter. Three different BESs are considered in this case. The main parameters of the BES 1, 2 and 3 are presented in Table 6.1, Table 6.2 and Table 6.3, respectively.

Table 6.1. Case 1. Parameters of BES1.

E_{nom} (Wh)	V_{nom} (V)	R (Ω)	P_{nom} (W)	Initial SOC (%)	Capacity (Ah)
1200	27.5	0.006303	1200	75	43.63

Table 6.2. Case 1. Parameters of BES2.

E_{nom} (Wh)	V_{nom} (V)	R (Ω)	P_{nom} (W)	Initial SOC (%)	Capacity (Ah)
1309	25	0.004773	1309	50	52.37

Table 6.3. Case 1. Parameters of BES3.

E_{nom} (Wh)	V_{nom} (V)	R (Ω)	P_{nom} (W)	Initial SOC (%)	Capacity (Ah)
1985	35	0.006169	1985	25	56.73

The initial conditions of the PV power plants are: PV power plant 1 (PV1): 800 W/m^2; PV power plant 2 (PV2): 900 W/m^2; and PV power plant 3 (PV3): 700 W/m^2. These operating conditions are changed to 600 W/m^2 at 1.5 s for all the PV power plants. The temperature is kept at 25ºC. The grid active power reference (P^*_{grid}) is set to 8.16 kW during the first 7.5 seconds (from 0 to 7.5 s), and it changes to 9.12 kW from 7.5 to 12 s. The grid reactive power reference (Q^*_{grid}) is set to 0 kVAr (unity power factor) and it changes to -0.1 kVAr at 5.5 second.

Fig. 6.1 shows the power dispatch for the BES along with the simulation. From 0 to 2.5s, the PV plants produce more power than the grid demand, so that the power excess is stored in the BES. The OPT-EMS decides the power to be stored into each BES according to their SOC values (Fig. 6.2), so that the BES 3 is charged with higher power because it has lowest SOC. From 2.5 to 7.5s, the total power generated by the three PV plants is almost equal to the power demanded by the grid, and thus, the EMS decides not to charge or discharge the BES. At 7.5 s, the grid demand increases, and the PV plants cannot fulfil the required power, and then, the BES are demanded to provide power, and thus, they are discharged. As the BES 1 has the highest SOC, it is discharged more than others.

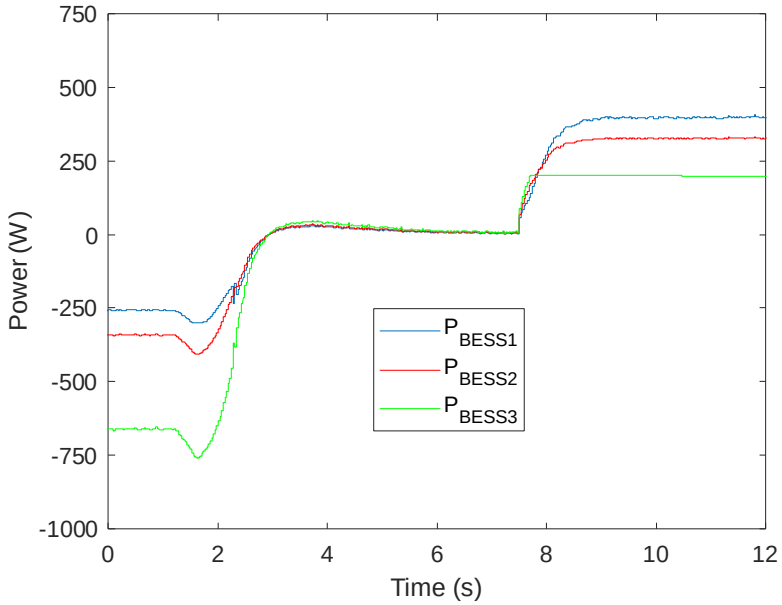

Fig. 6.1. Case 1. BES powers.

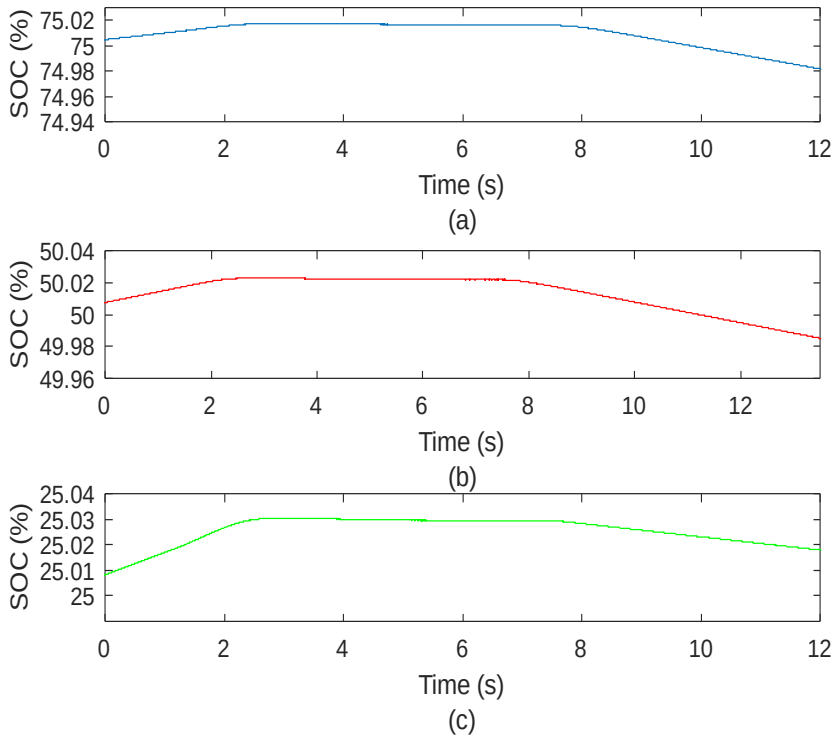

Fig. 6.2. Case 1. BES SOC: BES1, BES2, and BES3.

The active and reactive power delivered to the grid are illustrated in Fig. 6.3. The results show that the EMS allows the active and reactive powers to be controlled according to the reference values along the simulation. The reactive power is controlled at 0 pu (unity power factor) during the first 5.5 s and at -0.1 pu from 5.5 s. The active power is changed from 1.7 pu to 1.9 pu at 7.5 s. At 2.5 s the performance of the EMS ensures that the system tracks the reference values despite the reduction in PV production owing to the change in incident radiation.

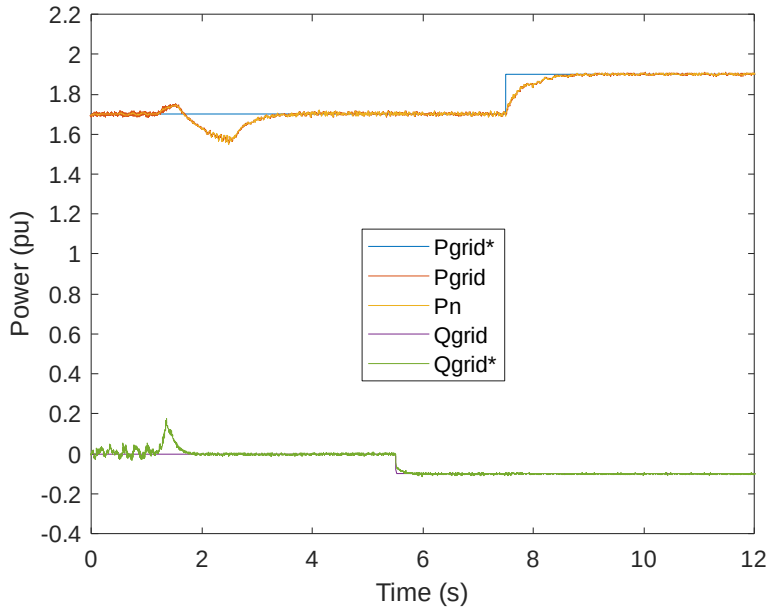

Fig. 6.3. Case 1. Grid active and reactive power.

The seven-level output voltage of the ES-qZS-CHBMLI with 3 cascade qZSI is shown in Fig. 6.4. (a), and the grid voltage and current are illustrated in Fig. 6.4. (b). Because the system operates with unity power during the first 5 seconds, the voltage and the current are in phase, as observed in Fig. 6.4. (b).

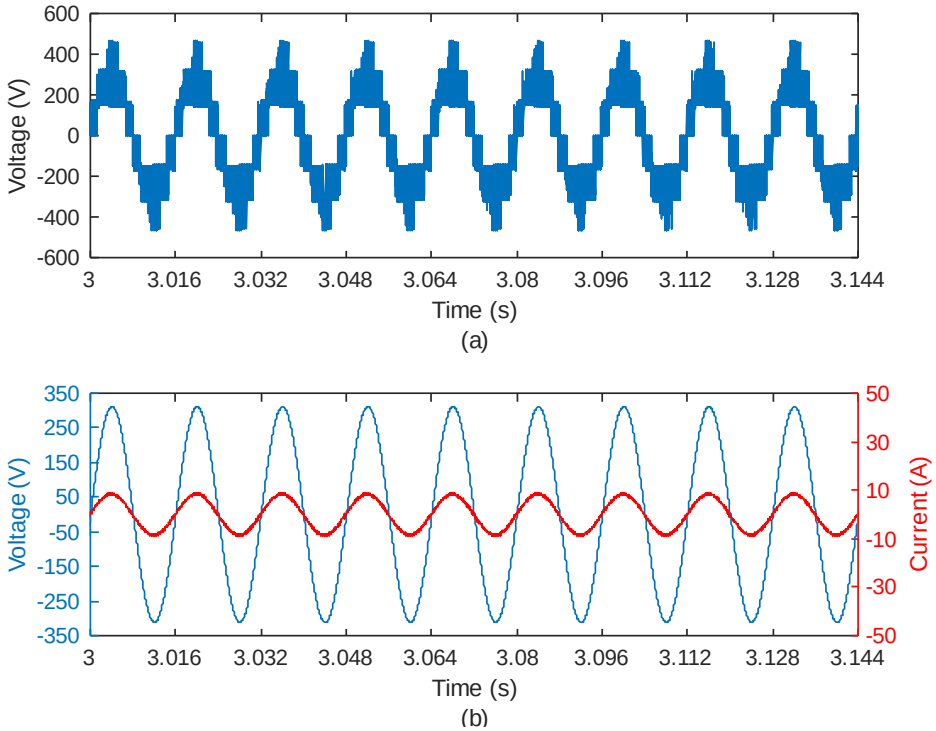

Fig. 6.4. Case 1. a) Seven-level output voltage of the ES-qZS-CHBMLI. (b) Grid voltage and current.

The BESS efficiency is illustrated in Fig. 6.5, where it can be seen that for both the charging and discharging modes, the efficiency is near the maximum value and when the BESS power is zero, the efficiency is maintained at 1. The simulation results prove that the proposed EMS can maintain the power at the reference values when the irradiation change or power reference increases, while the BES efficiency is optimized.

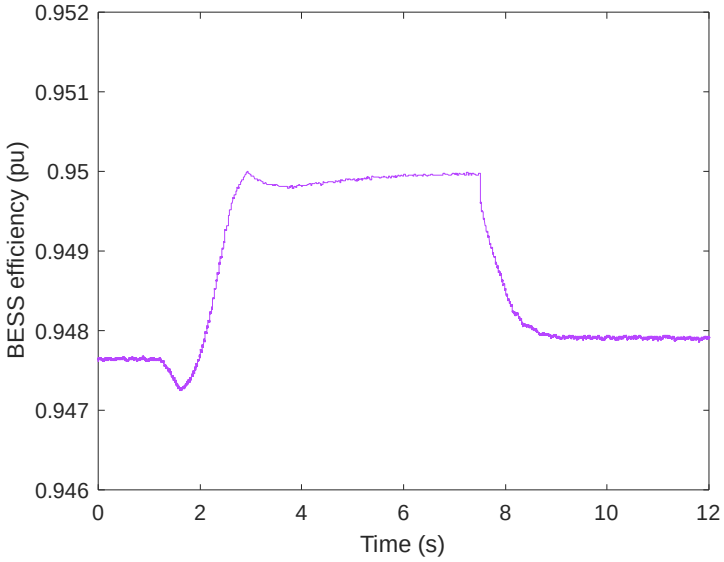

Fig. 6.5. Case 1. Grid active and reactive power.

An optimal EMS for a grid-connected ES-qZS-CHBMLI with three modules in series and PV power generation was proposed here. The EMS was based on optimizing the BES efficiency and lifetime through introducing an objective function and is solved by a nonlinear solver called fmincon function. The optimizer constraints were set to meet the grid demand, consider the SOC values between minimum and maximum values, and power distribution based on BES SOC. The simulation results showed that the proposed control system effectively controlled the power injected to the grid under different irradiation conditions and reference setpoints while the EMS equilibrated the BES power.

6.1.2. Case 2. A. Simulation results: Hybrid PV and WT power sources – EMS: OPT- SOC – MPC

The hybrid power plant under study here is composed of a 5-kW wind turbine and two 4.8 kW independent PV power plants, with a layout of six modules in parallel and two in series for each PV plant, whose total rated power is 14.4 kW. The results used to evaluate the proposed EMS in the previous part, under variable energy resources (solar irradiation and wind speed) and active and reactive power references defined by the system operator are presented and discussed in this section. These results are compared with those obtained from a conventional EMS based on the BES SOC and balancing power algorithm, denoted as SOC-EMS, which was used in [143] and almost similar model predictive control (MPC) EMS used in [139]. Taking advantage of the qZSI, a Lithium-Ion BES is connected in parallel with the capacitor $C_{2,i}$ of each qZSI, without an additional DC/DC converter. Three different BES are considered in this study under different initial conditions. The main parameters of the BES 1, 2 and 3 are presented in Table 6.4. The BES can operate between a maximum SOC of 90% and a minimum SOC of 20% to avoid issues in BESs that can reduce their lifetime, which are considered in the implemented EMS.

Table 6.4. Case 2.A. Parameters of BESs.

Param / **Battery**	E_{nom} (Wh)	V_{nom} (V)	R (Ω)	P_{nom} (W)	*SOC* (%)	*Capacity* (Ah)
BES1	1200	27.5	0.1261	1200	30	43.63
BES2	1571	30	0.1146	1571	50	52.37
BES3	1986	35	0.1234	1900	85	56.73

Fig. 6.6 illustrates the operating conditions of the RES of the hybrid power plant: solar radiation and output power of each PV power plant (PV1 and PV2), and the wind speed and WT output power. PV power plant are considered to work under different irradiances conditions. The initial conditions of the PV power plants are: PV power plant 1 (PV1): 800 W/m2; PV power plant 2 (PV2): 850 W/m2. The operating conditions for PV1 changes at t= 50, 55, 70 s to 750, 800, 850 W/m2 and for PV2 changes at t= 50, 55, 70 s to 800, 870, 900 W/m2. The temperature is kept at 25^{o} C for both PV plants. A real wind pattern is used for WT with wind speeds between 9 and 11 m/s.

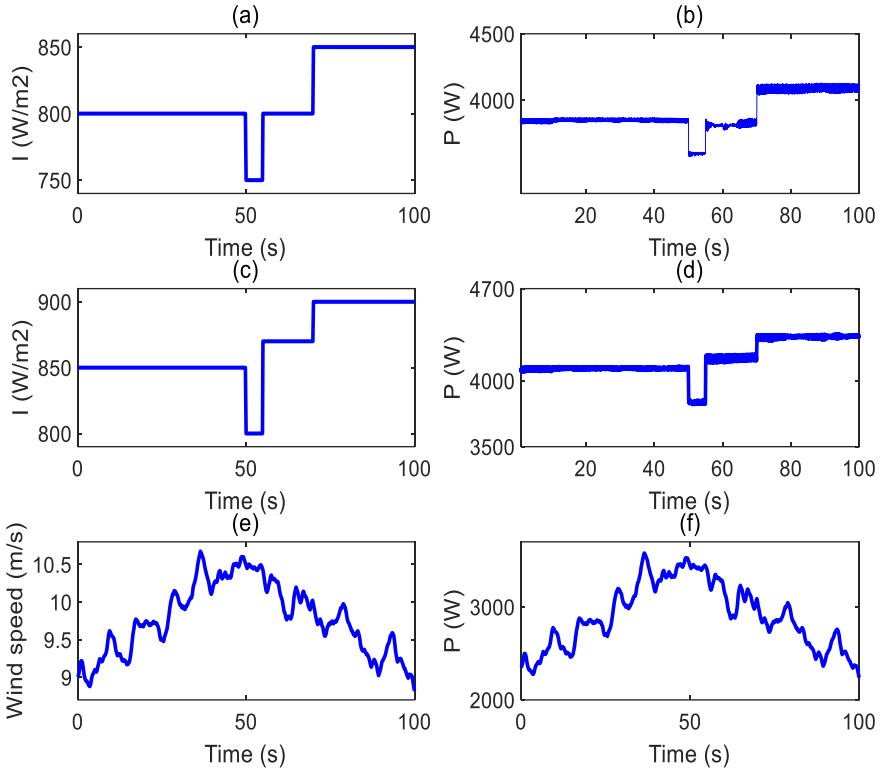

Fig. 6.6. Case.2. A. (a) PV1 irradiance, (b) PV1 output power, (c) PV2 irradiance, (d) PV2 power plant, (e) wind speed, (f) WT output power.

Table 6.5 presents the grid active and reactive power reference profiles used to evaluate the performance of the control systems during the simulation. The grid active power references are increased during the first 40 s and decreased for the rest of the simulation to evaluate the hybrid power plant in the charging and discharging modes of the BES. In addition, positive and negative references of grid reactive power are considered to evaluate the hybrid power plant under generation and consumption of reactive power.

Table 6.5. Case 2.A. Parameters of grid references.

Time (s)	***P* (pu)**	***Q* (pu)**
0	2.28	0
10	2.46	0
15	2.46	- 0.1
20	2.5	- 0.1
30	2.55	- 0.3
40	2.5	0
50	2.2	0
55	1.825	0
60	1.75	0
70	1.75	0
75	1.75	0.1
80	1.7	0.1
90	1.65	0.1

The simulation setup parameters are represented in Table 6.6, where the power sources, grid base and filter parameters, simulation sample time, and inverter nominal voltage are given.

Table 6.6. Case.2. A. Parameters of the simulation setup.

Param	*Value*	*Unit*
P_{pv1}	4800	W
P_{pv2}	4800	W
P_{WT}	5000	W
V_{base}	220√2	V
I_{base}	15.42	I
S_{base}	4800	W
D_{nom}	0.2	-
f_{nom}	50	Hz
R_f	0.001	Ohm
L_f	0.005	H
Ts	10^{-6}	S
$V_{nom\text{-}dc}$	159.7	V
$Kp\text{-}_{battery\text{-}current}$	0.035	-
$Ki\text{-}_{battery\text{-}current}$	2.5	-

The results obtained for all EMSs for the active and reactive powers delivered to the grid are shown in Fig. 6.7. As can be observed, three EMS achieve suitable control of the active and reactive powers of the hybrid power plant delivered with the grid. The hybrid power plant can track the changes in the active and reactive powers by properly controlling the RES, BES and qZSI, despite the changes in the incident radiation of the PV power plants, and the wind speed incident on the WT.

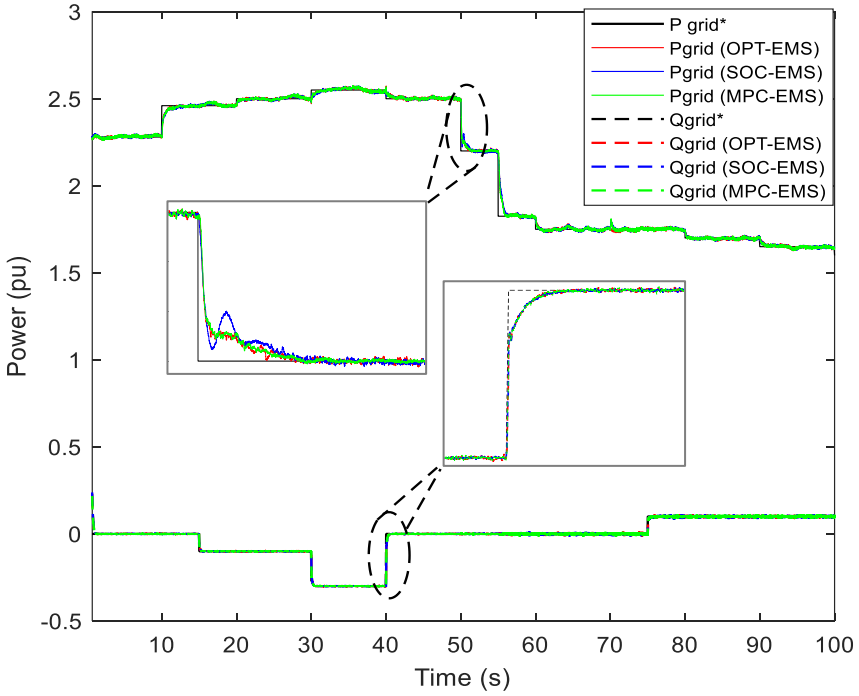

Fig. 6.7. Case.2. A. Grid active and reactive power.

Fig. 6.8 shows the BES power for tree EMS and Fig. 6.9 presents the BES SOC and how the EMS charge or discharge the BES during the simulation with the following initial SOC:

BES1=30% < BES2=50% < BES3=85%. From 0 to 50s, the power demanded by the system operator is higher than the power generated by the RES, and therefore, the BES operate in the discharging mode. From 50 to 55s, the total power generated by the RES is almost equal to the power demanded by the grid, and thus, the EMS decides not to intensively charge or discharge the BES (some of the BES are lightly discharged). After the second 55, the RES produce more power than the grid demand, and thus, the excess power is stored in the BES .

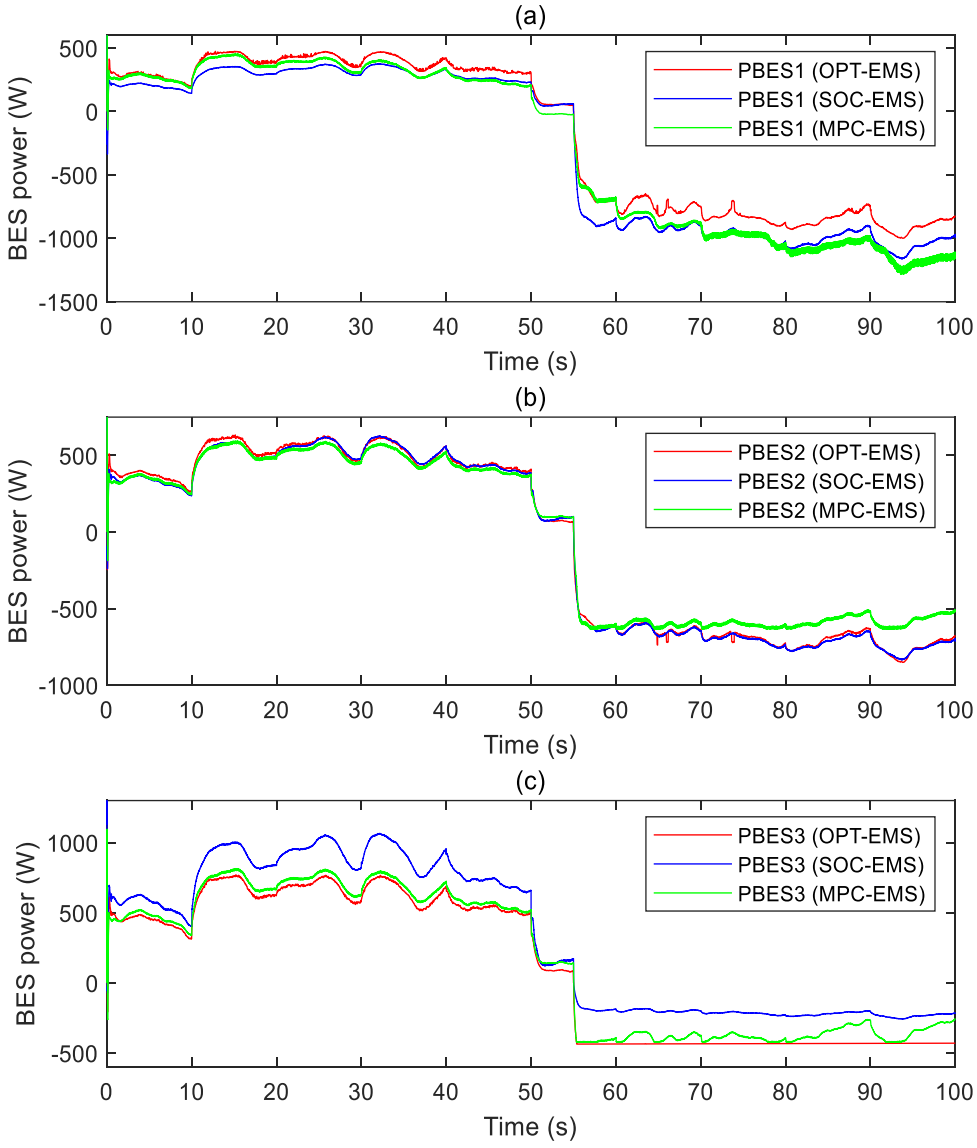

Fig. 6.8. Case.2. A. BES power for OPT-EMS, SOC-EMS, and MPC-EMS: (a) BES1, (b) BES2, and (c) BES3.

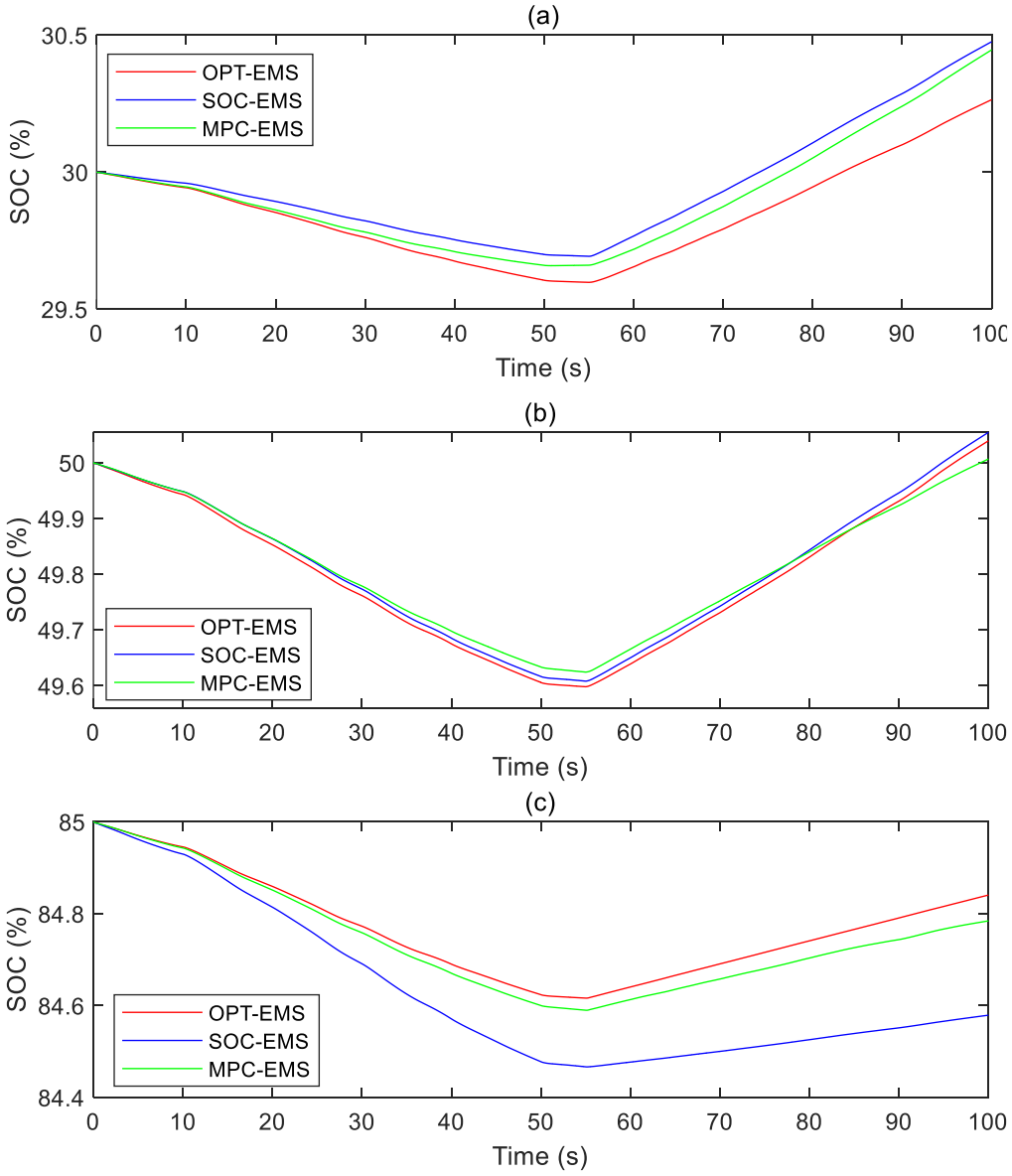

Fig. 6.9. Case.2. A. BES SOC: (a) BES1, (b) BES2, and (c) BES3.

In all EMS, the BES2 (with an intermediate initial SOC) is discharged and charged in practically the same manner, with an intermediate power compared to BES1 and BES3. The BES1 (with the lowest initial SOC) is the least discharged and the most charged BES in three EMS but presents a higher discharge power and a lower charge power in the OPT-EMS. The BES3 (with the highest initial SOC) is the most discharged and the least charged BES in both EMS, but has a higher discharge power and a lower charge power in the SOC-EMS because in this EMS the distribution among the BES depends on the BES SOC. The maximum values of the BES discharging and charging powers obtained with the OPT-EMS are lower than those obtained with the SOC-EMS and MPC- EMS to increase the global BES efficiency while properly dispatching power among the BES. From 55 s, the BES3 is charged with the OPT-EMS according to the power limit defined by equation (5.42), whereas the BES3 with the SOC-EMS is charged with a lower power because the SOC-EMS prioritizes charging the BES1 with the lowest SOC.

Fig. 6.10 shows the BES efficiency for both EMS, where it can be seen that the efficiency is near the maximum value when the BES power is near zero. This means that the lower the BES

power, the greater the efficiency. The results show that the OPT-EMS has higher efficiency, and the higher differences in the BES efficiency between the EMS appear with the highest BES powers, such as in seconds 25 and 33.

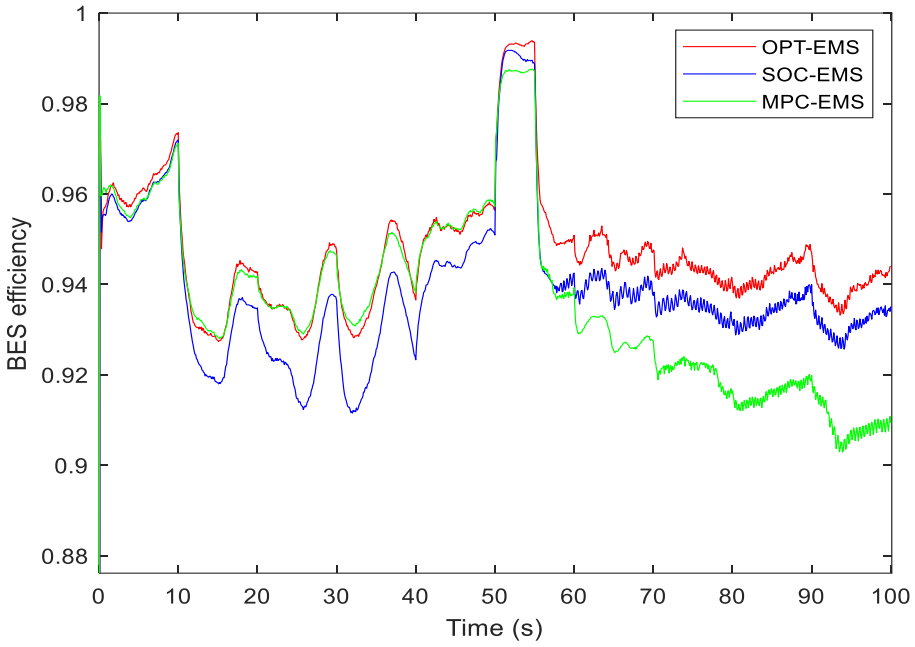

Fig. 6.10. Case.2. A. BES efficiency found by EMSs.

The seven-level output voltage of the BES-qZS-CHBMLI with 3 cascade qZSI and the grid voltage and current with unity power factor are illustrated in Fig. 6.11.

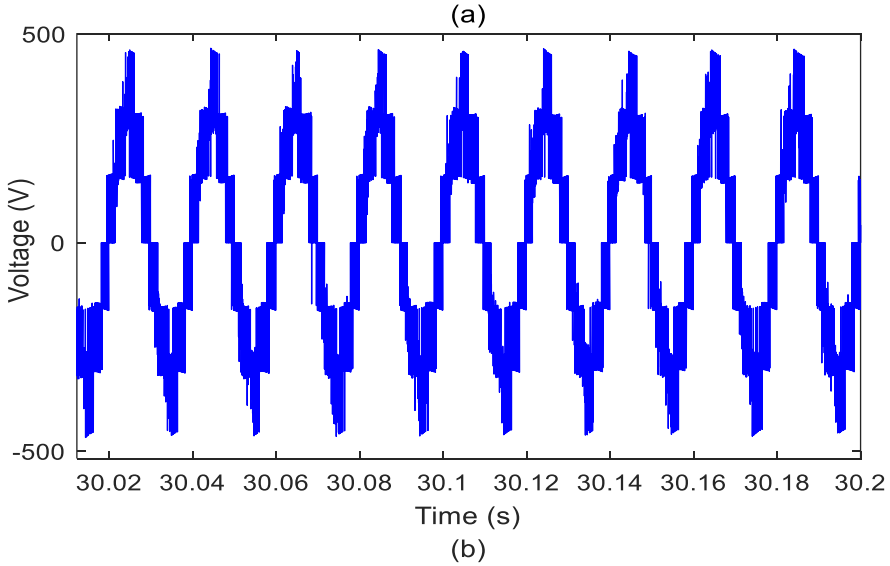

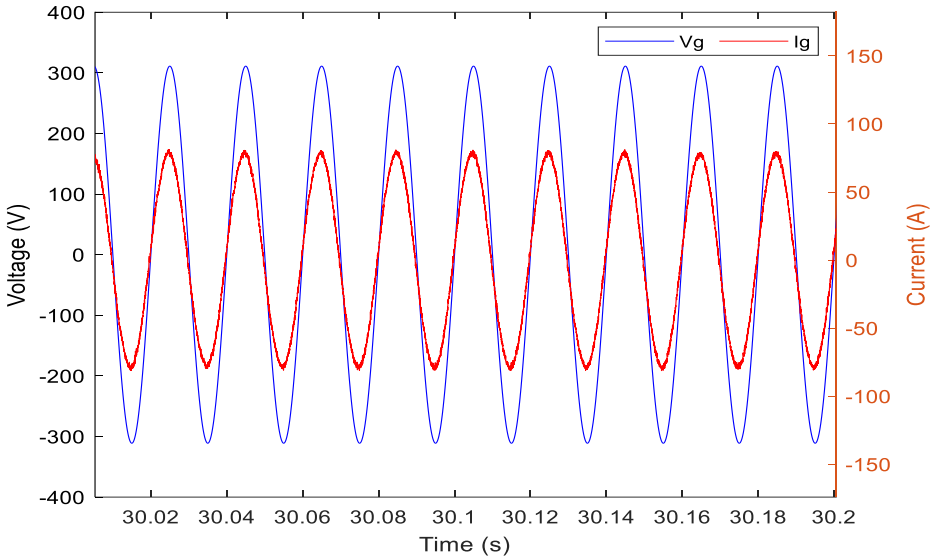

Fig. 6.11. Case.2. A. (a) Seven-level output voltage of the BES-qZS-CHBMLI, and (b) Grid voltage and current.

Table 6.7 compares the results obtained by the three EMSs in terms of global BES efficiency of the hybrid power plant (calculated by equation (5.38)), mean values of $P_{BES,i}^{max,dischar}$ and $P_{BES,i}^{max,char}$, and Integral Time Absolute Error (ITAE) for the grid active (*P*) and reactive power (*Q*), which is calculated as follows:

$$ITAE = \int_0^T t|e(t)|dt \tag{4.20}$$

where e(t) is the error between the grid active (reactive) power reference and the measured active (reactive) power, and T is the time considered for the study.

Table 6.7. Case.2. A: Comparison of EMSs

Parameter	SOC-EMS	MPC-EMS	OPT-EMS
Mean value of η_{BES}	0.9380	0.9366	0.9464
Mean value of $P_{BES,i}^{max,dischar}$ (W)	807.26	640.22	594.23
Mean value of $P_{BES,i}^{max,char}$ (W)	-861.52	-980.98	-720.71
$ITAE(P)$	40.38	40.37	40.40
$ITAE(Q)$	12.84	12.84	12.85

The results show that not only the OPT-EMS tracks properly the grid active and reactive power references, but also increases significantly the global BES efficiency of the hybrid power plant (+0.9% and +0.37% for a 100s simulation) compared to SOC-EMS and MPC-EMS, respectively. The mean values of $P_{BES,i}^{max,dischar}$ and $P_{BES,i}^{max,char}$ achieved with the OPT-EMS are

respectively almost 220W and 140W smaller than with the OPT-EMS and; 46W, 386W for MPC-EMS, and therefore, the proposed OPT-EMS dispatches the power among the BES with smaller power differences among them, instead of prioritizing a greater discharge of the BES with the highest SOC or higher charge of the BES with the lowest SOC, which reduces global BES efficiency of the hybrid power plant.

6.1.3. Case 2. B. Experimental Results: Hybrid PV and WT power sources – EMS: OPT- SOC - MPC

In this part experimental results are sought to verify the performance of the proposed EMS. The experiments with OPAL-RT real-time simulator OP4510 are performed, and RT-LAB environment is used to program and visualize the model. Through the analogue input/output ports, the integration of a simulator with the external hardware devices is achieved. Moreover, the optimal EMS is implemented in a dSPACE MicroLabBox prototyping unit that allows real time monitoring, evaluation, and control. Finally, the observation signals are transferred to the digital storage oscilloscope (DSO)and the total hardware connection is schemed in Fig. 6.12 To use OPAL-RT test-bed, the overall power system must be divided into subsystems on RT-Lab and the individual core must be allocated to them. The real-time batteries power, the grid voltage and signals obtained from the digital simulator at the analogue output ports is observed through DSO. A sampling frequency of 100 kHz has been considered during real-time implementation.

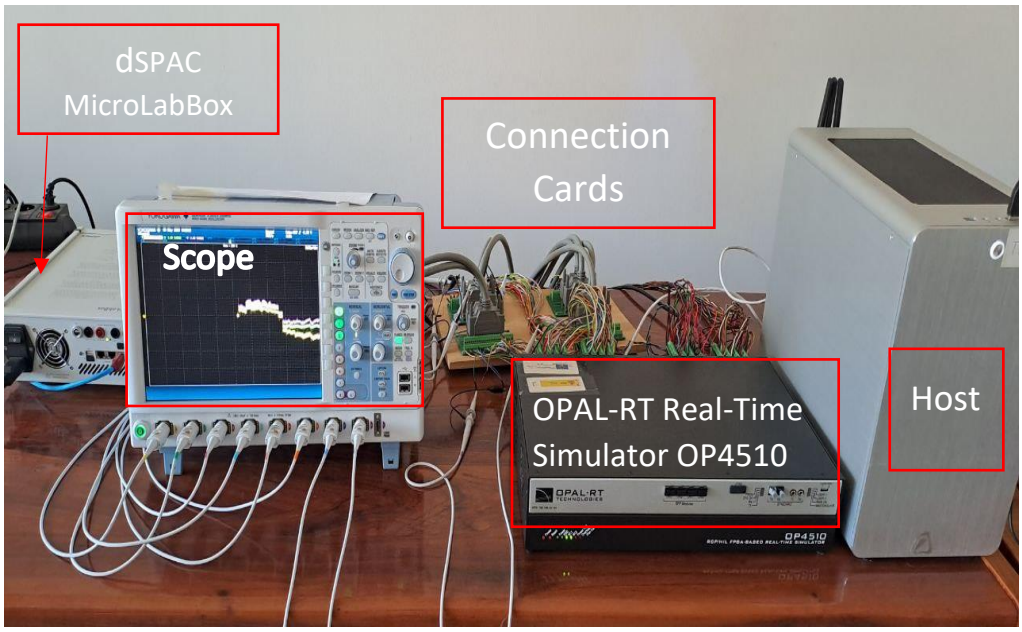

Fig. 6.12. Case.2. B Experimental setup with OPAL-RT- real-time simulator OP4510.

Fig. 6.13. **(**a). shows the experimental results of the grid parameters including active and reactive power, and Fig. 6. 13. (b). shows voltage, current, and the seven-level output voltage of the BES-qZS-CHBMLI. The power of each BESs (PB1, PB2, and PB3) obtained with the OPT-EMS, SOC-EMS, and MPC-EMS are shown in Fig. 6.14. (a. b. and c), respectively. For all 3 EMSs, during the discharging mode, the BES 3 is discharged higher than BES 2 and BES 1; and similarly, during the charging mode, BES 1 is charged most owing to its low SOC. The experimental results are consistent with the simulation results.

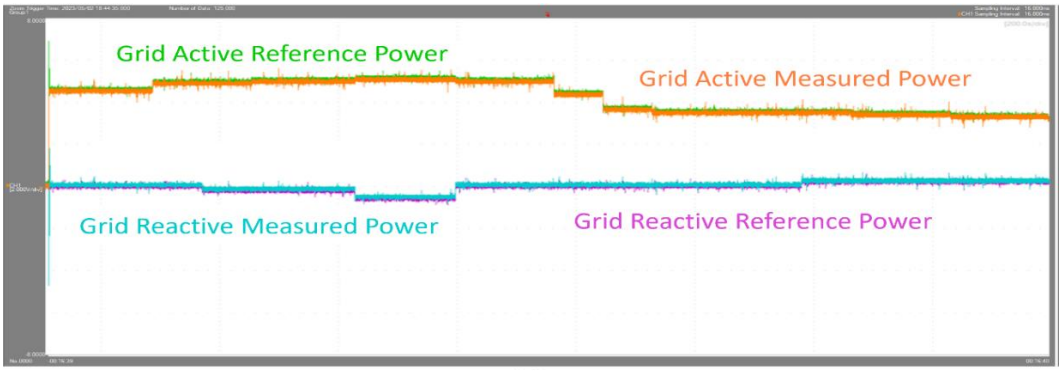

(a)

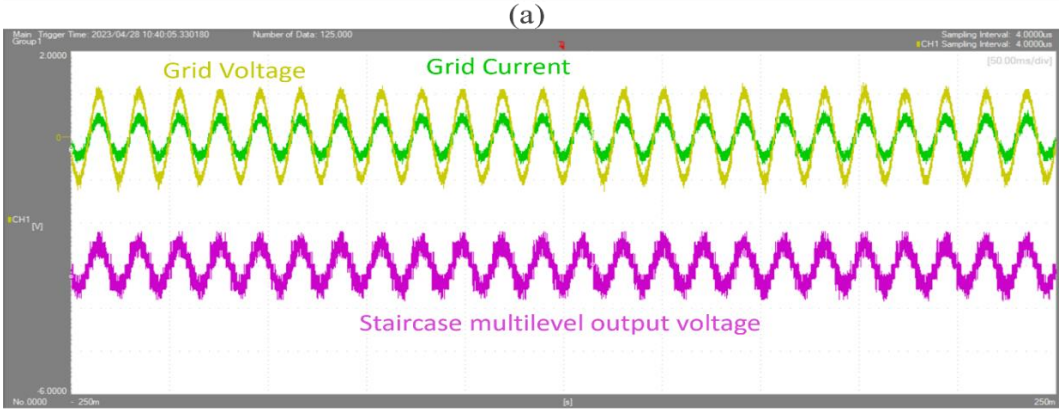

(b)

Fig. 6.13. Case.2. B. Experimental results for: (a) OPT-EMS grid active and reactive power, (b) OPT-EMS grid voltage and current, and Seven-level output voltage of the BES-qZS-CHBMLI.

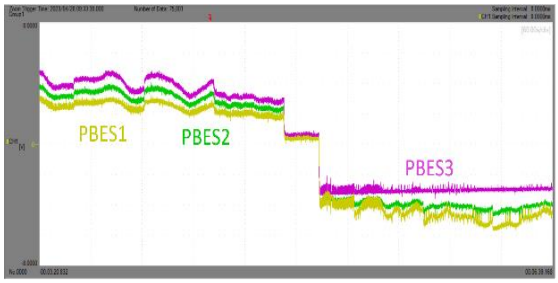

(a)

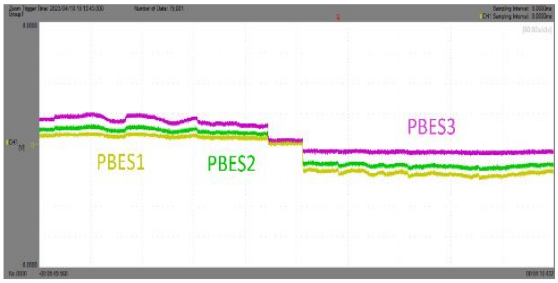

(b)

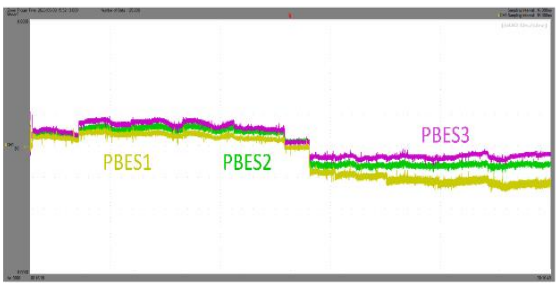

(c)

Fig. 6.14. Case.2. B. Experimental results for BES power: (a) OPT-EMS, (b) SOC-EMS, and (c) MPC-EMS.

This subsection presented controls and EMSs for the optimal operation of a grid-connected hybrid power plant with WT, PV power plants, and different BES integrated into a BES-qZS-CHBMLI. The optimal operation for the MPPT of the WT and PV power plants, connected to the input of the qZSI connected in series, was achieved by controlling the shoot-through duty ratio of each qZSI, whereas the active and reactive powers delivered to the grid were controlled by acting on the modulation index of each qZSI. The optimal operation of the BES integrated into the ES-qZS-CHBMLI was performed by implementing an EMS (OPT-EMS) based on optimizing the BES efficiency of the hybrid power plant while satisfying the system power balance and providing the active and reactive powers required by the grid. A constrained nonlinear multivariable algorithm was applied to solve the optimization problem and determine the optimal power of each BES, considering the maximum BES power capacity, limited values of the BES SOC (operation between a maximum and minimum SOC to avoid reducing the BES lifetime), and available power as constraints. The proposed OPT-EMS was compared, under variable renewable energy resources (solar irradiation in the PV power plants and wind speed in the WT) and active and reactive power references defined by the system operator, with a conventional EMS (SOC-EMS) and an MPC-EMS based on distributing the BES power proportionally to the BES SOC. The results showed that, when compared with the SOC-EMS and MPC-EMS, the OPT-EMS achieved suitable tracking (with similar values to those obtained by the SOC-EMS and MPC-EMS) of the active and reactive powers demanded by the grid from the power generated by the RES and the support of the BES, while dispatching efficiently the excess/deficit power among the BES with a higher global BES efficiency of the hybrid system (+0.9% and +0.37%) for a 100 s simulation, which could significantly increase over time.

6.1.4. Case 3. Hybrid PV and WT power sources – EMS: FLC- OPT- SOC

The main goal of this subsection is to evaluate the performance of fuzzy logic controller (FLC)suggested as EMS in section 5.3.2 to compare the results with SOC and OPT EMSs. The systems' inputs and conditions are considered the same as previous subsection composing of hybrid RES of two PV power plant and one WT as the sources of modules.

Fig. 6.15 shows the BES power for tree EMSs and Fig. 6.16 presents the BES SOC and how the EMS charge or discharge the BES during the simulation with the following initial SOC:

BES1=30% < BES2=50% < BES3=85%. From 0 to 50s, the power demanded by the system operator is higher than the power generated by the RES, and therefore, the BES operate in the discharging mode. After the second 50, the RES produce more power than the grid demand, and thus, the available power is stored in the BES. In all EMS, the BES2 (with an intermediate initial SOC) is discharged and charged in practically the same manner, with an intermediate power compared to BES1 and BES3. The BES1 (with the lowest initial SOC) is the least discharged and the most charged BES in three EMS but presents a higher discharge power and a lower charge power in the OPT-EMS. The BES3 (with the highest initial SOC) is the most discharged and the least charged BES in both EMS, but has a higher discharge power and a lower charge power in the SOC-EMS because in this EMS the distribution among the BES depends on the BES SOC.

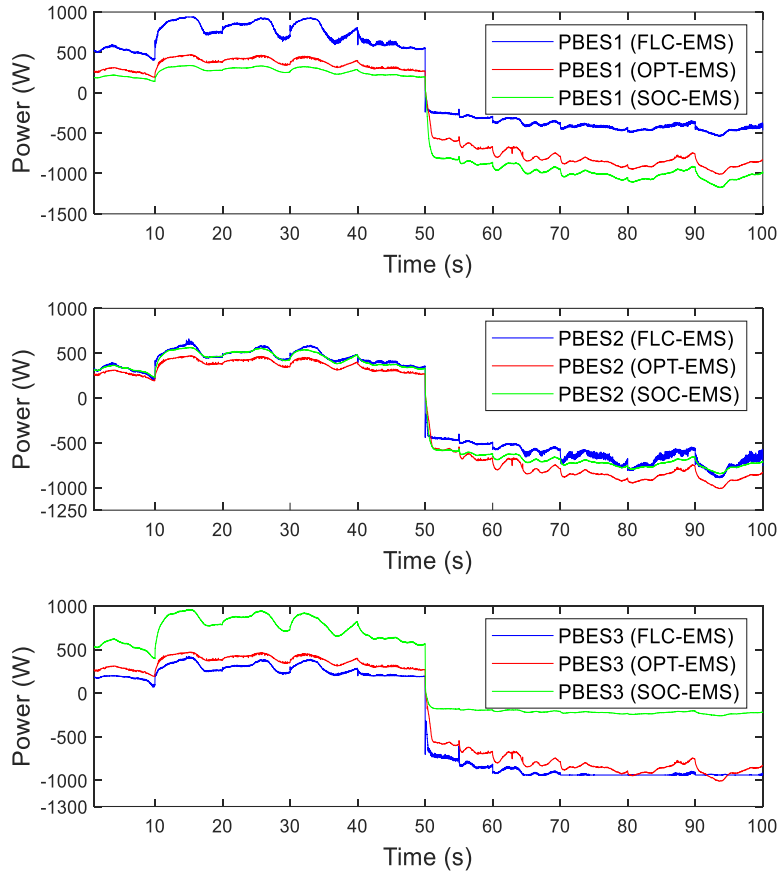

Fig. 6.15. Case.3. Results for BES power: (a) OPT-EMS, (b) SOC-EMS, and (c) FLC-EMS.

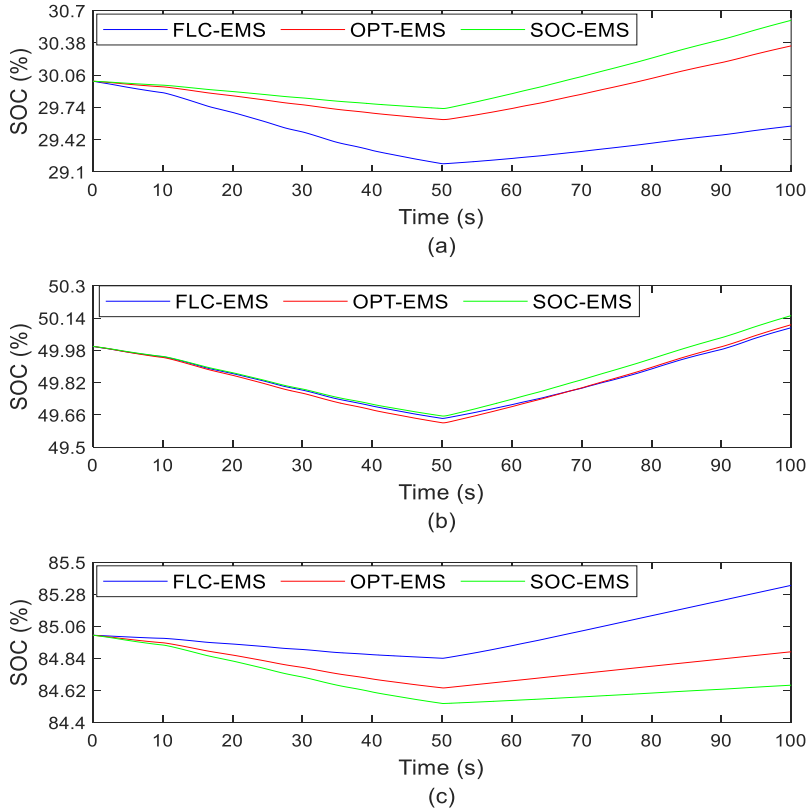

Fig. 6.16. Case.3. BES SOC: (a) BES1, (b) BES2, and (c) BES3.

The results obtained for three EMSs for the active and reactive powers delivered to the grid are shown in Fig. 6.17. As can be observed, three EMS achieve suitable control of the active and reactive powers of the hybrid power plant delivered with the grid. Among all, FLC-EMS has a better response in terms of overshoot and settling time, as can be seen in the zoom parts. The hybrid power plant can track the changes in the active and reactive powers by properly controlling the RES, BES and qZSI, despite the changes in the incident radiation of the PV power plants, and the wind speed incident on the WT.

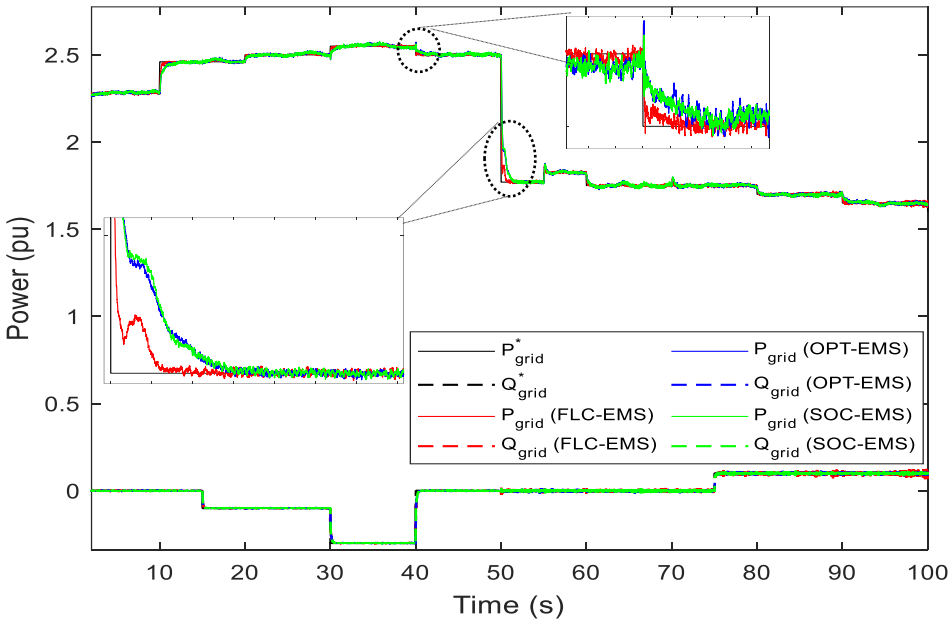

Fig. 6.17. Case.3. Grid active and reactive power

Fig. 6.18 shows the BES efficiency for both EMS, and as mentioned before the lower the BES power, the greater the efficiency. The results show that the OPT-EMS has the highest efficiency, and FLC-EMS has a higher efficiency compared to SOC-EMS.

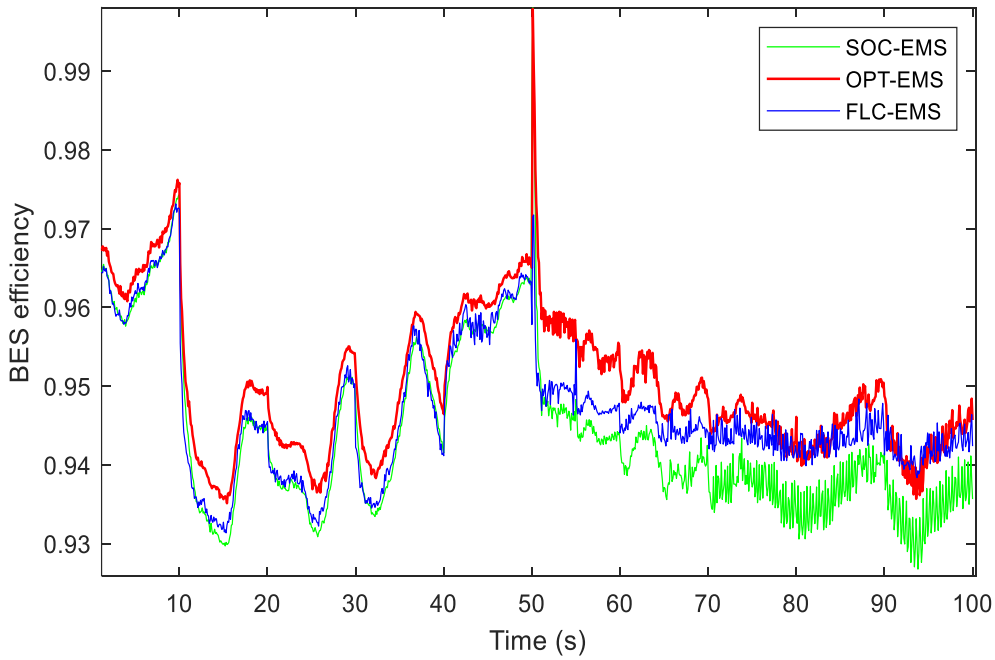

Fig. 6.18. Case.3. BES efficiency.

An error analysis has been sought to compare EMSs tracking performance and see which one satisfy the grid operator faster and track the reference power more accurately. Fig. 6.19 shows the error and histogram plots for the proposed EMS in this subpart. As it can be seen clearly that error distribution in SOC-EMS is vaster compared to others, while FLC-EMS has the least number of bar and closer to zero. It is due to the fact that when the grid power changes based on the reference power, FLC-EMS has a better dynamic performance and passes the transient modes faster than others.

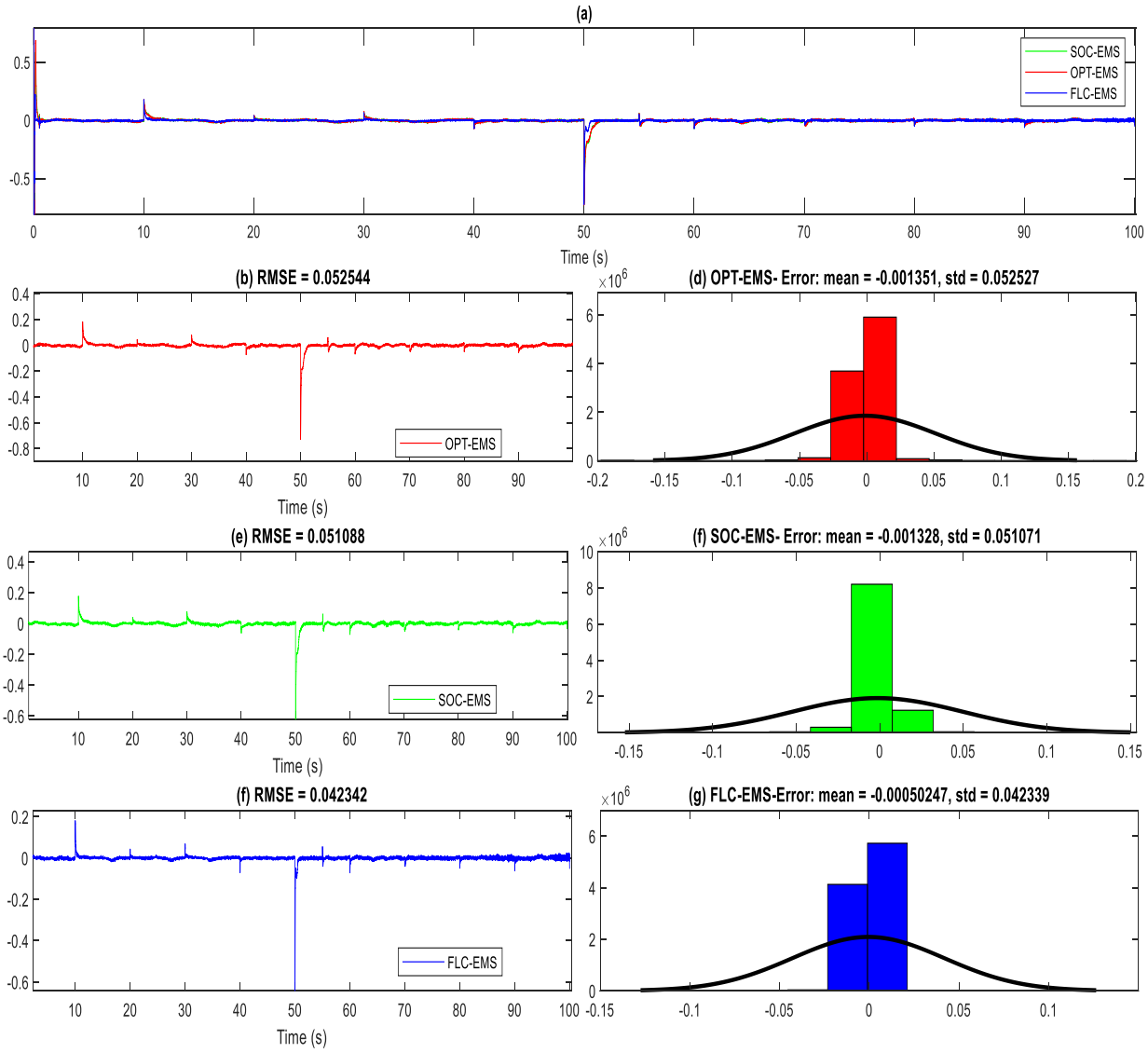

Fig. 6.19. Case.3. EMSs' errors analysis

Table 6.8 compares the results obtained by the three EMSs in terms of global BES efficiency of the hybrid power plant and the gap between the operator requested power and transferred power toward grid. It proves that FLC-EMS has more adaptive response and track better reference grid power, while OPT-EMS tries to increase global BES efficiency and has the highest mean efficiency value.

Table 6.8. Case.3: Comparison of EMSs

Parameter	SOC-EMS	FUZZY-EMS	OPT-EMS
Mean value of η_{BES}	0.9380	0.9371	0.9464
Mean error	-0.001328	-0.0005	-0.001351
RMSE error	0.051088	0.042342	0.052544
$ITAE(P)$	40.38	33.28	40.40
$ITAE(Q)$	12.84	12.84	12.85

6.1.5. Case 4. PV power plants – EMS: Multiagent RL

This subpart shows and discusses the obtained simulation results obtained by RL to evaluate this EMS. Reinforcement Learning Toolbox in MATLAB is used to simulate the RL-based EMS. The total system power is 14.400 kW, including of three 4.8 kW PV plants, with a layout of 6 modules in parallel and 2 in series for each PV power plant. The BES is a Lithium-Ion BES parallel with the capacitor C_{2_n}. Three different BES were considered in this subpart. The main parameters of the BES 1, 2 and 3 are presented in Table 6.9, respectively.

Table 6.9. Case.4: Parameters of BES

Param / Battery	E_{nom} (Wh)	V_{nom} (V)	R (Ω)	P_{nom} (w)	SOC (%)	Capacity (Ah)
BES1	1200	27.5	0.1261	1200	75	43.63
BES2	1571	30	0.1146	1571	50	52.37
BES3	1986	35	0.1234	1900	25	56.73

Discount factor γ is considered 0.93 that agents explore the whole environment as possible and learning rate α is set to 1e-3, fast enough to avoid long training periods, and slow enough to let the agent learn.

Fig. 6.20 illustrates the operating conditions of the RES of the cascaded series PV power plants. The irradiance of the PVs changes at 3 s, and therefore, the PV generation decreases.

The results obtained for RL-EMS for the active and reactive powers delivered to the grid are shown in Fig. 6.21. At 3 s, the grid power reference changes from 1.7 pu to 1.9 pu to evaluate both charging and discharging modes. A suitable control of the active and reactive powers of the RE power plant is seen, where the grid operator is satisfied with requested power. The power plant can track the changes in the active and reactive powers by properly controlling the RES, BES and qZSI, despite the changes in the incident radiation of the PV power plants, and the grid reference variation.

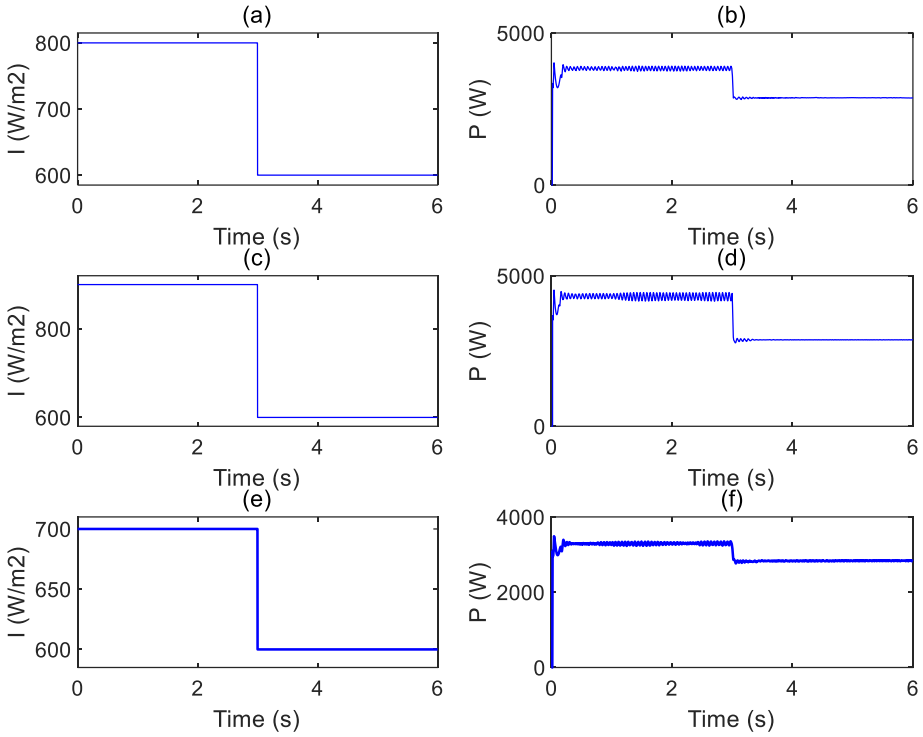

Fig. 6.20. Case.4. (a). PV1 irradiance, (b) PV1 output power, (c) PV2 irradiance, (d) PV2 power plant, (e) PV3 irradiance, (f) PV3 output power.

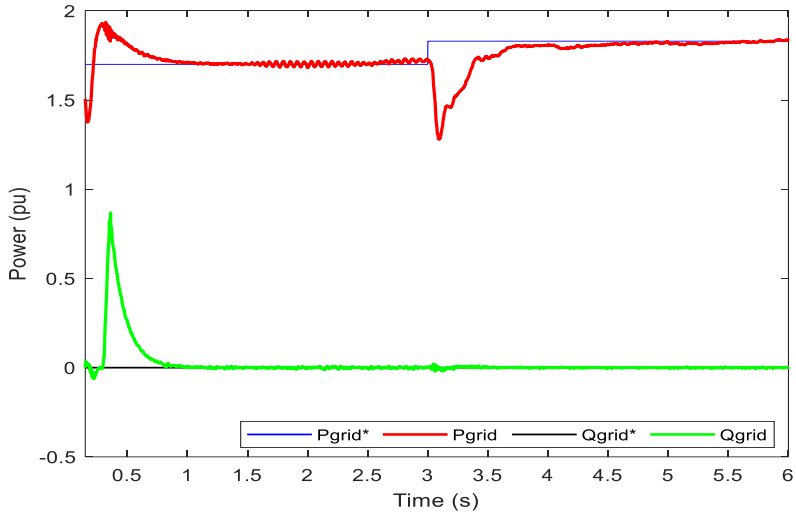

Fig. 6.21. Case.4. Grid active and reactive power.

Fig. 6.22 shows the power dispatch for the BES along the simulation. From 0 to 3 s, the PV power plants produce more power than the grid demand, and the power excess is stored in the BES. The RL decides the power to be stored into each BES while considering the maximum BES power limitations defined by equations (5.4.2,3). Therefore, BES 3 is charged with the highest power because it has the lowest SOC. From 3 to 6 s, the total power generated by the three PV power plants is higher than the power demanded by the grid, and thus, the EMS discharges the BES while considering the maximum power limitations of the BES. As BES 1 has the highest SOC, it is discharged more than others, while it was charged the least.

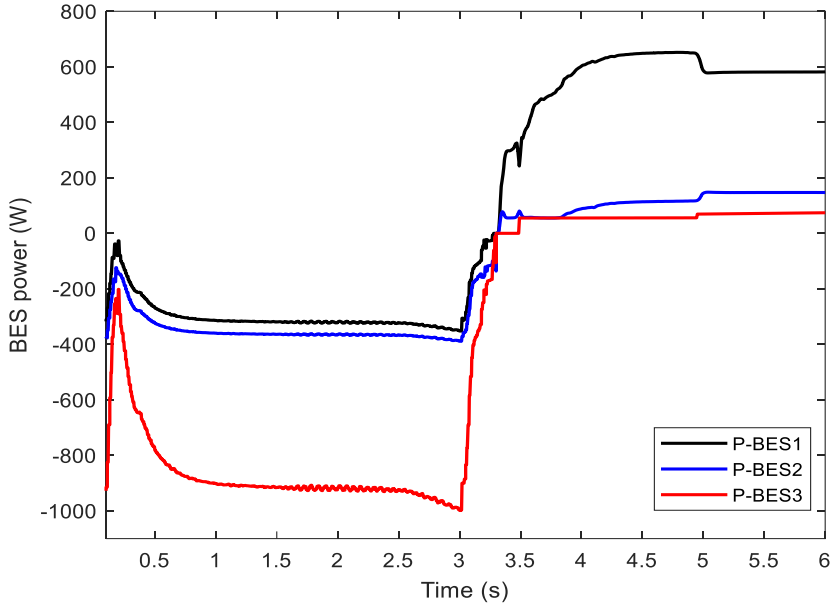

Fig. 6.22 Case.4. BES power

Fig. 6.23 shows the BES SOC and how the RL charges or discharges the BES during the simulation with the following initial SOC: BES1=75% < BES2=50% < BES3=25%. The SOC changing rate is decided by the EMS based on SOC levels. From 0 to 3 s, the RES produce more power than the grid demand, and the excess power is stored in the BES and SOC values increase. From 3 to 6 s, the power demanded by the system operator is higher than the power generated by the RES, and the BES operate in the discharging mode and SOC values start decreasing. To see how well the dc-voltage control is working, the inverter output voltage must be checked. The seven-level output voltage of the BES-qZS-CHBMLI with 3 cascaded qZSI and the grid voltage and current with unity power factor are illustrated in Fig. 6.24. The total seven-level voltage is the summation of three 150 V module output voltage. Sinusoidal waveforms are achieved for the grid current and voltage after the filter, synchronized with the grid.

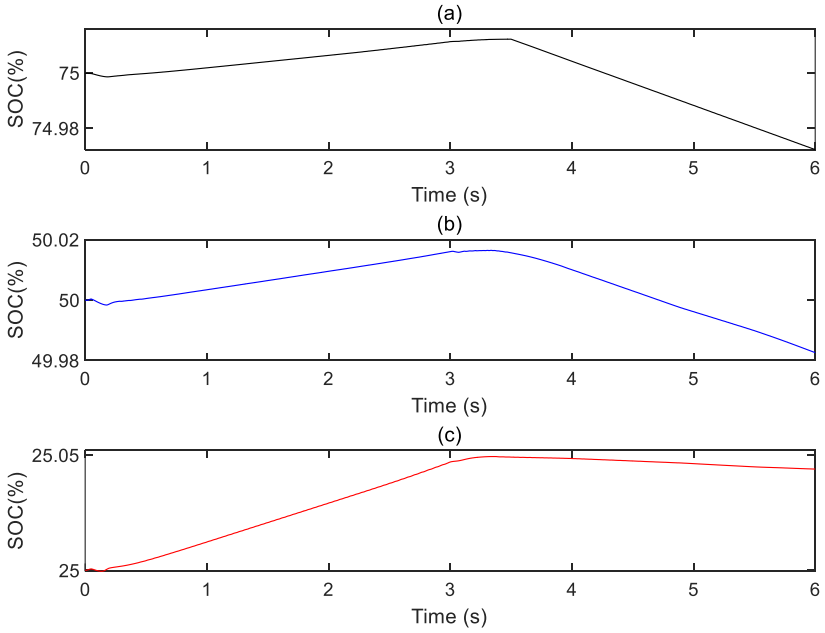

Fig. 6.23. Case.4. BES SOC: (a) BES1, (b) BES2, and (c) BES3.

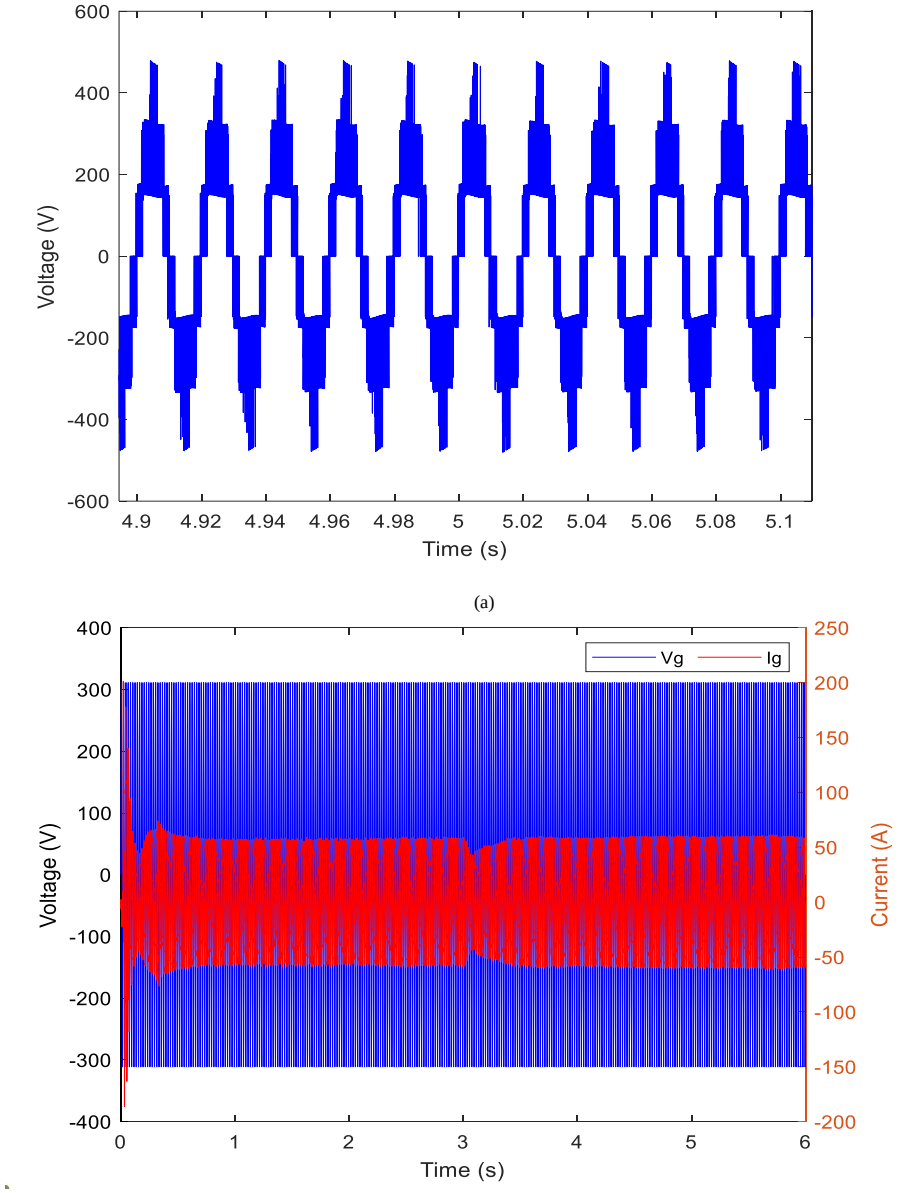

Fig. 6.24. Case.4. (a) Seven-level output voltage of the ES-qZS-CHBMLI. (b) Grid voltage and current.

The obtained results prove that the RL-based EMS dispatches power between BES by setting the increasing or decreasing SOC rates based on the initial SOC levels and the BES nominal parameters, while meeting the grid demand.

An intelligent RL EMS for a grid-connected ES-qZS-CHBMLI with three modules in series and PV power generation was proposed herein. Based on the BES efficiency and lifetime, a maximum charging and discharging power level was set for each battery, and the proposed RL agents were trained separately to meet the grid demand, maintaining the SOC between minimum and maximum values, and with a power distribution based on the SOC of each BES. The simulation results proves that the RL algorithms effectively dispatch power between batteries and the power is appropriately transferred to the grid under reference setpoints and different irradiation conditions, while the EMS equilibrated the BES power.

6.1.6. Case 5. A. PV power plants – EMS: Single-Agent RL- Training

In this subpart a single-agent RL algorithm is trained for three cascaded modules composed of three PV cells and simulation interval of 8 seconds. However, it is not acceptable to evaluate its performance for a short time simulation. Therefore, this agent is trained for 8 seconds with PV power sources and will be tested in the next subpart for 100 seconds simulation time and with hybrid configuration of WT and PV sources. It is the advantage of using intelligent RL algorithms to be trained based on the system conditions and not simulation time. However, some crucial factors must be taken into account. The first one is initializing every episode by random values around the specified range. It means if the simulation is going to be run for example 5000 times, in every time it initializes with random irradiance values and grid power references. For example, every time simulation is runed, the PV irradiances must be valued between 400 to 1000 W/m^2 and the reference grid power be varied between 1.6 to 2.5 pu. It makes the algorithm a super adaptive one that works under a wide range of conditions.

Fig. 6.25 visualizes the rewards attained in every episode and the way the agent has tried to increase accumulated reward by receiving less penalty. After almost 54 hours it can be said that the agent has learnt to do the dedicated tasks. The average reward started by -6×10^{-5} at the beginning of training and little by little the agent learnt how to behaves and it can be seen that in the last episode the average reward reached by almost -5000.

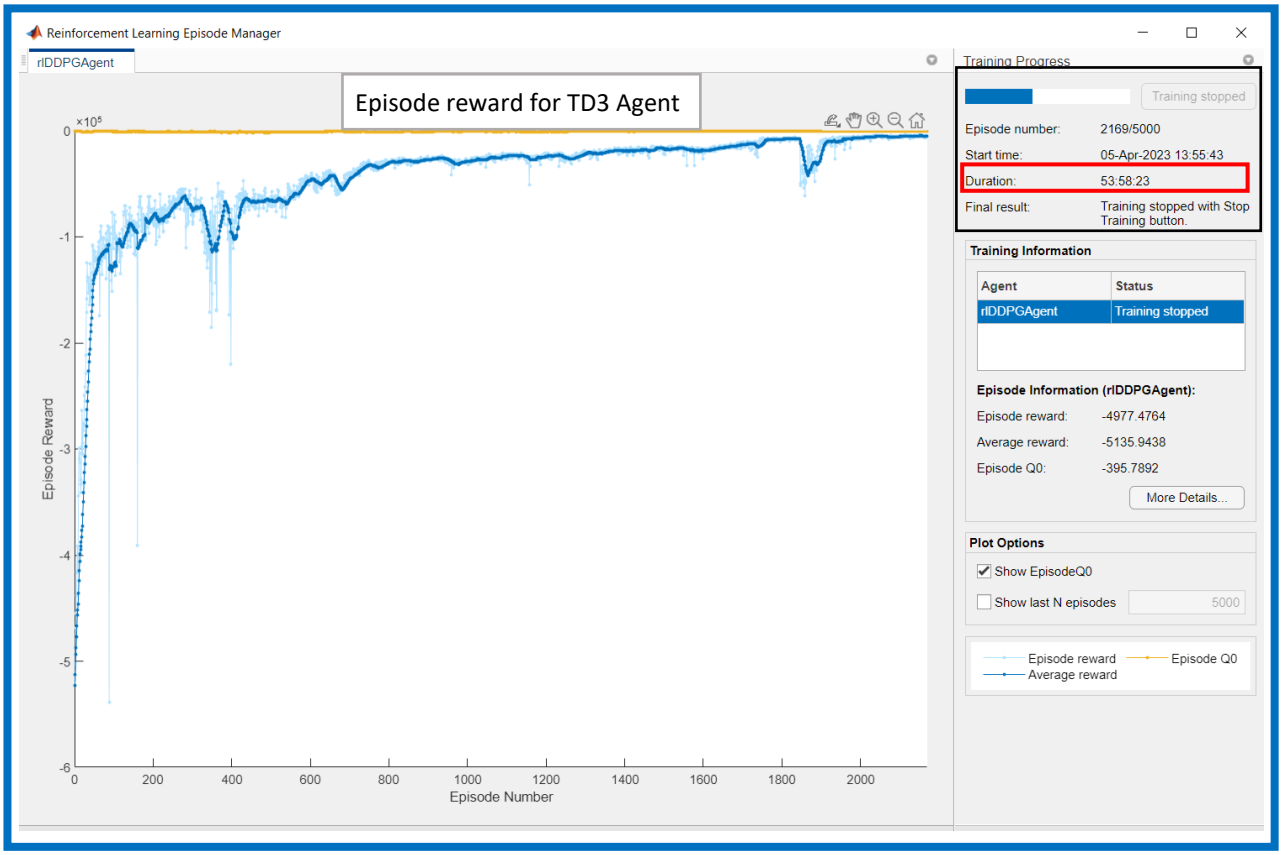

Fig. 6.25. Case.5. A. Reward plot for TD3 agent

Fig. 6.26 Shows the irradiances of the first simulation, that forces the system to change the mode from charging to discharging at second 3.

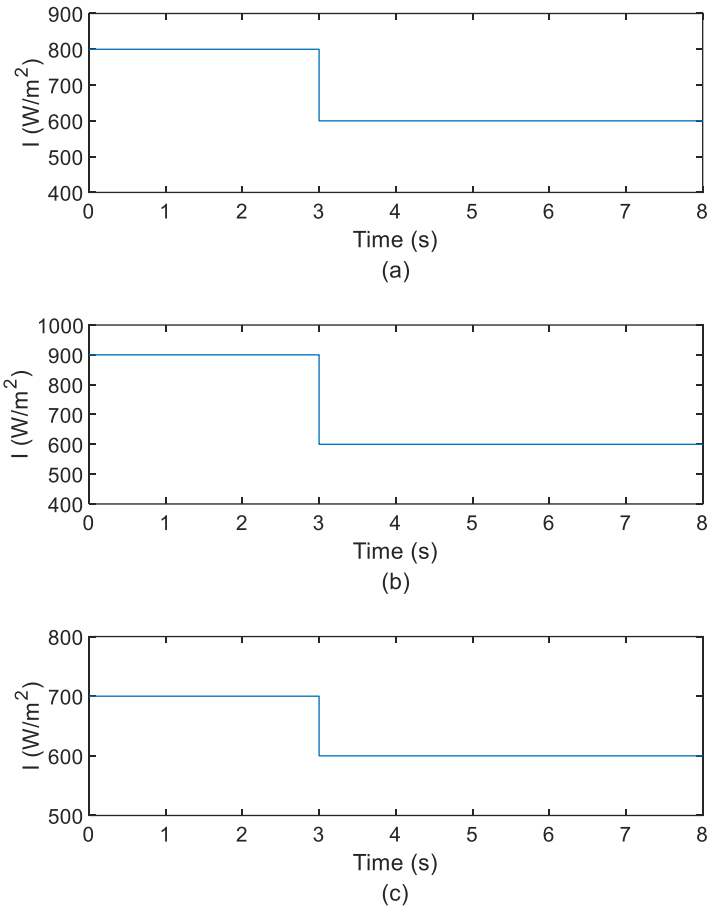

Fig. 6.26. Case.5. A. PVs irradiance (a). IRR. 1, (b). IRR. 2, and (c). IRR. 3.

Fig. 6.27 illustrates the BES powers that are dispatched based on the SOC values that is shown in Fig. 6.28.

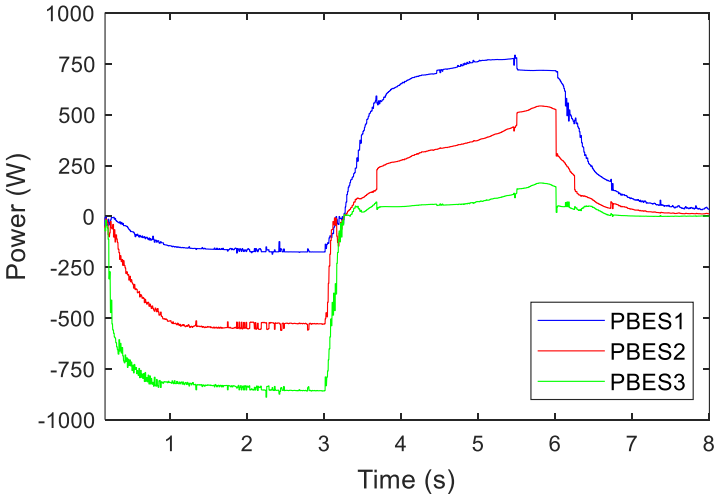

Fig. 6.27. Case.5. A. Output BESs power

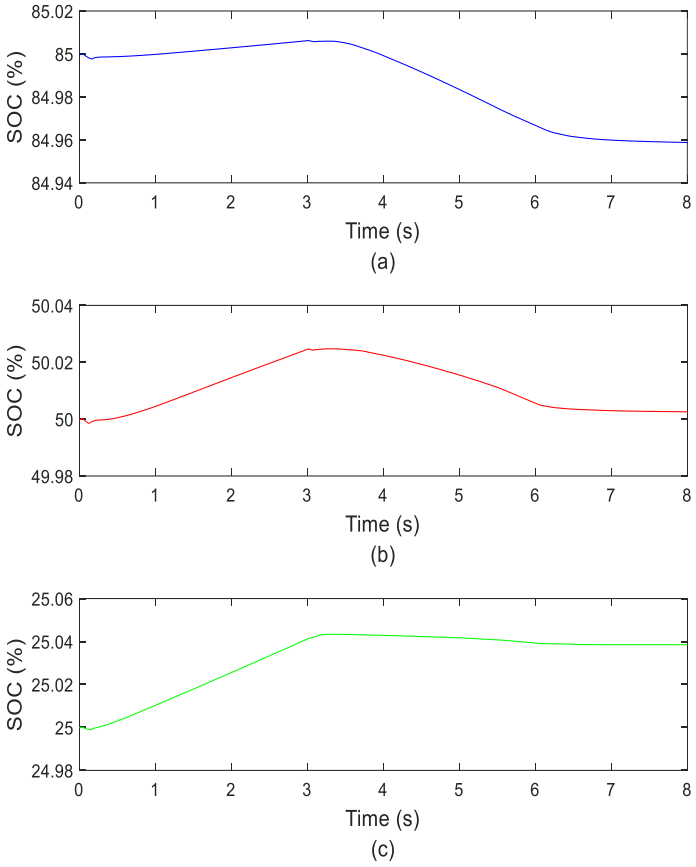

Fig. 6.28. Case.5. A. BESs SOC: (a). BES1, (b). BES2, and (c). BES3.

Fig. 6.29 Shows grid active and reactive power references and measured along with the simulation. By seconds 3 and 6, the grid power reference is changed in a way that by the 6ths the demanded power is reduced and there is no need to discharge power anymore and the RES power are not enough for charging BESs, and only are considered for satisfying the grid request.

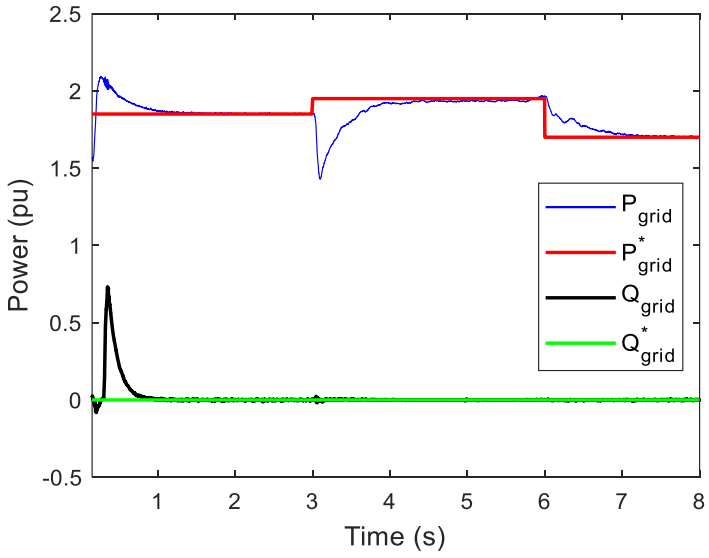

Fig. 6.29. Case.5. A. Grid active and reactive power

Now that the agent performance has been checked and it proved its well dispatching BES power based on SOCs and meeting demand, it can be tested for a hybrid configuration and longer simulations in the next subpart.

6.1.7. Case 5.B. Hybrid PV and WT power sources – EMS: Single-Agent RL Algorithm- Testing

The hybrid power plant under study here is based on Fig. 6. 6 composed of a 5-kW wind turbine and two 4.8 kW independent PV power plants, with a layout of six modules in parallel and two in series for each PV plant, whose total rated power is 14.4 kW. The results used to evaluate the proposed single-agent RL EMS, under variable energy resources (solar irradiation and wind speed) and active and reactive power references defined by the system operator.

Fig. 6.30 illustrates the output BESs power dispatched based on the SOC values that can be found in Fig. 6.31 It is totally normal that the responses seems a little noisy as the agent trained for the previous simulation conditions in subpart Case.5.A and used here to be tested for other conditions. Moreover, sample time of training is considered 1e-3 that is far bigger than Simulink sample time (1e-5) to raise the speed of simulation.

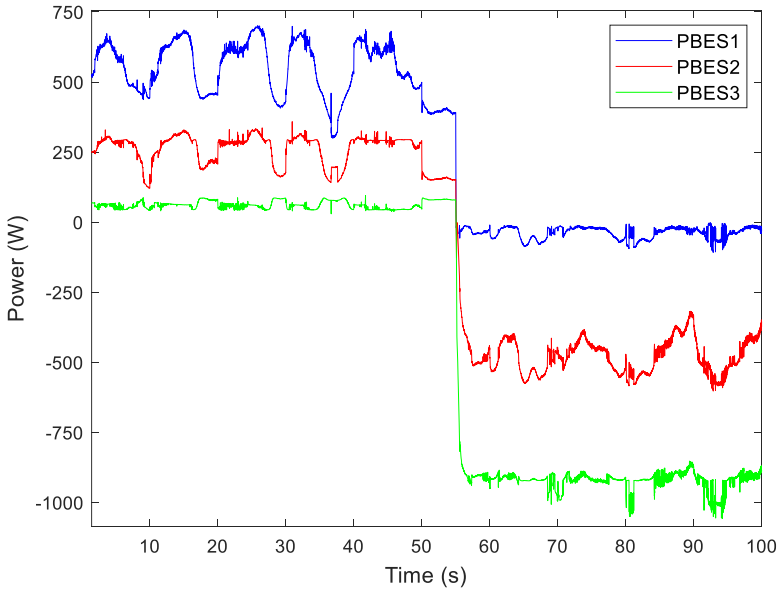

Fig. 6.30. Case.5. B. Output BESs power

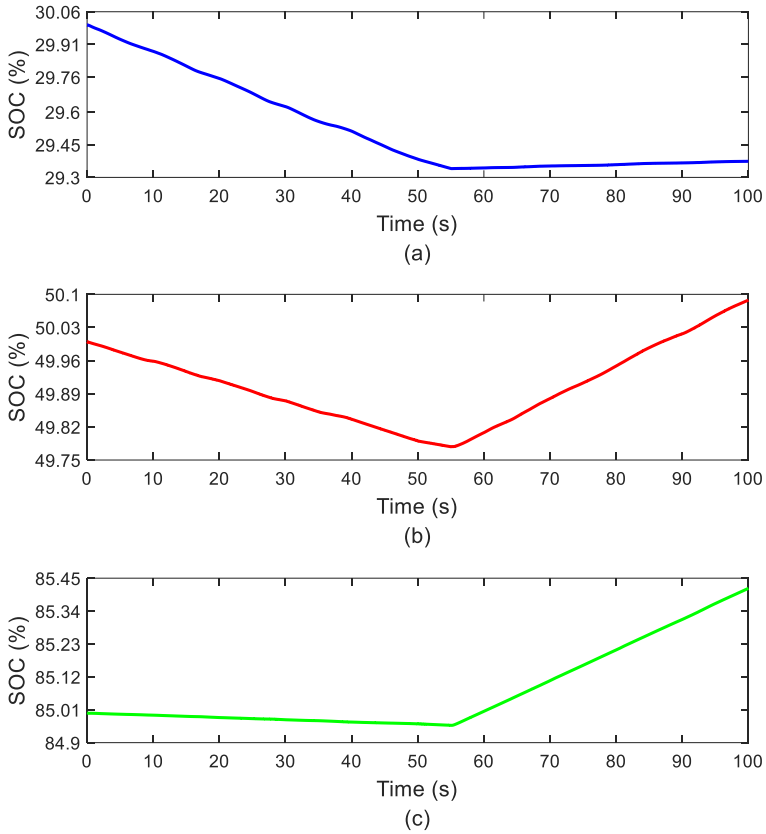

Fig. 6.31. Case.5. B. BESs SOC: (a). BES1, (b). BES2, and (c). BES3.

Fig. 6.32 Shows grid active and reactive power references and measured along with the simulation. Based on the Table 6.5. Case.2. A, the grid active and reactive power reference is changed. Notwithstanding the bumpy road, the grid power tracks well the operator requests appropriately. Even in second 50 that system changes its mode by a step change (slop 90°), the agent rapidly changes the BES power references to track the grid reference power. It proves how RL-EMS is adaptive and trustworthy.

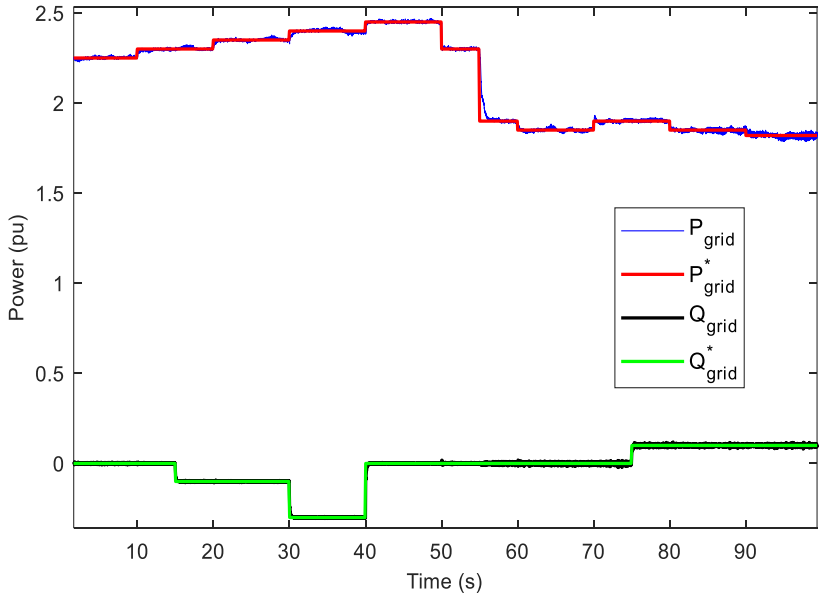

Fig. 6.32. Case.5. B. Grid active and reactive power

6.1.8. Case 6. Single WT power source – Adaptive MPPT and passive reinforcement learning algorithm for pitch angle control

This part presents the results of the controllers designed to receive the most efficient power of a WT. The proposed controller is evaluated by using FAST8 for a real experimental 600 kW WT (Controls Advanced Research Turbine, CART3, located at National Renewable Energy Laboratory), whose parameters are given in Table 6.10 The CART3 is a conventional three-bladed upwind variable-speed variable blade-pitch-to-feather-controlled WT turbine. This WT is modeled using a two-mass model and a validated aero-elastic simulator called FAST8 (Fatigue, Aerodynamics, Structures, and Turbulence) [37]. FAST8 tool allows to implement an accurate model of the WT in different aero-dynamical and environmental conditions.

Table 6.10. Case.6: Parameters of CART3

Parameters	Value
Rated rotational speed	1600 rpm
Rated power	600 kW
Cut-in wind speed	4 m/s
Cut-out wind speed	25 m/s
Rated wind speed	≈12 m/s
Maximum rotor torque	162 kN.m
Rated torque	3524.37 N.m
$C_{P,Max}$	0.4658
Radius	21.64 m
ρ	1 kg/m^3
λ_{OPT}	7.1
N_{gear}	43.164

Region 2 is defined from 431.65 to 1472 rpm speed, and region 2.5 from 1472 to 1584 of the maximum generator speed of 1600 rpm. Evaluating Eq. (1) with the CART3 parameters (K = 6541.75 N.m/(rad/s)^2), the torque in Region 2 is given by T_g = 6594.6 *W^2 N-m. The new K is K_{NEW}=0.000892, and thus T_g= (.000892*1600^2)N-m , where β is fixed at 3.7°.

In Region 3, a gain corrected PI controller (GC-PI) for the blade pitch angle is designed on the speed error (between the filtered generator speed and the rated generator speed. To find the PI gains, the WT parameters (A, B) must be chosen. By considering initial conditions of wind speed, rotor speed and pitch angle as V_0 = 14.6 m/s, ω_0= 41.7 rpm, and β_0=3.7 degrees, these WT parameters at this operating point are determined: *A*= -0.924, *B*= -3.302.

As suggested in [132], δ =1 and ω = 0.6 rad/s are chosen for higher performance. So, equation (5.5) can be written as follows:

$$(1 + 3.302k_D)s^2 + (0.924 + 3.302k_P)s + (3.302k_I) = 0 \quad (6.1)$$

K_D > -0.302, K_P > -0.27, K_P>0

By applying equations (5.6), (5.7), K_P, K_i can be calculated: K_P =0.083, K_i=0.109. These parameters, obtained from the linearized system, allow to achieve nearly the best performance for pitch angle control among all CART3 controllers and such controller is hardly challengeable. A scheduled PI controller as a function of blade pitch angle (GC-PI controller) to reach a better performance in smaller angles. The K_p and K_i are calculated online with the following equation (β_0 = 3.7°):

$$\beta_{GC} = 1 / \left(1 + (\beta_C / \theta_K) \right), \text{where } \theta_K = 3.7 * (\pi / 180). \quad (6.2)$$

where β_c and β_{Gc} are the collective pitch and revised pitch angles, respectively.

Therefore, the controller proposed here is compared with an adaptive pitch controller designed for the CART3, GC-PI controller. The proposed adaptive pitch controller can cover more uncertainties for CART3 in the base of online calculation of K_P and K_i parameters.

Because of limitations in the FAST tools, the FAST model does not include any blade-pitch actuator dynamic effects. To command a real blade pitch angle, an additional actuator dynamic block is added. The proposed GS-RL-RANFIST2 and GC-PI controllers are tested in the CART3 under step and random wind pattern. The GC-PI controller is an adaptive controller designed and tested by NREL. Hence, the GS-RL-RANFIST2 performance is compared with the proved GC-PI controller.

6.1.8.1. *Step wind speed test*

In order to evaluate the controllers' robustness to the model uncertainties, the performance of them obtained under step wind disturbances (one step raise and different pace steps) are shown in Fig. 6.33 and Fig. 6.34.

By comparing these dynamic responses, it can be seen that the GC-PI controller cannot provide consistently optimal dynamic performance when the wind speed is increased in steps. When the wind speed changes, the GS-RL-RANFIST2 can eliminate the effect of the shift of operating points, and therefore, it provides a better transient response with smaller overshoot and faster settling time, over the whole operation range. In the wind step of 12 to 18 m/s, the settling time for the rotor speed response is 16 s for the GC-PI and 9 s for the GS-RL-RANFIST2, and the maximum overshoot is 0.8 for the GC-PI and 0.62 for the GS-RL-RANFIST2. The power is better captured by the proposed controller by 71.92 W for 7 steps in the wind pattern.

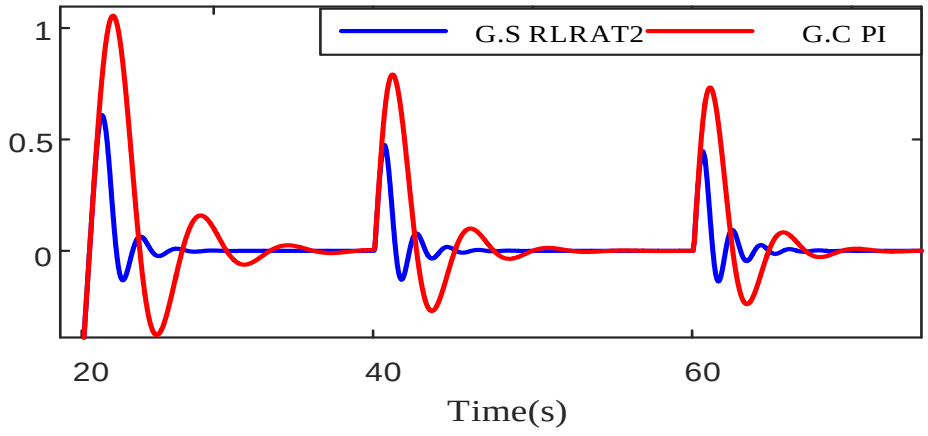

(a) Control input acceleration (rad/s)

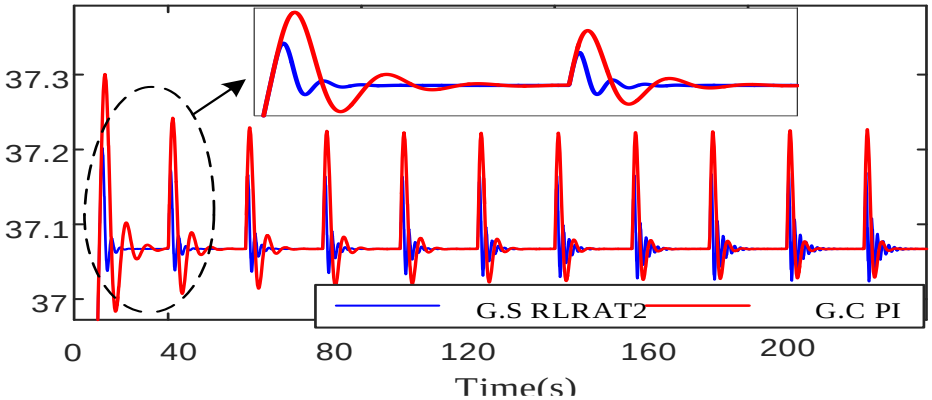

(b) rotor speed (rad/s)

Fig. 6.33. Case. 6. Dynamic response comparison under one step raise: (a) control input acceleration; (b) rotor speed

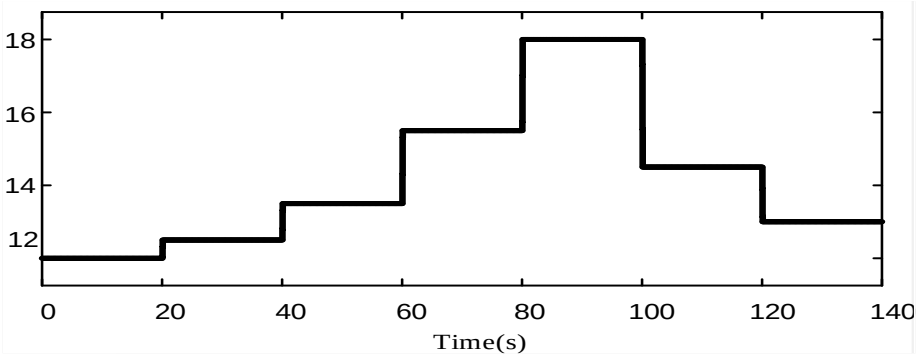

(a) wind step pattern (m/s)

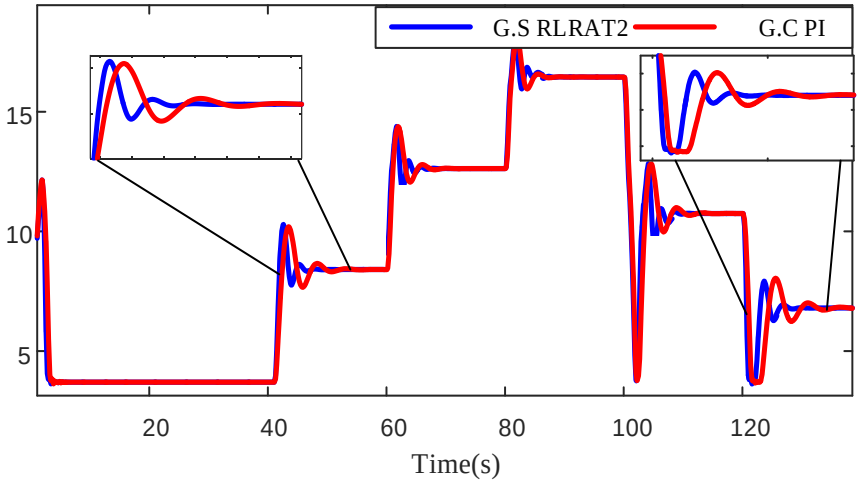

(b) pitch angle (degree)

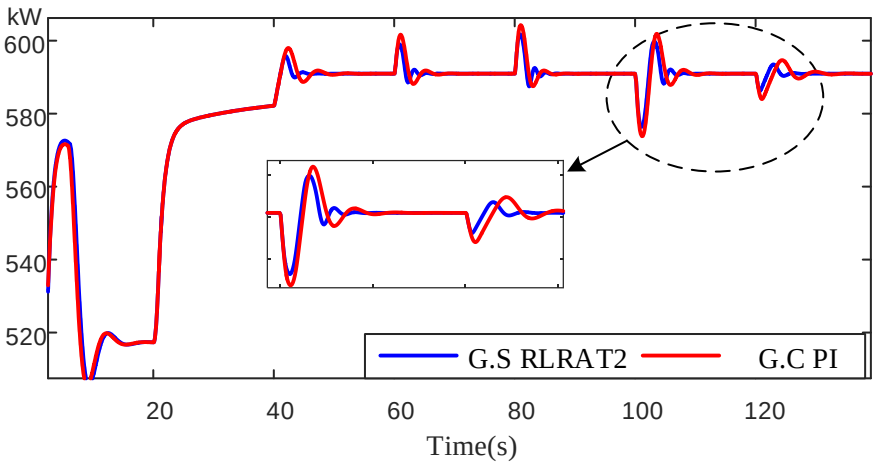

(c) generator power (kW)

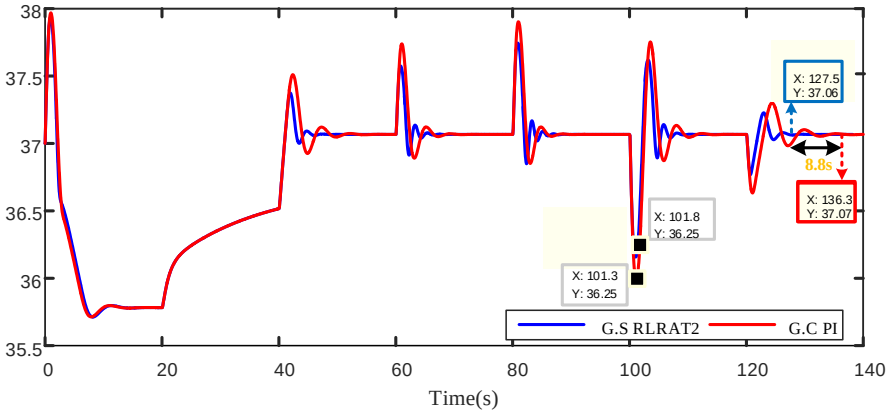

(d) rotor speed (rad/s)

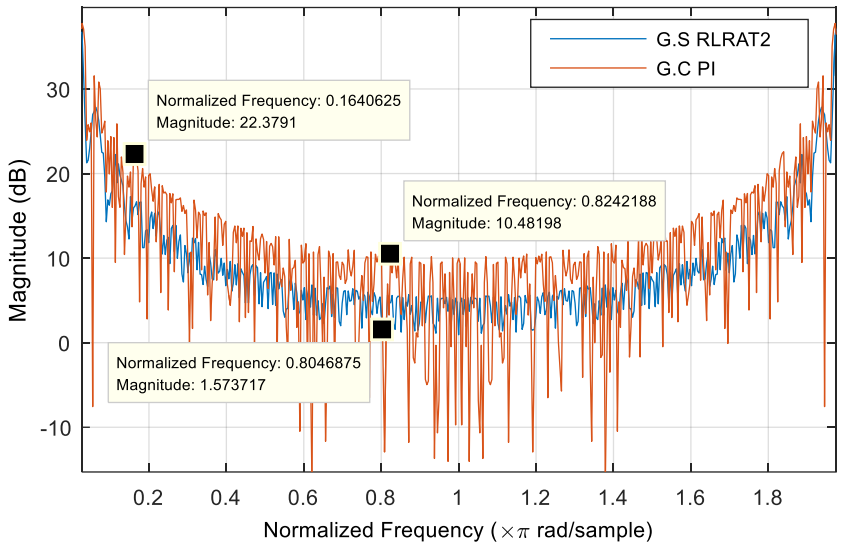

(e) frequency response of error speed

Fig. 6.34. Case.6. Dynamic response comparison of the controllers under different pace steps

The magnitude response estimations between [0 2π] and 512 points for the error signals are shown in Fig. 6.34. (e). It is clear that the proposed controller smooths the error for both low

and high frequency by less than 5 dB fluctuations rate, when this value is approximately 20 dB for the G.C PI.

6.1.8.2. Random wind speed test

The turbulent wind code with different mean wind speed and turbulence intensity is created by using TurbSim from NREL, which is a stochastic, full-field, turbulent-wind simulator and numerically simulates 3-dimensional wind velocity vectors by time series at points in a vertical rectangular grid. The wind speed is chosen in the range from 10 m/s to 20 m/s, as shown in Fig. 6.35.

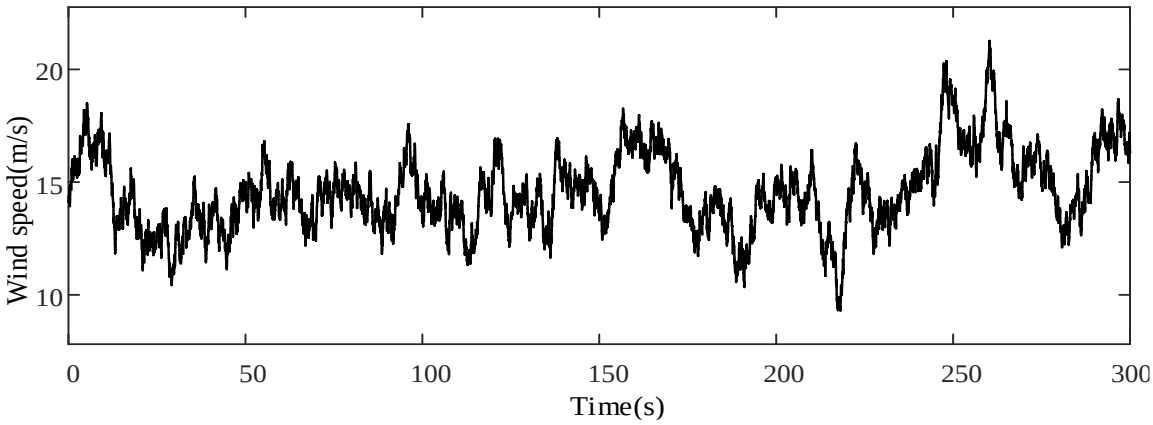

Fig. 6.35. Case.6. Turbulent wind pattern

The results obtained from FAST8 are illustrated in Fig. 6.36, Fig. 6.37, Fig. 6.38. where the speed error acceleration, pitch angle, generator power, generator speed and generator torque are shown respectively. The control performances are compared under heavy wind changes.

The log frequency scale for the control error signals is shown in Fig. 6.36.(a) and the phase delay in Fig. 6.36.(b). The marked points show the value of delays for both controllers.

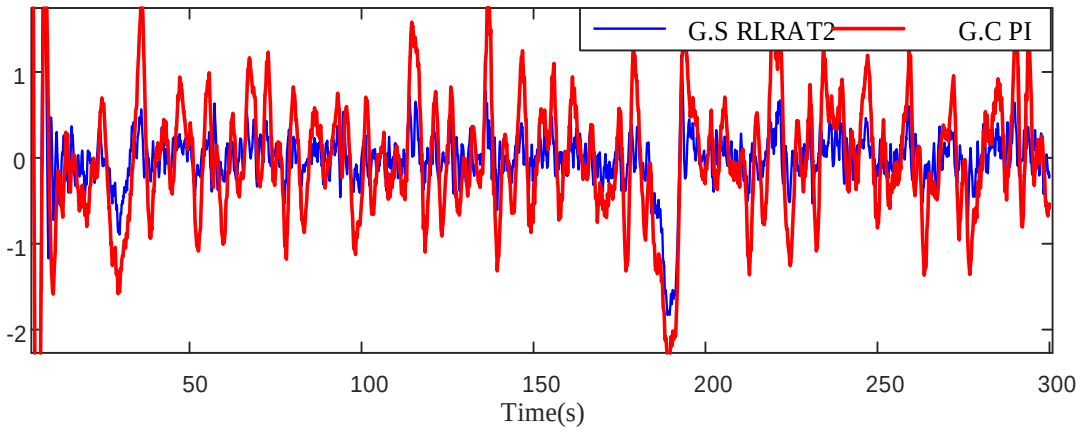

(a) Speed error acceleration (rad/s)

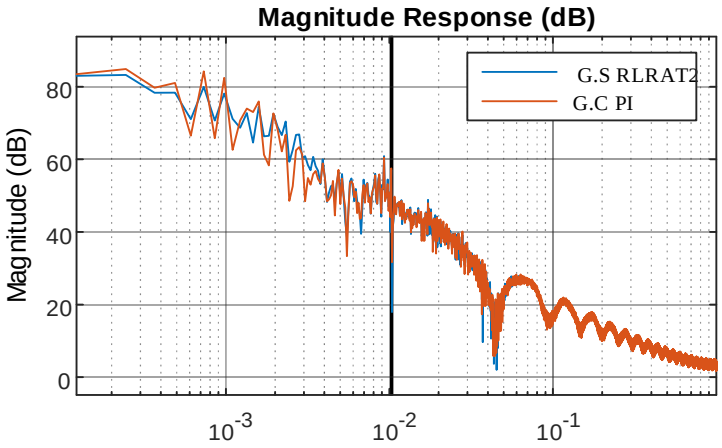

(b) Magnitude response (dB)

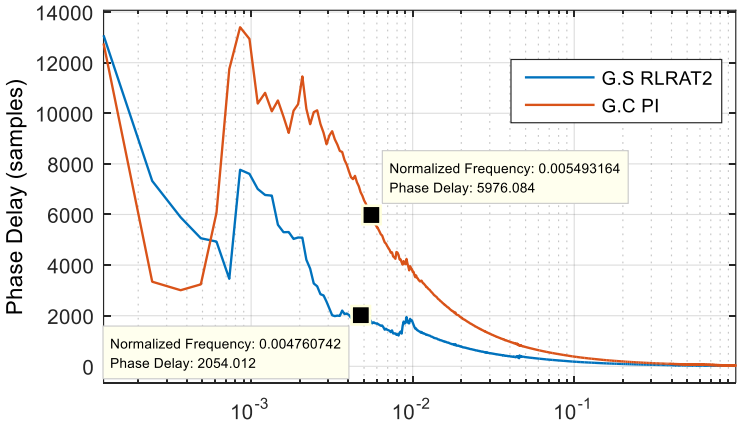

(c) Phase delay

Fig. 6.36. Case.6. Time and frequency responses for speed error acceleration

In region 3, the aim is to regulate the rotor speed to a certain set point while keeping constant generator torque. Additional fluctuations and unwanted movements of the pitch control signal for the GC-PI controller can be seen in Fig. 6.37. (a, b). and not for the GS-RL-RANFIST2. This is due to the fact that GC-PI controller is a linear controller, and its control gains are optimized at one operation point, while the GS-RL-RANFIST2 is a nonlinear controller, whose control gains are suitable for the whole wind speed regions, based on the cancellation of nonlinearities and gain scheduled technique. The GS-RL-RANFIST2 tunes several sets of gains around several operating points, while the G.C PI only tunes one pair of gains of PI. Fig. 9b shows that the magnitude of fluctuations is notably reduced by using the developed controller.

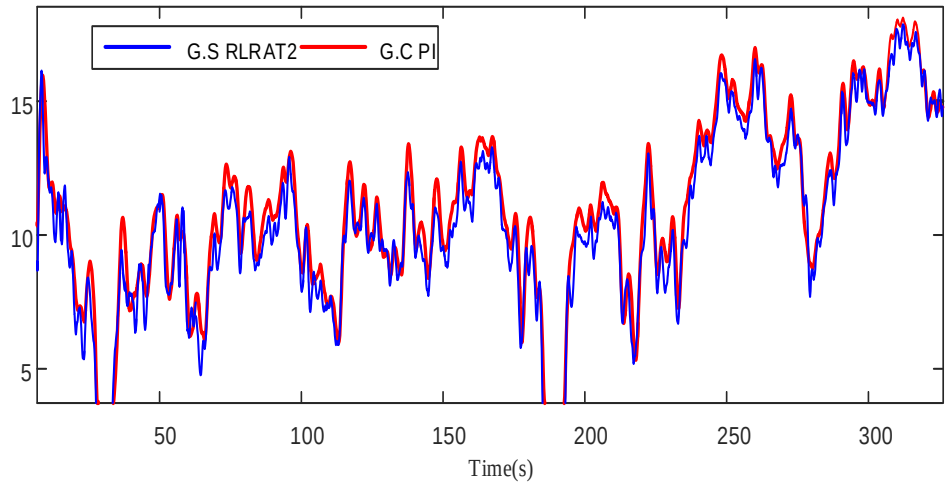

(a) Pitch control signal (deg)

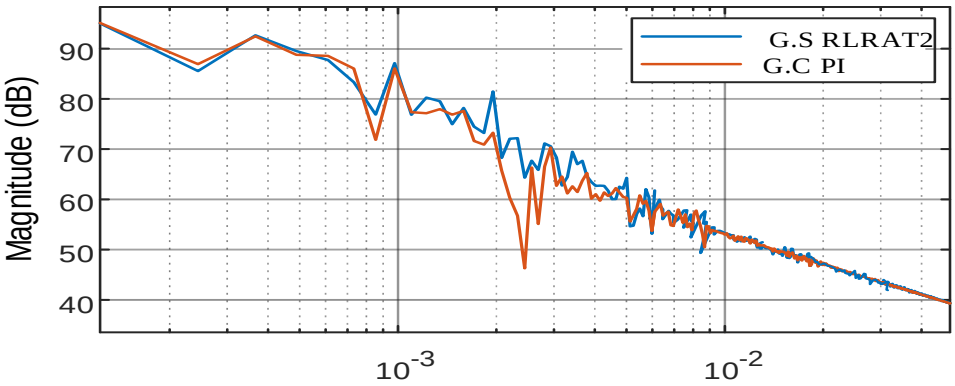

(b) Pitch frequency response (log)

Fig. 6.37. Case.6. Time and frequency domain responses for pitch angle acceleration

Fig. 6.38. (a)-(c) show the results of the output power, generator speed, and torque, in which the stable oscillations band confirm the robustness of the developed controller to the model uncertainties.

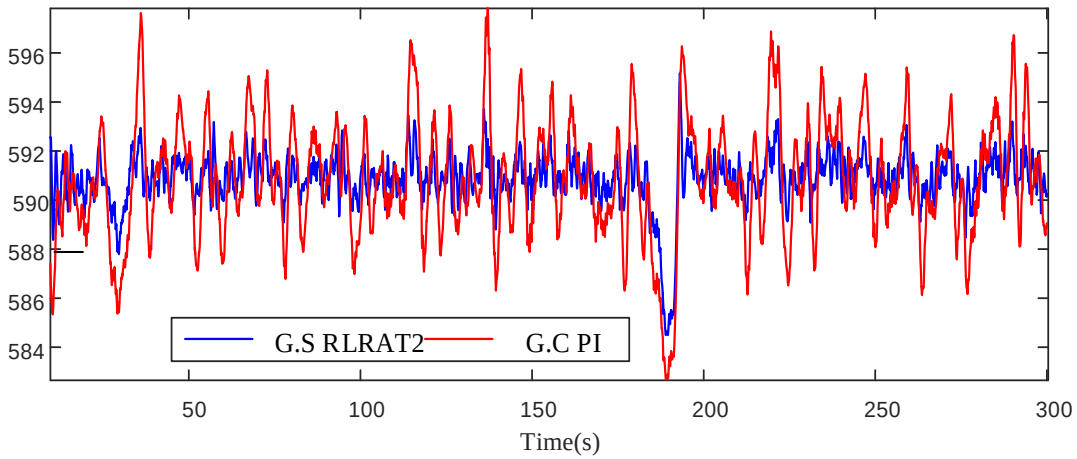

(a) Generator power (kW)

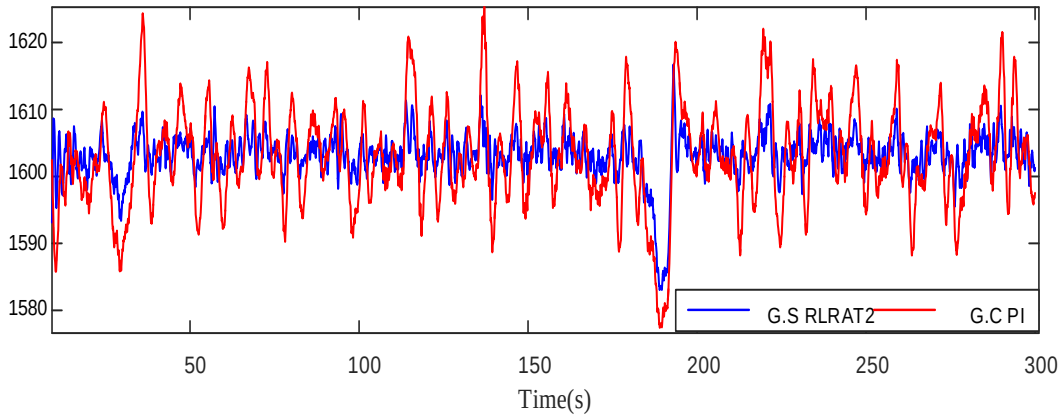

(b) Generator speed (rpm)

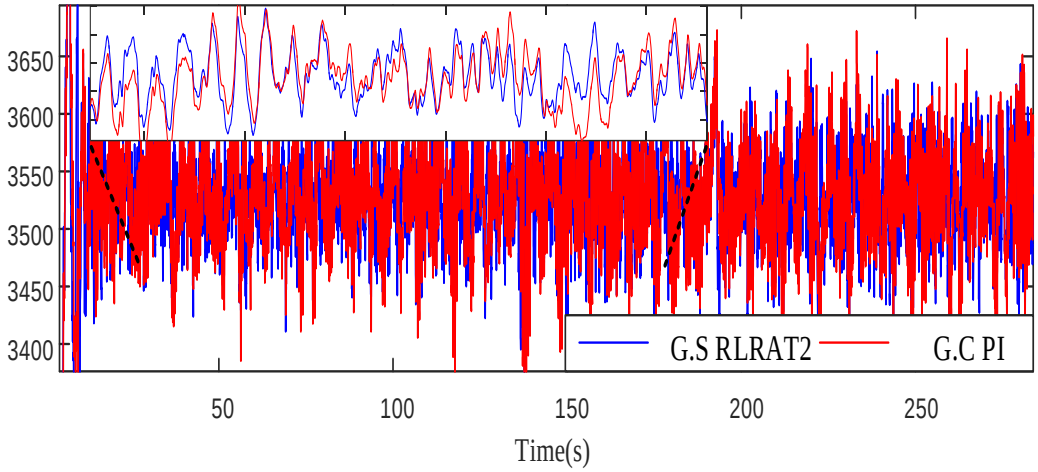

(c) Generator torque (N.m)

Fig. 6.38. Case.6. Results obtained for the CART3: (a) generator power (kW); (b) generator speed (rpm); (c) generator torque (N.m)

The data are visualized using box-plot and histogram plot in Fig. 6.39 to show the error intensity. Both plots represent the normalized error distribution for each controller. The results show that the distributed error between -3,3 has a twice better concentration around zero for the proposed controller. It can also be observed that the mean of the rotor speed regulation error obtained with the proposed controller is intensified around the zero more than the GC-PI controller. Furthermore, for the proposed controller, the mean error is 0.004017 and error STD is 0.8, while, for the GC-PI, these parameters are 0.008557 and 0.539, respectively.

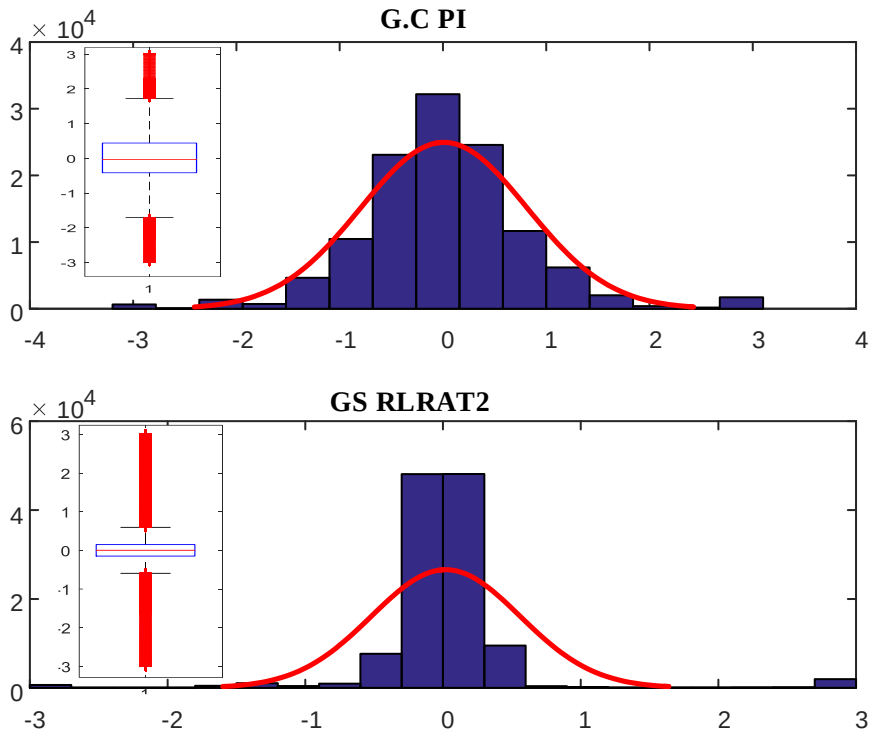

Fig. 6.39. Case.6. Comparison of the speed error acceleration by boxplot and histogram plot

For stability purposes, the generator speed (167.5516 rad/s) is considered lower than its real rated speed and the maximum torque is set in 3524.37 N.m, as usual for CART3, and therefore, the output power would be limited less than the rated value (600 kW), as seen in Fig. 6.38. (a). In this respect, the mean power generated with the GC-PI is 584.86 kW, whereas the mean power generated with the GS-RL-RANFIST2 is 588.61 kW. Any system, whose internal structure or internal model is unknown, could be controlled by the proposed method. The advantages of the proposed method are the reduction of the complexity of the controller design by diminishing the number of rules used in fuzzy type-2, the possibility of covering more modes of the system nonlinearity by using the recurrent structure and reducing human experience in controller design.

*6.1.8.3. **Longer simulation for comparative study and load analysis***

To evaluate the controller efficiency for a longer period and carry out the damage equivalent load (DEL) analysis, the output results of CART3 during 4000s are provided in this study, Fig. 6.40.

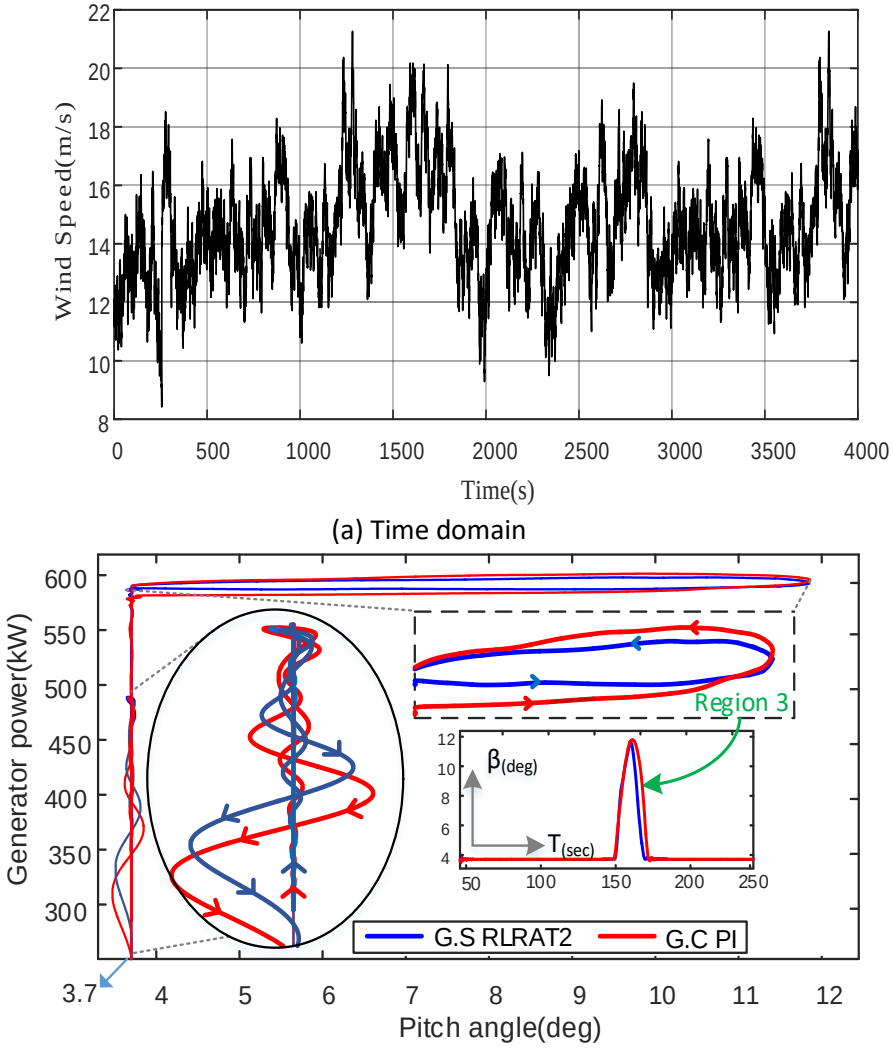

(a) Time domain

(b) Generator power (kW) versus pitch angle (deg)

Fig. 6.40. Case.6. Results for 4000 s simulation (a). Wind pattern (b). Pitch angle curve

On the other hand, the aerodynamic and electrical efficiency are used to evaluate the controller performance for a longer period of time, which can be obtained respectively by:

$$\eta_{aero}(\%) = \frac{\int_{t_0}^{T} P_a dt}{\int_{t_0}^{T} 0.5\rho\pi R^2 C_{P_{opt}} dt} \tag{4.43}$$

$$\eta_{elec}(\%) = \frac{\int_{t_0}^{T} P_e dt}{\int_{t_0}^{T} 0.5\rho\pi R^2 C_{P_{opt}} dt} \tag{4.43}$$

Table 6.11 represents the analytical comparison based on different parameters for both conventional and proposed control strategies. The parameters used are: the mean of the generated power, positive mean speed error (error of speed above zero), standard deviation (STD) of the speed error, aerodynamic and electrical efficiency, captured energy in windy months (from November to March) and captured energy for the WT lifespan (20 years). The enhanced value is calculated as the modulus of the difference between the value obtained by

the GS-RL-RANFIST2 and that achieved by the GC-PI controller. It shows that, at the interval of windy months (from November to March, with mean wind speed 15% and turbulence intensity 13%), the proposed controller achieves to capture 500kWh more energy than the GC-PI, and, by analogy, 30 MWh more energy for the turbine lifespan (20 years).

Table 6.11. Case.6: Comparison of the control strategies.

	Power mean (kW)	**mean error**	**STD**	η_{aero} **(%)**	η_{elec} **(%)**	**Captured energy (kWh)** (November to March)	**Captured energy (kWh) (20 years)**
G.C PI	5.6887e5	0.6	0.8301	87.47	74. 05	1638e3	9966e7
G.S RLRAT2	5.6904e5	0.3381	0.6724	94.08	76. 38	1688e3	9969e7
Enhanced value	164.3461	0.2619	0.1577	6.61	2.33	500	30e3

The lower values of positive mean error and STD demonstrate the superiority of the proposed control for the speed control. The results prove that the GS-RL-RANFIST2 is a promising control algorithm for improving the energy capture of an existing wind turbine operating in region 3, without the need to know the turbine model and measure the wind speed.

To evaluate the mechanical loads, the moment value of blade I, tower moment and rotor thrust are considered as load variables.

Fig. 6.41 compares the time domain and frequency domain responses of GC-PI and GS-RL-RANFIST2, in which the performance and load indices of proposed controller and GC-PI of the NREL controller are evaluated for the 4000s simulation (with mean wind speed 15% and turbulence intensity 13%). Local edge-wise bending moment (Spn2MLxb1), flap-wise tip acceleration (TipALxb1), in-plane bending moments (RootMxb1), out-of-plane bending moments (RootMyb1), pitching moments (RootMzb1), tower-base fore-aft bending moment (TTDspFA), tower force (TwHt2FLxt) and Rotor thrust (RotThrust) are the load variables considered in this study and shown in Fig. 6.41.

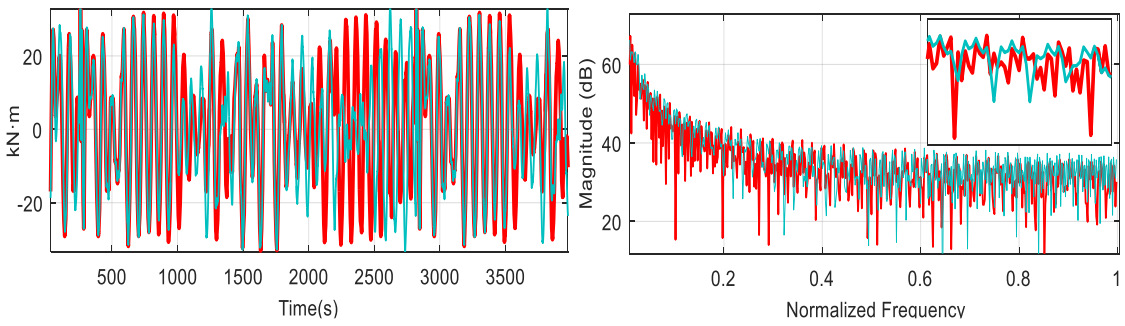

Fig. 6.41 Case.6. Moment variations on blade I, tower and rotor as a function of time and frequency; blue line (GS-RL-RANFIST2), red line (GC-PI)

Fig. 6.42 show the bar charts of the normalized DEL value calculated using NREL's MCrunch [144] for the GC-PI and GS-RL-RANFIST2.

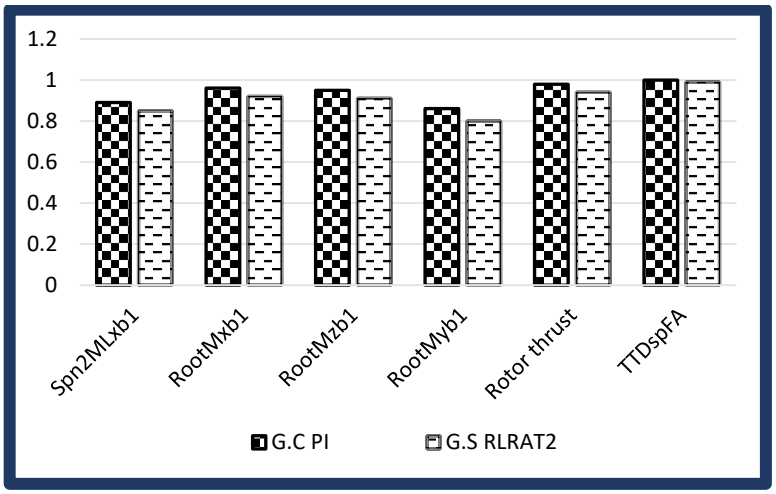

Fig. 6.42. Case.6. Normalized DEL values of the selected load variables for CART3

There is no doubt that the proposed controller achieves better DEL values for the blade moments than tower moments and shaft torsional rate. The bar charts proves that the DELs of most load variables achieved by the GS-RL-RANFIST2 controller are lower than those obtained by the GC-PI controller.

6.2. Comparison of EMSs

In this chapter five, different EMSs including SOC, MPC, OPT, FLC, and RL EMS have been proposed and discussed for the supervisory control system.

SOC-EMS is the simplest one that not only does not have complexity in designing, but also shows sufficiently good tracking of demanded power. Although MPC is a little difficult to be tuned, but it has a better response competed to SOC-EMS in tracking requested power. FLC proves its superiority over all other EMSs in well tracking of grid reference power. Needless to say, that the number of rules makes this EMS complicated and a boring simulation running time. OPT shows the best efficiency value as it designed for this purpose, however, needs a better sample time to track the reference power more accurate. At the end, RL algorithm proves that it can be a trustworthy EMS while it can accept multi-objective tasks. The multiagent RL dispatched power between BESs appropriately based on the SOC values and tracked the grid reference power. However, it is not recommended as learning of two agents is more complicated than a single-agent one. The single-TD3-agent showed a fantastic performance in the sight of the author as it was trained for totally other modules' sources, another references of power sources and PV irradiances, and simulation conditions. And when it tested in other environment, it proved its robustness, well tracking performance, adaptive behaviour, and fast response.

CHAPTER SEVEN

CAPÍTULO SIETE

7

7. Conclusions, contributions and future works

In this chapter, the most relevant contributions of this thesis are highlighted, and conclusions drawn from each control system are presented. Based on the simulation/experimental results of the hybrid configurations, concluding remarks are given. Finally, future research works to advance in the framework of this study are suggested.

7.1. Conclusions

A comprehensive study for the optimal operation of a grid-connected hybrid power plant with WT, PV power plants, and different BES integrated into a BES-qZS-CHBMLI was sought. BESs showed their benefits in compensating intermittent characteristics of RES. For incorporating of BESs to qZS-CHBMLI, five different EMS configurations were proposed and tested under varied operating conditions. The simulation with variable active and reactive power grid demand, varying PV plants' irradiances, and fluctuating incoming wind speed were sought.

All EMSs were able to address the grid demand and attain constant power generation regardless of the sun irradiance values, wind speed, and demanded power. It was seen that the active and reactive power grid requirements were successfully fulfilled by all the five EMS configurations. Moreover, other control objectives were presented to have a broad controlled configuration. P, Q control loops, modulation techniques, MPPT algorithms, and pitch angle control methods are among them that have been studied and implemented for our case of study.

The first EMS called SOC-EMS for BES-qZS-CHBMLI was used to dispatch power between BESs based on the SOC values. The simplicity and effectiveness of the SOC-EMS makes it applicable in practice that can be used in other topologies. Appropriate tracking of grid reference power, maintaining the BES SOCs in a specific-safe range of maximum charging and discharging, and sorting and releasing energy based on the BESs nominal power, were the advantages of this suggested EMS.

The second EMS called MPC-EMS was suggested for BES-qZS-CHBMLI to divide power between BESs. Notwithstanding the fact that tuning a model predictive control appropriate for our complicated case of study is a tough assignment, MPC-EMS showed that can do the work more efficiently than SOC-EMS. The appropriate power despatching between BESs is achieved based on SOCs values and whenever grid operator called for more power, MPC-EMS rapidly responded by releasing the proper amount of power.

The third EMS called FLC-EMS was proposed for BES-qZS-CHBMLI to share available power among BESs in a manner of prioritizing power sharing based on the BES SOC values. This fuzzy logic controller is suggested by author with four inputs (gap between production and demand, and SOC values) and three BESs reference powers as the outputs of FLC. The rule table has 180 rules only including inequality SOCs to reduces the complexity of controller, however, it is easy to write all other conditions based on the presented table. The results found by FLC-EMS showed the best adaptive performance among all EMSs. The faster response with less overshoot at the time of changing the grid reference power was the main feature of this EMS. Regardless of the RES source and output powers, FLC-EMS satisfy the grid demanded power quickly while cares about BES SOCs.

The fourth EMS called OPT-EMS was mainly introduced to enhance BESs efficiency and lifetime issues. OPT-EMS defined the BES power reference of the BES integrated into the ES-qZS-CHBMLI. It was not only as an efficiency function optimizer, but also OPT-EMS satisfied the system power balance and provided the active and reactive powers requested by grid operator. The objective function introduced in this EMS was based on a total BES efficiency value found by every single BES efficiency and power. The BES power constraints proposed to be limited during optimization process, forced the algorithm to oversee the depth of the BES charging and discharging. It was found that it can be more efficient utilization of BESs if the potential power is divided among them BESs in an approach of DOD and SOC balance. Therefore, rather than sorting most of the energy in the BES with the least SOC or releasing energy by BES with the most SOC, it was commented that other BESs (not BES with the most or least SOC) must receive or produce power as much as it can be possible based on the defined power constraints. Beside all these tasks, OPT-EMS showed proper tracking of the grid reference power.

The fifth and the last EMS that proposed in this thesis, was RL-EMS that implemented through multiagent and single agent algorithms. TD3 suggested as it performed better than other continues agents like DDPG and PPO agents. It was witnessed a breathtaking result when an agent trained for 8 seconds and only PV plants were used as the source of modules and then the trained agent was tested for a 100 second simulation time, a hybrid RES configuration, and different produced and requested powers. It proved that the agent had not been trained for a specific operation condition. This was owed of using a local function that initialized the simulation parameters different and varying in every time that simulation ran. Appropriate tracking of grid reference power, maintaining the BES SOCs in a specific-safe range of maximum charging and discharging, and sorting and releasing energy based on the BESs nominal power, were the responsibilities of this suggested EMS.

MPPT and pitch angle control strategies were also sought in this thesis that consisted of intelligent and conventional approaches. P&O algorithm was used in the multilevel configuration to execute MPPT process. Moreover, an adaptive PI control was also used for MPPT of a variable-speed WT and another passive RL algorithm was proposed in the same WT as the pitch angle controller. Comparing RL algorithm with the adaptive PI, dynamic response of RL was faster and gentler that leaded to more power extraction and optimal WT utilization.

7.2. Main contributions of the thesis

Along the progress of this thesis, several contributions have been made to the field of study. These are summarized here.

- A thorough review of the literature has been carried out to explore the different topologies applied for high power system applications of RES. As multilevel converters have caught more attention, different types of them have reviewed and cascaded multilevel inverters stated more in details. Additionally, various energy management system having been applied for the system under study reviewed and compared in different aspects.
- A BES-qZS-CHBMLI has been implemented and connected to a grid. Finding active and passive elements of impedance network, calculating parameters of the grid filter, finding RES power output appropriate for the required power level, and selecting BES

type and nominal and initial parameters were sufficiently complicated for such a knotty structure.

- Different control strategies for hybrid RES system comprising WT, PV, and BES for BES-qZS-CHBMLI have been squeegeed, modelled, and compared under different scenarios. These control systems have been targeted to the control systems of the (a). MPPT employed in the WT and PV power sources, (b). PQ control delivered to the grid, (c). modulation methods applied for multilevel cascade converter structure, (d). various EMSs proposed and implemented for power dispatching among BESs.

- The comparative studies included evaluation under nonidentical and varying PVs' irradiances, fluctuating wind with a ramp block in the wind pattern, and variable grid demand, and more importantly, integrating nonidentical BESs with different types and parameters. All the previous works have used a configuration of power plant based on a BES-qZS-CHBMLI integrating the same PV systems and BESs into each module in series, while in this thesis integration of PV or WT sources with different nominal power in each module have been sought.

- Different energy management systems have been proposed and compared to each other from various aspects. SOC-EMS and MPC-EMS applied in other works are implemented in the same manner to be compared with the new EMSs proposed in this thesis. The indexes of comparison were reference power tracking performance, SOC and DOD analysis, and BES global efficiency values. BES efficiency has overlooked in all previous work in designing EMS for BES-qZS-CHBMLI configurations.

- A new fuzzy logic controller has been proposed as EMS for the configuration under study. FLC was designed to track as much reference power as possible while prioritizing the amount of charging and discharging based on the BES SOC values. The proposed FLC showed an adaptive behaviour better than all other EMSs. This was due to the fact that fuzzy table and rule base were defined for every single circumstance of the system. Moreover, the number of membership functions and their placement were designed not only for the topology under study, but also for other systems using three BESs in their modules.

- Another new EMS developed herein was OPT-EMS using fmincon Matlab function. This one specifically designed to enhance BESs global and local efficiencies while it was obliged to dispatch power based on SOC values and grid requests. The main contribution of this EMS was introducing an objective function with specific constrains in order to take BESs efficiencies into consideration. The constrains considered BES nominal and initial parameters to maintain the received or produced power unique for every BES. Beside all, it showed an acceptable performance in tracking reference power and meeting demand while limiting SOC values between safe ranges. The experimental results obtained for comparing SOC-MPC- OPT EMSs.

- Another main novelty of this thesis is using reinforcement learning algorithm for managing energy in BES-qZS-CHBMLI configurations. At first a multiagent RL proposed, where one agent for charging and another one for discharging mode were designed. Training came much easier and faster by using external actions producing zero vectors when the mode of the BESs (charging or discharging) is not business of specific agent working in contrary mode. Another idea in designing this multiagent algorithm was

separating reward function and observation parameters for agents independent of each other. Then, a single agent trained for a short simulation interval but with random initialization in every simulation running. The agent to be trained, the simulation ran 5000 time and each time: with different RES input values, nonidentical reference grid pattern, and different BES parameters. This procedure made the RL algorithm super adaptive and util for other simulation conditions. It was tested in a longer simulation interval, in a hybrid RES configuration, and totally different circumstances. The RL-EMSs appropriately satisfied the demanded grid power and dispatched available power among BESs based on the SOC values. The constrained defined for OPT-EMS were used in the reward function of RL-EMS to somehow cares about BESs efficiencies.

- Another contribution was implementing a passive reinforcement learning that was solved by PSO algorithm. Using transfer learning was the key factor of this controller. In a way that for each step, training started with the data had obtained in the previous stage. Using unsupervised FCM clustering and fuzzy type-2 made a huge difference in controlling pitch angel in intensive fluctuating conditions. Implementing this system in CART3 real wind turbine by FAST simulator was also another contribution.

7.3. Future works

The research works carried out throughout the progress of this thesis have contributed to the existing knowledge in the field, being the most relevant results published in peer-reviewed scientific journals. Nonetheless, there is still a broad potential to exploit in the study of EMS configurations. Hence, the following approaches are proposed for exploration as future works in this topic.

- Increasing the number of modules to increase the energy level of configuration. Using RES in power systems is widely increasing and therefore utilizing them entails using multilevel configurations. Increasing the number of levels and therefore battery storages help to have a higher energy level.

- Using fuzzy logic type-2 instead of type-1, to makes the FLC-EMS more adaptive to varying conditions. Tufan Kumbasar in Istanbul University has recently (2018) introduced a fuzzy type-2 toolbox that is so similar the Matlab type-1 toolbox. Different fuzzy type reducer algorithms are also provided in this toolbox.

- Using fuzzy logic or model predictive control in designing reward function will improve the behaviour of the RL algorithm. It can help to reduce the training time and adaptivity of agent to RES energy fluctuations.

- Modulation with RL algorithm is another suggestion. We have designed a RL modulation technique in a paper for multi modular inverter with totally 50 submodules in upper and lower arms. DQN agent as discrete agent was suggested and tested. Therefore, DQN agent is suggested to achieve modulation goals. The advantage of using RL can be the enhanced frequency switching if the agent fulfils the goals with less actions. In addition, the balance of thermal stress between IGBT switches should be considered to equalize the lifetime expectation of semiconductors and to enhance the current capability of multilevel configurations.

- Using transfer learning is suggested during RL designing to make the training less complicated and less time consuming. Matlab has the option of training a pretrained agent to follow the training with more gaols and requests. Moreover, the approach of transferring data suggested for pitch controller, could be used for RL-EMS to enhance its' performance.
- To increase the BES efficiency, in RL-EMS, a reward term of (global efficiency) × e5 is suggested to encourage the TD3 agent to enhance efficiency during training. This term can be in logarithmic form to give a huge reward for a small enhance in efficiency.

References

[1] H. Zhu, K. Ouahada, and A. M. Abu-Mahfouz, “Transmission Loss-Aware Peer-to-Peer Energy Trading in Networked Microgrids,” *IEEE Access*, vol. 10, pp. 126352–126369, 2022, doi:10.1109/ACCESS.2022.3226625.

[2] International Energy Agency (2015), Energy and Climate Change – World Energy Outlook Special Briefing for COP21. IEA, Paris. doi:http://www.worldenergyoutlook.org/media/news/WEO2015_COP21Briefing.pdf. (accessed June 2016).

[3] D. Saygin, R. Kempener, N. Wagner, M. Ayuso, and D. Gielen, “The Implications for Renewable Energy Innovation of Doubling the Share of Renewables in the Global Energy Mix between 2010 and 2030,” *Energies (Basel)*, vol. 8, no. 6, pp. 5828–5865, Jun. 2015. doi: http://dx.doi.org/10.3390/en8065828.

[4] O. Ellabban, H. Abu-Rub, and F. Blaabjerg, “Renewable energy resources: Current status, future prospects and their enabling technology,” Renewable and Sustainable Energy Reviews, vol. 39, pp. 748–764, Nov. 2014, doi: 10.1016/j.rser.2014.07.113.

[5] IRENA (2016), Renewable Energy Benefits: Measuring the Economics, January 2016. IRENA, Abu Dhabi. doi:http://www.irena.org/menu/index.aspx?mnu=Subcat&PriMenuID=36&CatID=141&SubcatID=690 (accessed June 2016).

[6] (IRENA, 2019), Renewable Power Generation Cost in 2018, 2018 International Conference on Computation of Power, Energy, Information, and Communication (ICCPEIC).

[7] European Commission. Climate Action - Paris agreement 2015. doi:http://ec.europa.eu/clima/policies/international/negotiations/paris/index_en.htm (accessed June 2016).

[8] International Energy Agency (2015), World Energy Outlook Special Report 2015: Energy and Climate Change. IEA, Paris. doi: https://www.iea.org/publications/freepublications/publication/weo-2015-special-report-2015-energy-and-climate-change.html (accessed June 2016).

[9] IRENA (2014), Remap 2030: A Renewable Energy Roadmap, June 2014. IRENA, Abu Dhabi. doi:http://www.irena.org/menu/index.aspx?mnu=Subcat&PriMenuID =36&CatID=141&SubcatID=422 (accessed June 2016).

[10] A. Bedawy, N. Yorino, K. Mahmoud, and M. Lehtonen, “An Effective Coordination Strategy for Voltage Regulation in Distribution System Containing High Intermittent Photovoltaic Penetrations,” IEEE Access, 2021, doi: 10.1109/ACCESS.2021.3106838.

[11] R. Georgious, R. Refaat, J. Garcia, and A. A. Daoud, “Review on Energy Storage Systems in Microgrids,” Electronics 2021, Vol. 10, Page 2134, vol. 10, no. 17, p. 2134, Sep. 2021, doi: 10.3390/ELECTRONICS10172134.

[12] M. Itoh, H. Takahashi, T. Fujii, H. Takakura, Y. Hamakawa, and Y. Matsumoto, “Evaluation of electric energy performance by democratic module PV system field test,” Sol. Energy

Mater. Sol. Cells, vol. 67, no. 1–4, pp. 435–440, Mar. 2001, doi: 10.1016/S0927-0248(00)00312-3

[13] S. Kijima, T. Nakada, “High-temperature degradation mechanism of Cu(In,Ga)Se2-based thin film solar cells,” Appl. Phys. Express, vol. 1, no. 7, pp. 0750021–0750023, 2008, doi: 10.1143/APEX.1.075002.

[14] T. Ameri, G. Dennler, C. Lungenschmied, C. J. Brabec, “Organic tandem solar cells: A review,” Energy Environ. Sci., vol. 2, no. 4, pp. 347–363, 2009, doi: 10.1039/b817952b

[15] A. Review, “The Applications of Polymers in Solar Cells :,” no. 3, pp. 1–46, 2019

[16] A. Luque and S. Hegedus, Handbook of Photovoltaic Science. 2003.

[17] M. Jørgensen, K. Norrman, and F. C. Krebs, “Stability/degradation of polymer solar cells,” Sol. Energy Mater. Sol. Cells, vol. 92, no. 7, pp. 686–714, 2008, doi: 10.1016/j.solmat.2008.01.005.

[18] M.-E. Yeoh and K.-Y. Chan, “Recent advances in photo-anode for dye-sensitized solar cells: a review,” Int. J. Energy Res., vol. 41, no. 15, pp. 2446–2467, Dec. 2017, doi: 10.1002/er.3764.

[19] P. Frankl, E. Menichetti, M. Raugei, S. Lombardelli, and G. Prennushi, “New Energy Externalities Developments for Sustainability ‘ Final report on technical data , costs and life cycle inventories of PV applications ,’” pp. 1–81, 2006.

[20] International Energy Agency (2013), Technology Roadmap - Wind energy 2013 Edition. IEA, Paris. doi: https://www.iea.org/publications/freepublications/ publication/Wind_2013_Roadmap.pdf (accessed June 2016).

[21] I. Hadjipaschalis, A. Poullikkas, V. Efthimiou, “Overview of current and future energy storage technologies for electric power applications,” Renew. Sustain. Energy Rev., vol. 13, no. 6–7, pp. 1513–1522, 2009, doi: 10.1016/j.rser.2008.09.028.

[22] C. V Govinda, S. V Udhay, C. Rani, Y. Wang, and K. Busawon, “A Review on Various MPPT Techniques for Wind Energy Conversion System,” in 2018 Internat2018 International Conference on Computation of Power, Energy, Information and Communication (ICCPEIC)

[23] Fang Zheng Peng, “Z-source inverter,” IEEE Trans. Ind. Appl., vol. 39, no. 2, pp. 504–510, 2003, doi: 10.1109/TIA.2003.808920.

[24] M. Shen, A. Joseph, J. Wang, F. Z. Peng, and D. J. Adams, “Comparison of traditional inverters and Z-source inverter for fuel cell vehicles,” IEEE Trans. Power Electron., vol. 22, no. 4, pp. 1453–1463, 2007, doi: 10.1109/TPEL.2007.900505.

[25] C. S. Lai, Y. Jia, L. L. Lai, Z. Xu, M. D. McCulloch, and K. P. Wong, “A comprehensive review on large-scale photovoltaic system with applications of electrical energy storage,” Renew. Sustain. Energy Rev., vol. 78, no. November 2016, pp. 439–451, 2017, doi: 10.1016/j.rser.2017.04.078

[26] X. Li, L. Yao, and D. Hui, “Optimal control and management of a large-scale battery energy storage system to mitigate fluctuation and intermittence of renewable generations,” J. Mod. Power Syst. Clean Energy, vol. 4, no. 4, pp. 593–603, 2016, doi: 10.1007/s40565-016-0247-y.

[27] A. A. Solomon, D. Faiman, and G. Meron, “Appropriate storage for high-penetration grid-connected photovoltaic plants,” Energy Policy, vol. 40, no. 1, pp. 335–344, 2012, doi: 10.1016/j.enpol.2011.10.019.

[28] H. Chen, T. N. Cong, W. Yang, C. Tan, Y. Li, and Y. Ding, “Progress in electrical energy storage system: A critical review,” Prog. Nat. Sci., vol. 19, no. 3, pp. 291–312, 2009, doi: 10.1016/j.pnsc.2008.07.014.

[29] A. P. Karpinski, B. Makovetski, S. J. Russell, J. R. Serenyi, D. C. Williams, “Silver – zinc : status of technology and applications,” no. February, 1999.

[30] P. P. Lopes and V. R. Stamenkovic, “Past, present, and future of lead–acid batteries,” Science (1979), vol. 369, no. 6506, pp. 923–924, Aug. 2020, doi: 10.1126/science.abd3352.

[31] N. Omar et al., Analysis of Nickel-Based Battery Technologies for Hybrid and Electric Vehicles. Elsevier Inc., 2014.

[32] O. M. Toledo, D. Oliveira Filho, and A. S. A. C. Diniz, “Distributed photovoltaic 122generation and energy storage systems: A review,” Renew. Sustain. Energy Rev., vol. 14, no. 1, pp. 506–511, 2010, doi: 10.1016/j.rser.2009.08.007.

[33] H. Akbari et al., “Efficient energy storage technologies for photovoltaic systems,” Sol. Energy, no. March, pp. 1–25, 2018, doi: 10.1016/j.solener.2018.03.052.

[34] IEC, “Electrical Energy Storage - White Paper,” Int. Electrotech. Comm., pp. 1–78, 2011, doi: 10.1002/bse.3280020501.

[35] A. Berrueta, A. Ursua, I. S. Martin, A. Eftekhari, and P. Sanchis, “Supercapacitors: Electrical Characteristics, Modeling, Applications, and Future Trends,” IEEE Access, vol. 7, pp. 50869–50896, 2019, doi: 10.1109/ACCESS.2019.2908558.

[36] “ESA - Energy Storage Association.” http://energystorage.org/ (accessed Aug. 28, 2018)

[37] S. Reddy Salkuti, “Electrochemical batteries for smart grid applications,” International Journal of Electrical and Computer Engineering (IJECE), vol. 11, no. 3, pp. 1849–1856, 2021, doi: 10.11591/ijece.v11i3.pp1849-1856.

[38] H. IBRAHIM, A. ILINCA, and J. PERRON, “Energy storage systems—Characteristics and comparisons,” Renew. Sustain. Energy Rev., vol. 12, no. 5, pp. 1221–1250, Jun. 2008, doi: 10.1016/j.rser.2007.01.023

[39] D. Deng, “Li-ion batteries: Basics, progress, and challenges,” Energy Sci. Eng., vol. 3, no. 5, pp. 385–418, 2015, doi: 10.1002/ese3.95.

[40] O. M. Toledo, D. Oliveira Filho, and A. S. A. C. Diniz, “Distributed photovoltaic 122 generation and energy storage systems: A review,” Renew. Sustain. Energy Rev., vol. 14, no. 1, pp. 506–511, 2010, doi: 10.1016/j.rser.2009.08.007

[41] Sarrias R, Fernández LM, Garcia CA, Jurado F. “Energy storage systems for wind power application.” International Conference on Renewable Energies and Power Quality (ICREPQ’10); Granada (Spain), 2010.

[42] H. Akbari et al., “Efficient energy storage technologies for photovoltaic systems,” Sol. Energy, no. March, pp. 1–25, 2018, doi: 10.1016/j.solener.2018.03.052.

[43] Hameer S, van Niekerk JL. “A review of large-scale electrical energy storage. ” Int J Energy Res 2015;39(9):1179-95.DOI: http://dx.doi.org/10.1002/er.3294

[44] R. Sarrias. Mena, “Wind Power Generation with Energy Storage System, ” Doctoral thesis, Cadiz University, 2016.

[45] S. H. Chung, H. Wang, F. Blaabjerg, and M. Pecht, “Reliability of power electronic converter systems”. 2016

[46] S. Piasecki, J. Zaleski, M. Jasinski, S. Bachman, M. Turzyński, “Analysis of AC/DC/DC Converter Modules for Direct Current Fast-Charging Applications,” Energies, vol. 14, no. 19, p. 6369, Oct. 2021, doi: 10.3390/en14196369.

[47] F. Roccaforte, F. Giannazzo, and G. Greco, “Ion Implantation Doping in Silicon Carbide and Gallium Nitride Electronic Devices,” Micro, vol. 2, no. 1, pp. 23–53, Jan. 2022, doi: 10.3390/MICRO2010002.

[48] Bimal K. Bose, “Modern Power Electronics and AC Drives, “ 1st ed. Prentice Hall, 2001. Accessed: Feb. 15, 2023. [Online]. Available: https://www.pearson.ch/HigherEducation/PrenticeHall/EAN/9780130167439/Modern-Power-Electronics-and-AC-Drives

[49] G. Zhang et al., “An extendable single-switch n-cell boost converter with high voltage gain and low components stress for renewable energy,” International Journal of Circuit Theory and Applications, vol. 48, no. 6, pp. 817–831, Jun. 2020, doi: 10.1002/cta.2801.

[50] A. Yazdani and R. Iravani, “Voltage-Sourced Converters in Power Systems”. Hoboken, NJ, USA: John Wiley & Sons, Inc., 2010. doi: 10.1002/9780470551578.

[51] B. Wu and M. Narimani, “High-Power Converters and AC Drives”: eBook, Wiley, Second Edition. 2016. doi: 10.1002/9781119156079.

[52] M. G. Taul, N. Pallo, A. Stillwell, and R. C. N. Pilawa-Podgurski, “Theoretical Analysis and Experimental Validation of Flying-Capacitor Multilevel Converters under Short-Circuit Fault Conditions,” IEEE Trans Power Electron, vol. 36, no. 11, 2021, doi: 10.1109/TPEL.2021.3075447.

[53] P. Boonchiam and N. Mithulananthan, “Diode-clamped Multilevel Voltage Source Converter Based on Medium Voltage DVR,” no. March, pp. 590–595, 2008.

[54] V. Sharna, “Diode Clamped Multilevel Inverter Switching Topology,” International Journal of Industrial Electronics and Electrical Engineering, no. 5, 2017.

[55] “Low voltage controls and distribution, ” available at http://www.siemens.com/

[56] Y. Liu, “Impedance source power electronic converters”, eBook, Wiley, pp. 1-424, Accessed: Feb. 15, 2023. [Online].Available: https://www.wiley.com/enes/Impedance+Source+Power+Electronic+Converters-p-9781119037071

[57] Y. Zhou, L. Liu, H. Li, “A high-performance photovoltaic module-integrated converter (MIC) based on cascaded quasi-Z-source inverters (qZSI) using EGANFETS,” IEEE Trans. Power Electron., vol.28, no.6, pp.2727–2738, 2013.

[58] Y. Liu, B. Ge, H. Abu-Rub, F. Z. Peng, "A modular multilevel space vector modulation for photovoltaic quasi-Z-source cascade multilevel inverters," in Proc. Twenty-Eighth Annual IEEE Applied Power Electronics Conference and Exposition (APEC), pp.714–718, 2013.

[59] L. Yang, D. Qiu, B. Zhang, G. Zhang, "A high-performance Z-source inverter with low capacitor voltage stress and small inductance," in Proc. 29th Annu. IEEE Applied Power Electronics Conf. Exposition (APEC), Mar. 16–20, 2014, pp. 2331–2337

[60] Y. Zhu, M. Chen, X. Lee, and Y. Tsutomu, "A novel quasi-resonant soft-switching Z-source inverter," in Proc. IEEE Int. Conf. Power and Energy (PECon), Dec. 2–5, 2012, pp. 292–297

[61] P. A. Bachurin, D. V. Makarov, A. V. Geist, M. V. Balagurov, and D. A. Shtein, "Z-source inverter with neutral point," in Proc. 14th Int. Conf. Young Specialists on Micro/Nanotechnologies and Electron Devices (EDM), July 1–5, 2013, pp. 255–258.

[62] O. Ellabban and H. Abu-Rub, "Z-Source Inverter: Topology Improvements Review: Z-Source Inverter,", IEEE Industrial Electronics Magazine, vol. 10, no. 1, pp. 6- 24, Mar. 2016, doi: 10.1109/MIE.2015.2475475

[63] D. Sun, B. Ge, F. Z. Peng, A. R. Haitham, D. Bi, and Y. Liu, "A New Grid-Connected PV System Based on Cascaded H-bridge Quasi-Z Source Inverter," IEEE International Symposium on Industrial Electronics, May.2012, doi: 10.1109/ISIE.2012.6237218.

[64] Y. Liu, B. Ge, H. Abu-Rub, F. Z. Peng, "An effective control method for quasi-Z-source cascade multilevel inverter based three-phase grid-tie photovoltaic power system," IEEE Trans. Ind. Electron., vol.61, no.12, pp.6794–6802, Dec. 2014.

[65] Y. Xue, B. Ge, F. Z. Peng, "Reliability, Efficiency, and Cost comparisons of MW-scale photovoltaic inverters," in Proc. IEEE Energy Conversion Congress and Exposition (ECCE), 2012, pp.1627–1634.

[66] Y. Zhou, L. Liu, H. Li, "A high-performance photovoltaic module-integrated converter (MIC) based on cascaded quasi-Z-source inverters (qZSI) using EGANFETS," IEEE Trans. Power Electron., vol.28, no.6, pp.2727 2738, 2013.

[67] D. Sun, B. Ge, F. Z. Peng, H. Abu-Rub, D. Bi, Y. Liu, "A new grid-connected PV system based on cascaded H-bridge quasi-Z source inverter," in Proc. IEEE International Symposium on Industrial Electronics (ISIE), 2012, pp.951–956.

[68] D. Sun, B. Ge, X. Yan, D. Bi, H. Zhang, Y. Liu, H. Abu-Rub, L. Ben-Brahim, F. Z. Peng, "Modeling, impedance design, and efficiency analysis of quasi-Z source module in cascade multilevel photovoltaic power system," IEEE Trans. Ind. Electron., vol.61, no.11, pp.6108–6117, 2014.

[69] Y. Liu, B. Ge, H. Abu-Rub, F. Z. Peng, "An effective control method for quasi-Z-source cascade multilevel inverter based grid-tie single-phase photovoltaic power system," IEEE Trans. Ind. Informat., vol.10, no.1, pp.399–407, Feb. 2014.

[70] D. Sun, B. Ge, F. Z. Peng, A. R. Haitham, D. Bi, and Y. Liu, "A New Grid-Connected PV System Based on Cascaded H-bridge Quasi-Z Source Inverter," IEEE International Symposium on Industrial Electronics, May.2012, doi: 10.1109/ISIE.2012.6237218.

[71] C. Roncero-Clemente, E. Romero-Cadaval, O. Husev, and D. Vinnikov, “P and Q control strategy for single phase Z/qZ source inverter based on d-q frame,” in IEEE International Symposium on Industrial Electronics, 2014. doi: 10.1109/ISIE.2014.6864932.

[72] O. Alonso, P. Sanchis, E. Gubia, L. Marroyo, “Cascaded H-bridge multilevel converter for grid connected photovoltaic generators with independent maximum power point tracking of each solar array,” IEEE 34th Annual Power Electronics Specialist Conference, PESC ’03, Acapulco, Mexico, vol. 2,pp. 731–735, 15-19 June, 2003.

[73] S. Rivera, S. Kouro, B. Wu, J.I. Leon, J. Rodriguez, L.G. Franquelo, “Cascaded H-bridge multilevel converter multistring topology for large scale photovoltaic systems,” IEEE International Symposium on Industrial Electronics, ISIE 2011, Gdansk, Poland, pp. 1837–1844, 27-30 Jun., 2011.

[74] Jayalakshmi, N. S., and D. N. Gaonkar. "Maximum Power Point Tracking for Grid Integrated Variable Speed Wind based DG System with Dynamic Load." International Journal of Renewable Energy Research (IJRER) 4, no. 2 (2014): 464-470.

[75] Neetu Singh, Dr. Bhupal Singh, “Design and Modeling of Wind Energy Conversion System Based on PMSG Using MPPT Technique” in International Journal of Scientific Research Engineering & Technology (IJSRET),Volume 5, Issue 2, February 2016.

[76] B. Lahfaoui, S. Zouggar, M. L. Elhafyani, M. Seddik. "Experimental study of P&O MPPT control for wind PMSG turbine." In Renewable and Sustainable Energy Conference (IRSEC), 2015 3rd International, pp. 1-6. IEEE, 2015.

[77] D L Manoj Kumar ,Dr. G.V.S.Krishna rao, “Modeling and MPPT Control of Hybrid WIND/PV/Fuel Cell Unit Energy Sources for Distributed Generation”, international Research Journal of Engineering and Technology (IRJET), Volume: 02 Issue: 04, July-2015.

[78] González, L. G., E. Figueres, G. Garcerá, and O. Carranza. "Maximum power-point tracking with reduced mechanical stress applied to wind-energy conversion-systems." Applied Energy 87, no. 7 (2010): 2304-2312.

[79] Sarkar, Joydeep, and Shridhar S. Khule. "A study of MPPT schemes in PMSG based wind turbine system." In Electrical, Electronics, and Optimization Techniques (ICEEOT), International Conference on, pp. 100-105. IEEE, 2016.

[80] B. Lahfaoui, S. Zouggar, M. Larbi, et al, " Real Time Study of P&O MPPT Control for Small Wind PMSG Turbine Systems Using Arduino Microcontroller." Energy Procedia (2017) DOI: 10.1016/j.egypro.2017.03.263.

[81] M. Gomez, E. Ribeiro, J. Estima, C. Boccaletti, and A. J. M. Cardoso, “Development of an effective MPPT method suitable to a stand-alone, low-cost wind turbine system,” in IECON Proceedings (Industrial Electronics Conference), 2016. doi: 10.1109/IECON.2016.7793128.

[82] Femia, Nicola, Giovanni Petrone, Giovanni Spagnuolo, and Massimo Vitelli. "Optimization of perturb and observe maximum power point tracking method." IEEE transactions on Power Electronics 20, no. 4 (2005): 963-973.

[83] R. Sitharthan, K. R. Devabalaji, A. Jees,"An Levenberg–Marquardt trained feedforward back-propagation based intelligent pitch angle controller for wind generation system", Renewable Energy, Vol. 22, pp.24-32, Dec. 2017.

[84] G. Abdalrahman, W. Melek, F. S. Lien, "Pitch angle control for a small-scale Darrieus vertical axis wind turbine with straight blades (H-Type VAWT)", Renewable Energy, Vol. 14, pp. 1353–1362, Dec. 2017.

[85] Luis M. Fernández, Carlos Andrés Garcia, Francisco Jurado, "Operating capability as a PQ/PV node of a direct-drive wind turbine based on permanent magnet synchronous generator", Renewable Energy, Vol. 35, No. 6, pp. 1308-1318, June. 2010.

[86] B. Boukhezzar, L. Lupu, H. Siguerdidjane, M. Hand, "Multivariable control strategy for variable speed variable pitch wind turbines", Renewable Energy, Vol. 32, No. 8, pp. 1273–1287, 2007.

[87] E. Hosseini, GH. Shahgholian, "Output power leveling for DFIG WTS using intelligent pitch angle control", Journal of Control, Measurement, Electronics, Computing and Communications, Vol. 58, No. 4, pp. 363–374, Apr. 2018.

[88] Zhang Xinfang, "Research on intelligent control of large-scale wind turbines", Ph.D. dissertation, North China Electric Power University, Beijing of China, pp19-86, 2004.

[89] J. Zhang, H. Wang, G. Hou, J. Zhang, "Generalized Predictive Control for Wind Turbine Systems", 5th IEEE Conference on Industrial Electronics and Applications, pp. 679-683, 2010.

[90] E. Hosseini, GH. Shahgholian, "Partial- or full-power production in WECS: a survey of control and structural strategies", European Power Electronics and Drives, Vol. 27, Issue. 3, pp. 125-142, Dec. 2017.

[91] L. Suganthi, S. Iniyan, A.A. Samuel, "Applications of fuzzy logic in renewable energy systems– A review", Renewable and Sustainable Energy Reviews, Vol. 48, pp. 585–607, Aug. 2015.

[92] J. Zhang, M. Cheng, Z. Chenand, X. Fu, "Pitch angle control for variable speed wind turbines", Proceeding of the IEEE/DRPT, pp. 2691–2696, 2008.

[93] T. L. Van, T.H. Nguyen, D.C. Lee, "Advanced pitch angle control based on fuzzy logic for variable-speed wind turbine systems", IEEE Trans. on Energy Conversion, Vol. 30, No. 2, pp. 578-587, Jan. 2015.

[94] M. D. Aldair, "Pitch angle control design of wind turbine using fuzzy-art network", Journal of Engineering and Development, Vol. 18, No. 4, pp. 39-51, 2014.

[95] Q. Bin, L. Pengcheng, W. Xin, Z. Wanli, "Pitch angle control based on reinforcement learning", Proceeding of the IEEE/CCDC, pp. 18-21, 2014.

[96] A.S. Yilmaz, Z. Özer, "Pitch angle control in wind turbines above the rated wind speed by multi-layer perceptron and radial basis function neural networks", Expert System and Application, Vol. 36, No. 6, pp. 9767-9775, 2009.

[97] A. B. Asghar, X. Liu, "Estimation of wind turbine power coefficient by adaptive neuro-fuzzy methodology", Neurocomputing, Vol. 238, pp. 227-233, May 2017.

[98] I. Villanueva, P. Ponce, A. Molina ,"Interval type 2 fuzzy logic controller for rotor voltage of a doubly-fed induction generator and pitch angle of wind turbine blades", International Federation of Automatic Control, pp. 2195–2202 , Jul. 2015.

[99] F. Z. Peng, "Z-Source Inverter," vol. 39, no. 2, pp. 504–510, 2003.

[100] F. Z. Peng, M. Shen, S. Member, Z. Qian, and S. Member, "Maximum Boost Control of the Z-Source Inverter," vol. 20, no. 4, pp. 833–838, 2005.

[101] M. Shen, J. Wang, A. Joseph, F. Z. Peng, L. M. Tolbert, and D. J. Adams, "Maximum Constant Boost Control of the Z-Source Inverter," Conf. Rec. 2004 IEEE Ind. Appl. Conf. 2004. 39th IAS Annu. Meet., vol. 1, pp. 142–147, 2004, doi: 10.1109/IAS.2004.1348400

[102] Y. Liu, B. Ge, H. Abu-Rub, and F. Z. Peng, "Overview of space vector modulations 125for three-phase Z-Source/quasi-z- source inverters," IEEE Trans. Power Electron., vol. 29, no. 4, pp. 2098–2108, 2014.

[103] Y. Liu, B. Ge, H. Abu-Rub, F. Z. Peng, "Phase-shifted pulse-width-amplitude modulation for quasi-Z-source cascade multilevel inverter based photovoltaic power system," IET Power Electron., vol.7, no.6, pp.1444–1456, June. 2014.

[104] Y. Liu, B. Ge, H. Abu-Rub, F. Z. Peng, "A modular multilevel space vector modulation for photovoltaic quasi-Z-source cascade multilevel inverters," in Proc. Twenty-Eighth Annual IEEE Applied Power Electronics Conference and Exposition (APEC), pp.714–718, 2013.

[105] S. G. Kadwane, A. Kadu, P. Fulzele Research, and D. Alviya Mahevashand, "Control Strategy for Closed Control of Quasi-Z Source Based Cascaded H-bridge Inverter; Control Strategy for Closed Control of Quasi-Z Source Based Cascaded H-bridge Inverter," 2021 Innovations in Power and Advanced Computing Technologies (i-PACT), 2021, doi: 10.1109/I PACT52855.2021.9696736.

[106] P. Manoj, K. Annamalai, S. Member, S. Dhara, G. Student Member, and V. T. Somasekhar, "A Quasi-Z-Source-Based Space-Vector-Modulated Cascaded Four-Level Inverter for Photovoltaic Applications," IEEE J Emerg Sel Top Power Electron, vol. 10, no. 4, p. 4749, 2022, doi: 10.1109/JESTPE.2021.3125695.

[107] Y. Zhou, S. Member, L. Liu, S. Member, and H. Li, "A High-Performance Photovoltaic Module-Integrated Converter (MIC) Based on Cascaded Quasi-Z-Source Inverters (qZSI) Using eGaN FETs," IEEE Trans Power Electron, vol. 28, no. 6, 2013, doi: 10.1109/TPEL.2012.2219556.

[108] P. Horrillo-Quintero, P. García-Triviño, R. Sarrias-Mena, C. Andrés García-Vázquez, and L. M. Fernández-Ramírez "Active and Reactive Power Sharing for PV Power Plants with Quasi-Z-source Cascaded H-bridge Multilevel Inverters," 4th International Conference on Smart Power & Internet Energy Systems (SPIES 2022), pp. 1956-1961, 2022.

[109] W. Liang, Y. Liu, and J. Peng, "A Day and Night Operational Quasi-Z Source Multilevel Grid-Tied PV Power System to Achieve Active and Reactive Power Control," IEEE Trans Power Electron, vol. 36, no. 1, 2021, doi: 10.1109/TPEL.2020.3000818.

[110] W. Liang, Y. Liu, and H. Abu-Rub, "State-of-charge balancing control for battery energy stored quasi-Z source cascaded multilevel inverter based photovoltaic power system,"

2015 IEEE Energy Conversion Congress and Exposition (ECCE), 2015, doi: 10.1109/ECCE.2015.7309662.

[111] B. Ge, Y. Liu, H. Abu-Rub, and F. Z. Peng, “State-of-Charge Balancing Control for a Battery-Energy-Stored Quasi-Z-Source Cascaded-Multilevel-Inverter-Based Photovoltaic Power System,” IEEE Transactions on Industrial Electronics, vol. 65, no. 3, 2018, doi: 10.1109/TIE.2017.2745406.

[112] P. Horrillo-Quintero, P. García-Triviño, R. Sarrias-Mena, C. Andrés García-Vázquez, and L. M. Fernández-Ramírez, “Control System for Quasi-Z-source Cascaded H-bridge Multilevel Inverter with PV Power Generation and Battery Energy Storage System,” Interdisciplinary Conference on Mechanics, Computers and Electrics (ICMECE 2022), Barcelona, Spain, 2022.

[113] A. Lashab, D. Sera, and J. M. Guerrero, “Model Predictive Control of Cascaded Multilevel Battery Assisted Quasi Z-Source PV Inverter with Reduced Computational Effort,” IEEE Energy Conversion Congress and Exposition (ECCE), Nov. 2019, DOI: 10.1109/ECCE.2019.8912551.

[114] E. Hosseini, E. Aghadavodi, Luis M. Fernández-Ramírez, "Improving response of wind turbines by pitch angle controller based on gain-scheduled recurrent ANFIS type 2 with passive reinforcement learning ", Renewable Energy (Elsevier), Vol. 157, pp. 897-910, May. 2020. DOI: https://doi.org/10.1016/j.renene.2020.05.060

[115] J.M. Jonkman, M.L. Buhl Jr, "FAST User’s Guide", NREL Report No. TP-500-38230, Golden, CO: National Renewable Energy Laboratory, pp. 1-125, Aug. 2005.

[116] The MathWorks Inc./Hydro-Québec. SimPowerSystems TM; 2016. Natick, MA.

[117] M. D. Aldair, "Pitch angle control design of wind turbine using fuzzy-art network", Journal of Engineering and Development, Vol. 18, No. 4, pp. 39-51, 2014.

[118] Q. Bin, L. Pengcheng, W. Xin, Z. Wanli, "Pitch angle control based on reinforcement learning", Proceeding of the IEEE/CCDC, pp. 18-21, 2014.

[119] A.S. Yilmaz, Z. Özer, "Pitch angle control in wind turbines above the rated wind speed by multi-layer perceptron and radial basis function neural networks", Expert System and Application, Vol. 36, No. 6, pp. 9767-9775, 2009.

[120] A. B. Asghar, X. Liu, "Estimation of wind turbine power coefficient by adaptive neuro-fuzzy methodology", Neurocomputing, Vol. 238, pp. 227-233, May 2017.

[121] A. Raj and R. P. Praveen, “Highly efficient DC-DC boost converter implemented with improved MPPT algorithm for utility level photovoltaic applications,” Ain Shams Engineering Journal, vol. 13, no. 3, 2022, doi: 10.1016/j.asej.2021.10.012.

[122] Z. Xie and Z. Wu, “A flexible power point tracking algorithm for photovoltaic system under partial shading condition,” Sustain. Energy Technol. Assessments, vol. 49, no. November 2021, p. 101747, 2022, doi: 10.1016/j.seta.2021.101747

[123] M. G. Taul, N. Pallo, A. Stillwell, and R. C. N. Pilawa-Podgurski, “Theoretical Analysis and Experimental Validation of Flying-Capacitor Multilevel Converters under Short-Circuit Fault Conditions,” IEEE Trans Power Electron, vol. 36, no. 11, 2021, doi: 10.1109/TPEL.2021.3075447.

[124] Y. Liu, H. Abu-Rub, and B. Ge, “Z-source/quasiZ-source inverters—derived networks, modulations, controls, and emerging applications to photovoltaic conversion,” IEEE Ind. Electron. Mag, vol. 8, no. 4, pp. 32–44, Dec. 2014.

[125] Y. Liu, H. Abu-Rub, B. Ge, F. Blaabjerg, O. Ellabban, and P. C. Loh, “Impedance Source Power Electronic Converters. ” Wiley-IEEE Press, 2016.

[126] Q.C. Zhong, X. Zang, “Impedance-Sum Stability Criterion for Power Electronic Systems with Two Converters/Sources.” IEEE Access, Vol. 7 pp.21254-21265, Jan. 2019. DOI: 10.1109/ACCESS.2019.2894338

[127] Y-M Chen, A. Q. Huang, and X. Yu, “A high step-up three-port DC-DC converter for stand-alone PV/battery power systems,” IEEE Transaction on Power Electron, Volume. 28, No. 11, Nov. 2013.

[128] Y. P. Siwakoti, F. Z. Peng, F. Blaabjerg, et al, “Impedance source networks for electric power conversion part II: review of control and modulation techniques”, IEEE Trans Power Electron, Vol. 30, No. 4, pp. 1887–1906, 2015, DOI: 10.1109/TPEL.2014.2329859.

[129] S. G. Kadwane, A. Kadu, P. Fulzele Research, and D. Alviya Mahevashand, “Control Strategy for Closed Control of Quasi-Z Source Based Cascaded H-bridge Inverter,” 2021 Innovations in Power and Advanced Computing Technologies (i-PACT), 2021, doi: 10.1109/I PACT52855.2021.9696736.

[130] P. Manoj, K. Annamalai, S. Member, S. Dhara, G. Student Member, and V. T. Somasekhar, “A Quasi-Z-Source-Based Space-Vector-Modulated Cascaded Four-Level Inverter for Photovoltaic Applications,” IEEE J Emerg Sel Top Power Electron, vol. 10, no. 4, p. 4749, 2022, doi: 10.1109/JESTPE.2021.3125695.

[131] Luis M. Fernández, Carlos Andrés García, Francisco Jurado, "Comparative study on the performance of control systems for doubly fed induction generator (DFIG) wind turbines operating with power regulation", Energy, Vol. 33, No. 9, pp. 1438-1452, Sep. 2008.

[132] A. D. Wright, L. J. Fingersh, "Advanced control design for wind turbines: Part 1: Control design, implementation, and initial tests", Nat. Renew. Energy Lab., Lakewood, CO, USA, Tech. Rep. NREL/TP-500- 42437, Mar. 2008.

[133] Shahnazi, "Observer-based adaptive interval type-2 fuzzy control of uncertain MIMO nonlinear systems with unknown asymmetric saturation actuators", Neurocomputing, Vol. 171, No. 1, pp. 1053-1065, January 2016.

[134] A. Taskin, T. Kumbasar, "An Open Source Matlab/Simulink Toolbox for Interval Type-2 Fuzzy Logic Systems", IEEE Symposium Series on Computational Intelligence, pp.1-13, Dec. 2015.

[135] M. Coquelet L. Bricteux M. Moens, et al, " A reinforcement-learning approach for individual pitch control ", Wind Energy, (2022), vol.25, no. 8, pp. 18-21, 2022.

[136] D. Hein, A. Hentschel, T. A. Runkler, S. Udluft, "Reinforcement Learning with Particle Swarm Optimization Policy (PSO-P) in Continuous State and Action Spaces", International Journal of Swarm Intelligence Research, Vol. 7, No. 3, Sep. 2016.

[137] J. Kennedy, R. Eberhart, "Particle swarm optimization", Proceeding of the IEEE/international Conference on Neural Networks, vol 4, pp 1942–1948, 1995.

[138] Z. Roumila, D. Rekioua, and T. Rekioua, “Energy management based fuzzy logic controller of hybrid system wind/photovoltaic/diesel with storage battery,” Int. J. Hydrogen Energy, vol. 42, no. 30, pp. 19525–19535, 2017, doi: 10.1016/j.ijhydene.2017.06.006.

[139] P. Horrillo-Quintero, P. García-Triviño, R. Sarrias-Mena, C. A. García-Vázquez, and L. M. Fernández-Ramírez, “Model predictive control of a microgrid with energy-stored quasi-Z-source cascaded H-bridge multilevel inverter and PV systems,” Appl Energy, vol. 346, p. 121390, Sep. 2023, doi: 10.1016/j.apenergy.2023.121390.

[140] R. Bellman, “A Markovian Decision Process.” Journal of Mathematics and Mechanics, vol. 6, no. 5, pp-679–684, 1957.

[141] Fujimoto, Scott, H.V. Hoof, D. Meger, “Addressing Function Approximation Error in Actor-Critic Methods,” ArXiv:1802.09477, 22 October 2018.

[142] J-H. Jung, E. Hosseini, M. Liserre, L. M. Fernández-Ramírez, “Reinforcement Learning Based Modulation for Balancing Capacitor Voltage and Thermal Stress to Enhance Current Capability of MMCs,” 2022 IEEE 13th International Symposium on Power Electronics for Distributed Generation Systems (PEDG), Kiel, Germany, June 2022.

[143] E. Hosseini, P. Horrillo-Quintero, P. García-Triviño, R. Sarrias-Mena, C. Andrés García-Vázquez, and L. M. Fernández-Ramírez “A Nonlinear Programming Solver based on Battery Efficiency Maximization for Quasi-Z-source Cascaded H-bridge Multilevel Inverter with PV and Battery,” 4th International Conference on Smart Power & Internet Energy Systems (ONCON), India, 2022.

[144] M. L. Buhl, "MCrunch user’s guide for version 1.00, " Nat. Renew. Energy Lab., Golden, CO, USA, Tech. Rep. NREL/TP-500-43139, May 2008.

List of publications

The following works have been published and submitted during the progress of this thesis:

Journal papers:

- **Ehsan Hosseini,** Ehsan Aghadavoodi, Luis M- Fernández-Ramírez. ''Improving response of wind turbines by pitch angle controller based on gain-scheduled recurrent ANFIS type 2 with passive reinforcement learning.'' Renewable Energy 2020; 157: pp. 897-910.
  DOI: https://doi.org/10.1016/j.renene.2020.05.060
  Journal Impact Factor (2022): 8.7 (**Q1**).

- **Ehsan Hosseini,** Pablo Horrillo-Quintero, Pablo García-Triviño, Raúl Sarrias-Mena, Carlos Andrés García-Vázquez, Luis M. Fernández-Ramírez. ''Optimal Energy Management System for Grid-Connected Hybrid Power Plant with Wind Turbine, PV Plants and Battery Energy-Stored Quasi-Z-source Cascaded H-bridge Multilevel Inverter.'' Energy Reports, Submitted Jul 2023.
  Journal Impact Factor (2022): 5.2 (**Q2**).

Conference proceedings

- **Ehsan Hosseini,** Pablo García-Triviño, Raúl Sarrias-Mena, Carlos Andrés García- Vázquez, Luis M. Fernández Ramírez. ''Reinforcement Learning based Energy Management System for Grid-Connected PV plants and Energy-Stored Quasi-Z-source Cascaded H-Bridge Multilevel Inverter.'' 23rd EEEIC International Conference on Environment and Electrical Engineering (EEEIC 2023); Madrid (Spain), 2023.

- **Ehsan Hosseini,** Pablo Horrillo-Quintero, Pablo García-Triviño, Raúl Sarrias-Mena, Carlos Andrés García-Vázquez, Luis M. Fernández Ramírez. ''A Nonlinear Programming Solver based on Battery Efficiency Maximization for Quasi-Z-source Cascaded H- bridge Multilevel Inverter with PV and Battery.'' IEEE Industrial Electronics Society Annual OnLine Conference (ONCON); India, 2022.
  DOI: https://ieeexplore.ieee.org/abstract/document/10126639.

- **Ehsan Hosseini**, Jun-Hyung Jung, Marco Liserre, Luis M. Fernández-Ramírez, ''Reinforcement Learning Based Modulation for Balancing Capacitor Voltage and Thermal Stress to Enhance Current Capability of MMCs.'' IEEE 13th International Symposium on Power Electronics for Distributed Generation Systems (PEDG); Kiel (Germany), 2022.
  DOI: https://ieeexplore.ieee.org/abstract/document/10126639.

Currículum Vitae

Información Personal

Nombre: Ehsan Hosseini

Fecha de nacimiento: 11 de junio, 1990

Lugar de nacimiento: Esfahan, Iran.

Email: ehsan.hosseini@uca.es

ORCID ID: https://orcid.org/0000-0003-4693-9008

Formación Académica

- Máster Universitario en Ingeniería Eléctrica, Universidad de Azad, Irán, Febrero 2016.
- Ingeniero Eléctrico, Universidad de Azad, Irán, Octubre 2012.

Experiencia Profesional

- Contrato de Formación de Personal Investigador, Universidad de Cádiz (Marzo 2022 – actualmente).
    - Proyecto de investigación: Nuevas soluciones para la mejora de la eficiencia e integración a red de plantas eléctricas híbridas basadas en energía eólica, solar fotovoltaica y almacenamiento de energía (PHESA) (Ref. PY20_00317). Entidad financiadora: Consejería de Transformación Económica, Industria, Conocimiento y Universidades de la Junta de Andalucía. Programa de ayudas a la I+D+i, en régimen de concurrencia competitiva, en el ámbito del Plan Andaluz de Investigación, Desarrollo e Innovación (PAIDI 2020). Proyectos de investigación orientados a los retos de la sociedad andaluza. Entidades participantes: Universidad de Cádiz. Duración, desde: 05/10/202 hasta: 30/06/2023. Cuantía de la subvención: 65.875,00€. Investigador responsable: Prof. Dr. D. Luis M. Fernández Ramírez. Nº de investigadores participantes: 10. Contratado como investigador: desde 05/05/2022 hasta 14/03/2023.
    - Proyecto de investigación: Control coordinado de microrredes multi-energía con vectores de electricidad, hidrógeno y gas - Coordinated control of multi-energy microgrids with electricity, hydrogen and gas vectors (CoMicroME-EleH2Gas) (Ref. TED2021-129631B-C32). Entidad financiadora: Ministerio de Ciencia e Innovación. Proyectos de Transición Ecológica y Transición Digital. Entidades participantes: Universidad de Cádiz, de Jaén y Politécnica de Cataluña. Duración, desde: 01/12/2022 hasta: 30/11/2024. Cuantía de la subvención: 138.000,00 €. Investigador responsable: Prof. Dr. D. Luis M. Fernández Ramírez. Nº de investigadores participantes: 9. Contratado como investigador: desde 15/03/2023 hasta 30/11/2024.

- Beca de Investigación en la División de Energías Renovables y Generación Distribuida, Universidad de Azad, Irán (Oct 2013 – Sep 2018).

Estancia de Investigación en el Extranjero

- Estancia de investigación en el *Centre ''Chair of Power Electronics''*, Kiel University, Alemania (6 meses, Sep 2021 – Mar 2022). Supervisores: Prof. Marco Liserre, Dr. Jun.

Idiomas

- **Inglés:** Certificación nivel B2, Cambridge (Dec 2018).
- **Español:** Certificación nivel B1, Escuela Oficial de Idiomas, San Roque, Cádiz (Jun 2023).

Producción científica

- Publicaciones en revistas indexadas en JCR-SCIE:
  - E. Hosseini, E. Aghadavodi, Luis M. Fernández-Ramírez, "Improving response of wind turbines by pitch angle controller based on gain-scheduled recurrent ANFIS type 2 with passive reinforcement learning ", Renewable Energy (Elsevier), Vol. 157, pp. 897-910, May. 2020.
    DOI: https://doi.org/10.1016/j.renene.2020.05.060
  - E. Hosseini, GH. Shahgholian, "Output Power Leveling for DFIG WTS Using Intelligent Pitch Angle Control", Journal for Control, Measurement, Electronics, Computing and Communications (Taylor & Francis-Automatika), Vol. 58, No. 4, pp. 363–374, Apr. 2018.
    DOI: https://doi.org/10.1080/00051144.2018.1455017
  - E. Hosseini, GH. Shahgholian, "Partial- or full-power production in WECS: a survey of control and structural strategies", European Power Electronics and Drives (Taylor & Francis-EPE), Vol. 27, Issue. 3, pp. 125-142, Dec. 2017.
    DOI: https://doi.org/10.1080/09398368.2017.1413161
  - E. Hosseini, E. Aghadavodi, GH. Shahgholian, H. Mahdavi-Nasab, "Intelligent Pitch Angle Control Based on Gain-Scheduled Recurrent ANFIS", Journal of Renewable Energy and Environment, Vol. 6, No. 1, pp. 36-45, Nov. 2019.
    DOI:https://www.academia.edu/download/88630392/article_95920_4c2576a7b0e5583fbb294609902819d8.pdf
  - E. Hosseini, GH. Shahgholian, "Different Types of Pitch Angle Control Strategies Used in Wind Turbine System Applications ", Journal of Renewable Energy and Environment, Vol. 4, No. 1, pp. 20–35, Nov. 2017.
    DOI: https://doi.org/10.30501/jree.2017.70103

- Publicaciones en actas de congresos internacionales con revisión por pares:

  - Ehsan Hosseini, Pablo García-Triviño, Raúl Sarrias-Mena, Carlos Andrés García- Vázquez, Luis M. Fernández Ramírez. ‘‘Reinforcement Learning based Energy Management System for Grid-Connected PV plants and Energy-Stored Quasi-Z-source Cascaded H-Bridge Multilevel Inverter.’’ 23rd EEEIC International Conference on Environment and Electrical Engineering (EEEIC 2023); Madrid (Spain), 2023.

  - Ehsan Hosseini, Pablo Horrillo-Quintero, Pablo García-Triviño, Raúl Sarrias-Mena, Carlos Andrés García-Vázquez, Luis M. Fernández Ramírez. ‘‘A Nonlinear Programming Solver based on Battery Efficiency Maximization for Quasi-Z-source Cascaded H- bridge Multilevel Inverter with PV and Battery.’’ IEEE Industrial Electronics Society Annual OnLine Conference (ONCON); India, 2022.
    DOI: https://ieeexplore.ieee.org/abstract/document/10126639.

  - Ehsan Hosseini, Jun-Hyung Jung, Marco Liserre, Luis M. Fernández-Ramírez, ‘‘Reinforcement Learning Based Modulation for Balancing Capacitor Voltage and Thermal Stress to Enhance Current Capability of MMCs.’’ IEEE 13th International Symposium on Power Electronics for Distributed Generation Systems (PEDG); Kiel (Germany), 2022.
    DOI: https://ieeexplore.ieee.org/abstract/document/10126639.

  - E. Hosseini, "Permanent magnet synchronous motor vector control with fuzzy logic controller", International Conference on Non-Linear System and Optimization in Computer and Electrical Engineering, Imaret Dubai, May. 2015.

  - E. Hosseini, M. Torki, "Dynamic stability enhancement in large power systems using fuzzy logic PSS", International Conference on Research in Science & Engineering, Turkey, Istanbul University, July. 2016.